2013

MODERNIZATION OF THE MOCK CIRCULATORY LOOP: ADVANCED PHYSICAL MODELING, HIGH PERFORMANCE HARDWARE, AND INCORPORATION OF ANATOMICAL MODELS

Charles Taylor
Virginia Commonwealth University

MODERNIZATION OF THE MOCK CIRCULATORY LOOP: ADVANCED PHYSICAL MODELING, HIGH PERFORMANCE HARDWARE, AND INCORPORATION OF ANATOMICAL MODELS

A dissertation submitted in partial fulfillment of the requirements for the degree of

Doctor of Philosophy at Virginia Commonwealth University

BY

CHARLES EDWARD TAYLOR

B.S., Bioengineering, UC San Diego, 2005

Director: Gerald E. Miller, Ph.D.

Department Chair of Biomedical Engineering

Virginia Commonwealth University

Richmond, Virginia

May, 2013

Acknowledgements

The author has always been blessed by having the opportunities to work for great individuals that have allowed him to grow and thrive in his research. His graduate advisor, Dr. Miller, is no exception. His support of my research and mentorship of my career path forward have been invaluable. The author would also like to thank the previous employers that saw the potential in him, and provided the opportunity to join excellent research. The experience gained from those employments played heavily in the success of this project. For those investments in his career he would like to thank Charles River Laboratories, Stanford Medical Center, and Kalypsys, Inc.

The authors family certainly deserves thanks for the support and guidance through this degree. It has always been important to the author that they are proud of his accomplishments and feel he has reached his full potential. Last, but certainly not least, the author would like to thank Amanda Bates for her commitment and perseverance. She has been a tremendous source of support through this very challenging degree.

"I have only made this letter longer because I have not had the time to make it shorter."

Blaise Pascal, (1623-1662) Lettres provinciales.

Table of Contents

List of Figures

List of Tables

List of Abbreviations

ABP	*Aortic Blood Pressure*
ANSI	*American National Standards Institute*
CFD	*Computational Fluid Dynamics*
DIAS	*Diastole*
FMEA	*failure modes and effects analysis*
FRACAS	*failure reporting, analysis and corrective action system*
GUI	*Graphical User Interface*
HIL	*Hardware-In-the-Loop*
HR	*Heart rate*
ICU	*Intensive Care Unit*
ISA	*International Society of Automation*
ISO	*International Organization for Standardization*
LA	*Left Atrium*
LV	*Left Ventricle*
LVAD	*Left Ventricular Assist Device*
MCL	*Mock Circulatory Loop*
NYHA	*New York Heart Association*
PID	*Proportional-integral-derivative*
PIV	*Particle Image Velocimetry*
PS	*Percent Systole*
RA	*Right Atrium*
RV	*Right Ventricle*
SV	*Stroke Volume*
SYS	*Systole*
UI	*User Interface*
VAD	*Ventricular Assist Device*
VI	*Virtual Instrument*

Abstract

MODERNIZATION OF THE MOCK CIRCULATORY LOOP: ADVANCED PHYSICAL MODELING, HIGH PERFORMANCE HARDWARE, AND INCORPORATION OF ANATOMICAL MODELS

By: Charles E. Taylor, Ph.D.

A dissertation submitted in partial fulfillment of the requirements for the degree of Doctor of Philosophy at Virginia Commonwealth University.

Virginia Commonwealth University, 2013.

Major Director: Gerald E. Miller, Chair of the Biomedical Engineering Department

A systemic mock circulatory loop plays a pivotal role as the in vitro assessment tool for left heart medical devices. The standard design employed by many research groups dates to the early 1970's, and lacks the acuity needed for the advanced device designs currently being explored. The necessity to update the architecture of this in vitro tool has become apparent as the historical design fails to deliver the performance needed to simulate conditions and events that have been clinically identified as challenges for future device designs. In order to appropriately deliver the testing solution needed, a comprehensive evaluation of the functionality demanded must be understood. The resulting system is a fully automated systemic mock circulatory loop, inclusive of anatomical geometries at critical flow sections, and accompanying software tools to execute precise investigations of cardiac device performance.

Delivering this complete testing solution will be achieved through three research aims: (1) Utilization of advanced physical modeling tools to develop a high fidelity computational

model of the in vitro system. This model will enable control design of the logic that will govern the in vitro actuators, allow experimental settings to be evaluated prior to execution in the mock circulatory loop, and determination of system settings that replicate clinical patient data. (2) Deployment of a fully automated mock circulatory loop that allows for runtime control of all the settings needed to appropriately construct the conditions of interest. It is essential that the system is able to change set point on the fly; simulation of cardiovascular dynamics and event sequences require this functionality. The robustness of an automated system with incorporated closed loop control logic yields a mock circulatory loop with excellent reproducibility, which is essential for effective device evaluation. (3) Incorporating anatomical geometry at the critical device interfaces; ascending aorta and left atrium. These anatomies represent complex shapes; the flows present in these sections are complex and greatly affect device performance. Increasing the fidelity of the local flow fields at these interfaces delivers a more accurate representation of the device performance in vivo.

1 Introduction

Heart disease remains the leading cause of death worldwide. Providing more sophisticated assessment technologies for the development of cardiac devices servicing this research seeks to synergize the delivery of more effective treatment options. The structure and function of the cardiovascular system is crucial to addressing the clinical and biomedical engineering aspects of congestive heart failure. With this understanding of the system and issues, it is clear that the current assessment protocols are lacking in appropriately evaluating device function in this complex application environment. Building from the excellent research in this field, the research objectives that seek to bridge this gap become clear.

1.1 Anatomy and physiology

The human circulatory system is a closed loop system comprised of two circulations that are in series; pulmonary and systemic. The human heart supports both of these circulations, and is divided into right and left sections to support the pulmonary and systemic circulations, respectively. Figure 1 illustrates the segregation of these two circulations and the oxygen content of the blood at the various stages of circulation between these systems. The heart is a positive displacement pulsatile pump; fluid flow is created by a moving physical boundary and occurs at intervals. The atria of the heart accept incoming flow from the veins, the ventricles eject the blood into the arteries leading away from the heart, and the valves prevent back flow. These structures and functions are mirrored in both the left and right heart. The geometry of the left and right structures reflects the characteristics of the circulations they are serving.

The pulmonary circulation accepts deoxygenated blood from the systemic circulation and returns oxygenated blood. The lungs are large vasculature beds where gas exchange takes place. Although the flows leaving and returning to the heart are circular conduit flows, the flow past the

alveoli represent sheet flow [1]. The flow through the lungs is low pressure and the tissues in this region are highly elastic. The pressure from ejection of the right ventricle into the lungs is roughly 15-30 mmHg and the return pressure to the left atrium is on the order of 3-14 mmHg [2]. These characteristics almost completely dampen the pressure pulse from the right ventricle ejection. This enables the pulmonary system to have a large flow capacity at low pressures.

The systemic circulation accepts oxygenated blood from the lungs and transfers it to the various organ systems of the body. Figure 2 illustrates the organ apportionment of the flow under healthy rest conditions. Due to the larger network and geometries of the vessels, this system is under higher pressure and is less elastic in nature [3]. It is able to change its elasticity and resistance to flow much more than that of the pulmonary system, as it uses these mechanisms to regulate the flow to specific organs. The systemic circulation's arterial pressures during ventricular ejection (systole) and filling (diastole) are those taken during clinical evaluations to assess patient health. The systemic arterial circulation normally operates at 100-140 mmHg in ventricular systole and 60-90 mmHg in diastole for healthy individuals; these are the pressures at the exit of the left ventricle [2]. The return pressure from the systemic circulation, via the vena cava, to the right atrium is roughly 3-8 mmHg.

The function of the heart has classically been described in a set of measurements that describe the timing and flow delivery; heart rate, percent systole, and stroke volume. The first two metrics describe the rate of contractions that eject blood from the ventricles and the percentage of time spent in systole versus diastole for each cycle, respectively. The third term describes the volume that is ejected for a particular beat. Other volume terms such as end systolic volume (ESV) and end diastolic volume (EDV) are important, but typically require medical imaging or catheter studies to determine [2]. Using heart rate and stroke volume, the

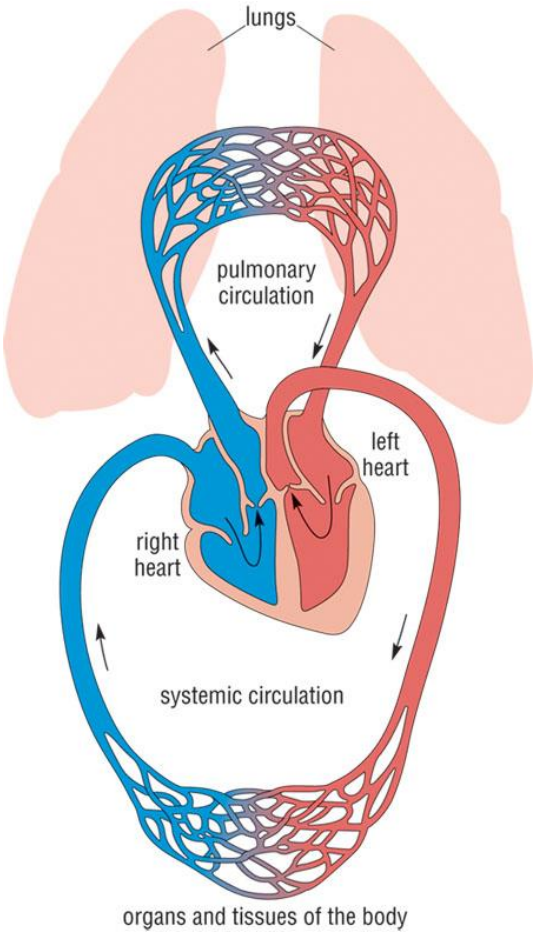

Figure 1: Illustration of the two circulatory systems in the body. Blue is deoxygenated blood and red is oxegynated blood.

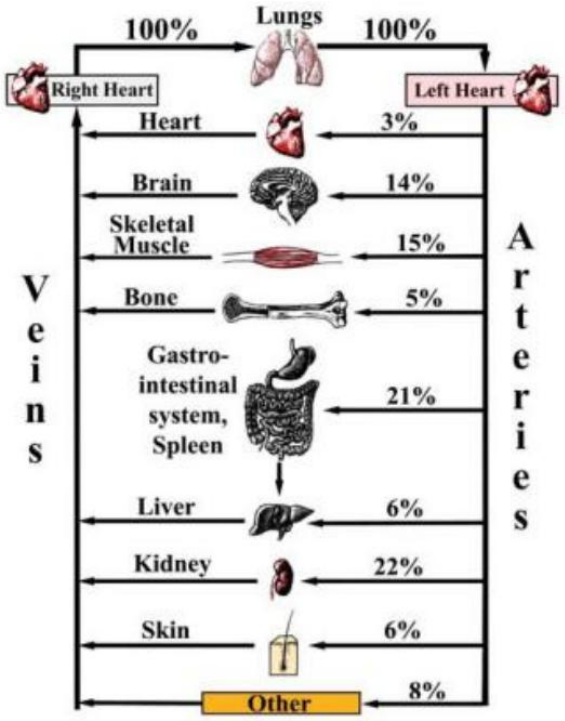

Figure 2: Blood flow apportionment in the cardiovascular system. The values presented are for a healthy individual at rest. For different levels of activity or disease state, flow apportionment can change drastically. Skeletal muscle, GI, and kidney flows can be respectively increased by exercise, digestion, and disease. Adapted from Iaizzo (2009).

cardiac output can be determined; this is the bulk volume pumped in a particular time period. These calculations are important metrics to assess cardiac function.

Governing the function of the cardiovascular system are various neural and physiochemical mechanisms that regulate the aforementioned soft tissue behavior and cardiac function. There exist fast acting neural controls that can rapidly change the contractility of the heart or systemic vascular resistance [4]. These neural controls are responsible for the swift

changes in cardiovascular conditions that work to maintain homeostasis during sudden events; hemorrhage, exercise, postural changes, etc.

Stretch receptors in the ascending aorta and carotid bodies act as blood pressure sensors for the nervous system. These sensors are distal to the left ventricle output, resulting in a fast detection of changes in blood pressure. Another set of controls are physiochemical based, such as aldosterone. Although there are some fast acting hormones, such as epinephrine, hormones tend to work on longer effect duration and may change the sensitivities to neural control mechanisms. The physiological control mechanisms of the cardiovascular system are complex, with new discoveries still being made. A comprehension of the multiple levels of effect and duration is important when simulating events and disease states that challenge devices tasked with maintaining appropriate circulatory conditions.

1.2 Clinical Aspect

The investment in cardiac medical devices is based not only on the large patient population that it services, but in the continued refinement of technology that has yet to fully satisfy the patient treatment outcomes seen in other fields. The development complexity stems from the highly conjugated nature of the diseases driving these interventions, the higher quality of life expectation for post-intervention, and the broadening of the recipient patient population demographics. With this continually evolving target, it is necessary to provide the research with tools that effectively allow it to assess efficacy against this increasing array of clinical performance expectations.

1.2.1 Heart Disease

Heart disease is the leading cause of death in world and it is estimated that 200 million people will be diagnosed with either congestive heart failure (CHF) or a defective heart valve

[5]. CHF is the inability of the heart to sufficiently maintain blood flow in the body; Table 1 shows that the degree of dysfunction is delineated by symptoms indicative of the stage of the failure [6]. Patient population statistics have shown that in a large percentage of individuals CHF is caused by ischemic heart disease, with other health issues (diabetes, obesity, hypertension) and lifestyle choices (cigarette smoking) being present as well [7]. Acute onset of CHF can also result from injury or illnesses that affect the cardiopulmonary system [8]. Heart valve disease, beginning with leaflet sclerosis (thickening) and possibly leading to stenosis (narrowing), causes undue stress on the heart and may lead to CHF as well [2].

The state of the disease is typically determined after some objective assessment, either medical imaging or catheter study, which results in an objective description of extent of disease (Table 2). The occurrence of valvular disease states is typically age related, but may be influenced by other health conditions (hypertension, diabetes) [9].

Table 3 represents patient examples produced by the NYHA for different degrees of functional capacities and objective assessments; symptoms are not always connected with objective proof and vice versa. The compounding issue of heart disease is the blend of physiochemical and biomechanical issues present. Medical devices play a role in patients where pharmaceutical and surgical interventions are not sufficient to properly address the treatment of these patients, alleviate symptoms and prolong survival.

Table 1: NYHA functional capacity guidelines.

Functional Capacity			
Identification		Symptoms	
Class	Description	At Rest	Activity
I	Patients with cardiac disease but without resulting limitation of physical activity.	They are comfortable at rest.	Ordinary physical activity does not cause undue fatigue, palpitation, dyspnea, or anginal pain.
II	Patients with cardiac disease resulting in slight limitation of physical activity.	They are comfortable at rest.	Ordinary physical activity results in fatigue, palpitation, dyspnea, or anginal pain.
IV	Patients with cardiac disease resulting in marked limitation of physical activity.	They are comfortable at rest.	Less than ordinary physical activity results in fatigue, palpitation, dyspnea, or anginal pain.
IV	Patients with cardiac disease resulting in inability to carry on any physical activity without discomfort.	Symptoms of heart failure or the anginal discomfort may be present even at rest.	If any physical activity is undertaken, discomfort is increased.

Table 2: NYHA objective assessment guidelines.

Objective Assessment	
Grade	Description
A	No objective evidence of cardiovascular disease.
B	Objective evidence of minimal cardiovascular disease.
C	Objective evidence of moderately severe cardiovascular disease.
D	Objective evidence of severe cardiovascular disease.

Table 3: NYHA patient examples with corresponding functional capacities and objective assessments.

Patient	Symptoms	Class	Clinical Assessment	Grade
1	Dyspnea at rest.	IV	Near total occlusion of the left main artery.	D
2	Mild dyspnea while climbing stairs.	II	Severe aortic stenosis	D
3	Angina at rest.	IV	Angiographically normal coronary arteries.	A
4	No cardiac symptoms.	I	Moderate pressure gradient across mitral valve.	C

1.2.2 Medical Device Challenges

With the large volume of end stage heart failure diagnoses annually, organ donation networks cannot sustain the required annual supply with cadaveric material. In order to sufficiently address this patient population, medical device development has produced many viable treatments in the form of total artificial hearts, ventricular assist devices, and prosthetic heart valves. Progress in the development of these devices has not only greatly decreased mortality, but has positioned some of these products as long term solutions. This length of application increases the expectation of continued and improved quality of life in the patient, which in turn challenges the performance of the device. Now, it must operate in a patient that is not confined to a bed and may be distant from medical professionals. This deepening of the complexity in a single patient is further complicated by the expanding medical device market. Brazil, Russia, India and China (BRIC) accounted for nearly 40% of the world population in 2010 and have become ever increasing consumers in the medical device market. The diversity of the populations between these countries calls into question the variance in cardiac function parameters (e.g. cardiac output, blood pressures) that might exist. This would add to the range of operation medical devices must operate within to target these patients demographics effectively. These compounding complexities in medical device development necessitate effective robustness and performance evaluation across a wide range of operating conditions.

1.3 Standards and Guidance Documents for In Vitro Testing

Evaluation of medical devices in vitro is a critical step in the performance validation and safety analysis. Guidance and regulatory documents seek to homogenize the in vitro evaluation process by prescribing conditions and calculations that should be applied. Due to the technological diversity of medical devices, and complexity of the physiological systems they

interface, there are many governing bodies that have constructed evaluation procedures to assess safety as it relates to their discipline [10,11]. For the purposes of evaluating ventricular assist devices and heart valves, the primary documents utilized for safety assessment are ISO documents 5840, 5198, and 14708-5. Executing these ISO certifications supports many of the requirements outlined in the draft guidance by the FDA, which in many cases directly refer to the ISO guidelines for experiments to be conducted [12]. Understanding the contents and requirements of these documents is crucial when designing the mock circulatory loops that will be utilized for these certifications.

Safety evaluation of cardiac valve prostheses is crucial due to the high cycle life expectancy of the device and the forces exerted during use. The ISO 5840 document that governs the safety assessment of cardiac valves prescribes in vitro experiments and in vivo animal trials that work to replicate the target operating conditions in humans [13]. Table 1 of the document outlines the pressure and flow conditions that simulate hypotensive, normotensive, and hypertensive conditions. Description of the flow rate waveform in Figure 1 of the document, and the RMS calculation for forward flow (Note 1), allow for appropriate comparison to the performance requirements in Table 2. For non-rigid heart valves, there is a requirement for use of compliant chambers to replicate the mounting tissues structural deformation that might affect the regurgitation of the valve. The application of the testing methods from ISO 5840 not only serve as regulatory compliance for products in pre-market approval, but as guidance for investigational conditions used by researchers [14–16].

Safety assessment of ventricular assist devices and total artificial hearts is a complex process due to the active nature of the devices and the multiple domains involved in the operation of the device (electrical, mechanical, etc.). Focusing on the complete assembly's

performance as a heart pump, there are two ISO guidance documents that assist in certifying performance and pumping safety: ISO 5198 and ISO 14708-5. The former pertains to all pumps, regardless of application, and details the appropriate means of characterizing performance [17]. It serves as the basis for the methods and testing outlined in ISO 14708-5, which details the evaluation schema for a pump destined for cardiovascular circulatory support [18]. ISO 14708-5 supersedes the AAMI TIR26:2000 document, which had many of its testing guidelines adopted into the ISO 14708 series. The 14708-5 document is specific to circulatory support devices, and is the fifth in a series of documents that describe safety for a wide range of implantable medical devices. Annex CC of the document details an exemplary set of physiological conditions for the assessment of a left ventricular assist device. There are no set conditions to evaluate against, rather suggested ranges of operation.

Safety assessment techniques and methodologies have been proposed to work in conjunction with the aforementioned hydrodynamic testing documents. These recommended practices are typically based on FMEA, FRACAS, or other failure identification methods [19–21]. ISO 14971 describes risk management techniques applied to medical devices, and serves as a guidance on product life cycle safety determination [22]. It is cited by many of the experimental standards as a means of identifying, or categorizing, failures. The adaptation of these failure identification methodologies to medical device safety assessments, and specifically cardiac prostheses, has gained momentum in recent years. However, it is still an industry consensus that there is no overarching failure assessment methodology that satisfies the multifaceted safety issues inherent to cardiac devices.

1.4 Cardiovascular Lumped Parameter Modeling

Lumped parameter modeling is used to simplify systems into discrete elements, and can be used to represent a simplified embodiment of a complex network [23]. The classic example of this technique is in electronics with the use of Norton and Thevenin equivalents to simplify larger circuits into a low element count model with the same response. This technique can be applied to hydraulic models as well, and has been used extensively to model the human circulatory system [24–26]. Aggregating the system effects of resistance to flow (peripheral resistance), expansion of volume under pressure (arterial compliance), and feed capacity (pulmonary supply) produces a model for left ventricular device evaluation that is quite effective. For flow based cardiac medical devices, the hydraulic interaction with the cardiovascular system is perceived at an inlet and outlet. Thus, the lumped parameter model is sufficient at representing the larger system responses at these interfaces without reproducing the entire cardiovascular system structure and function. Mock circulatory loops provide in vitro simulation of the circulatory conditions present in vivo for the purpose of evaluating methods of restoring cardiac performance. These testing scaffolds provide the ability to evaluate cardiac assist device performance under various circulatory conditions. Most mock systemic circulatory loops employ a lumped parameter model for the simulation of arterial compliance, peripheral resistance and venous volume [27–29].

1.4.1 Peripheral Resistance

Peripheral resistance in the human systemic circulation is produced by the transition of larger diameter arteries to smaller diameter arterioles and capillaries. These arterioles provide the largest pressure drop in the systemic circulation, and are capable of mediating change in resistance through vasoconstriction and vasodilatation [30]. This diameter change is effected by

smooth muscle cells imbedded concentrically in the wall of the vessel that constrict the wall circumferentially to achieve smaller flow path diameters [3]. Resistance to flow produces a pressure gradient, with the higher pressure being developed upstream. With the extensive network of vasculature in the systemic circulation, the resistance is not only developed by reduction of cross-sectional area, but also by the length of the restrictive vasculature [1,3].

Disease states may physiologically alter peripheral resistance, or the body's response capabilities. Hypertension is a leading medical concern, which can lead to heart disease and decreased organ function [30]. This elevated blood pressure state is indicative of the increased back pressure caused by systemic flow resistance. Many patients that are recipients of ventricular assist devices exhibit pathological states of peripheral resistance.

In terms of the peripheral resistance, this methodology assumes that all resistance to flow experienced by ventricle, or ventricular assist device (VAD), can be summated into a single resistive term [3]. This single resistance is exemplified by a single resistance device in the mock circulatory loop. This one device must have a range of operation that encompasses the resistance developed by all the arterial vasculature for every condition that is to be simulated by the mock circulatory loop. A classical design for peripheral resistance simulation in a mock circulatory loop is the presence of a clamped section of tubing [27]. The clamping mechanism is typically a hand clamp that is manually actuated [29]. Proportional pinch valves have been employed in cases where automated clamping of the tube is desired [28,31]. The resistance to flow in these designs results from the decrease in the flow path cross section area as the tubing is compressed.

1.4.2 Arterial Compliance

Arterial compliance provides the capacitance of the circulatory system, which is crucial in maintaining the blood pressure during ventricular diastole and dampening pressure waves.

The use of compliance chambers for simulating the elastic effects of circulatory tissue provides an effective means of lumped parameter testing; the entirety of elastance in the system being simulated is represented in a singular device. Compliance values in the human population vary according to age, sex, and health [32,33]. Compliance chambers that are capable of simulating a range of settings provide an in vitro method for assessing a device's performance for a prescribed compliance value. Compliance has been found to change during pathological events as well, which is consistent with the biomechanics of the arterial tissues [3,32,34]. For a complete mock circulatory loop investigation of a device, it becomes necessary to simulate a range of compliance values and include the capability to change the compliance during pumping.

There are three main design types for compliance chambers in mock circulatory loops; membrane-based chambers [33], spring-based chambers [35], and pneumatic only chambers [36]. The first is the architecture chosen for this design due to the accuracy with which the membrane can be measured for volume expansion in the compliance calculation, and this structure’s low hydraulic impedance. The spring-based designs are more complex in their hermetic seals, and are subject to higher impedance due to the seal friction. The use of a non-membrane design provides an effective means of compliance, but poses the challenge of accurate liquid volume change measurement. Mass flow sensors must be used for the pneumatic system in order to use ideal gas laws for volume and pressure correlations. Ultrasonic liquid level sensors can be used, but are dependent on the system fluid physical properties and do not account for sloshing at the surface. The membrane design provides a geometrical constraint for accurate volume expansion determination, is not dependent on system fluid physical properties, and lacks the seal friction of spring loaded piston designs.

1.4.3 Venous Supply

The venous system returns blood to the heart, with the pulmonary veins carrying oxygenated blood and the systemic veins carrying deoxygenated blood. Venous tissue is highly elastic and the flow operates at near atmospheric pressure. The volume of blood in the systemic veins is much higher than that in the arterial network; the pulmonary circulation is not that disproportioned. This high flow return capacity in the venous system supplies the necessary preload to the ventricles, so that appropriate end diastolic volumes can be reached for the prescribed cardiac function level. If this flow capacity is not in place, ventricular filling insufficiency results. In the case that a ventricular assist device is in use, venous collapse may occur if the pump overdraws the venous systems volume capacity and creates a suction event.

Mock circulatory loops that are simulating only the systemic cardiovascular systems typically employ a reservoir to deliver a constant pressure head to the left atrium [37–39]. This is an appropriate means of dampening the return flow oscillations, to deliver the near constant pressure that exists in the pulmonary veins. Mock circulatory loops simulating both the pulmonary and systemic circulations may not employ the reservoirs, and may just use compliance chambers to model the venous return. The limitations of these methods are twofold; reservoirs do not allow for venous return conditions to change and closed loop systems have issues with inertial effects that may misrepresent the changes in venous return conditions. Modifying the inertial effects in a hydraulic system can be challenging, as this characteristic is governed by dimensions of the components. Utilizing actuators and numerical models may provide a means of simulating these inertial effects, and circumvent the issues seen with hydraulic only methods [40].

1.5 Anatomical Models

Effective in vitro assessment of cardiac devices employing the use of non-anatomically derived geometry has been shown to have limitations when understanding the devices impact on the surrounding anatomy. The technological progression in this field has necessitated that accurate geometry is employed in experiments, and the means of achieving this demand has been met. The capability of researchers to extract geometry from medical imaging modalities, fabricate a representative model from material of choice, and integrating those geometries into experimental studies has become a fairly common practice. The options available to researchers in pursuit of developing these models are varied, with a common denominator being the funding available. Effort and price are inversely proportional, with quality of the model becoming more equal in the spectrum with the rapid advancement in open source tools.

1.5.1 CAD Model Development

The primary step in developing an anatomical model is the decision of what to base the geometry on. Constraining this decision to the practice of basing the model on patient data, the medical image dataset must be acquired. Researchers have typically used geometry that they have commissioned, or through acquisition of anonymous patient data. There also exists the Visible Human Project through the National Library of Medicine, which is a publicly accessible database of multiple imaging modalities (CT, MRI, cryo-slice, etc.) [41]. The image set must be a compilation of slices from the same individual that serve as a volume scan of the anatomy of interest. The modality used should be reflective of that medium's capability in capturing the boundaries of the tissue of interest, and the resolution necessitated for the model.

The method of extracting the geometry from the images is termed segmentation. It is the practice of segmenting the region of interest from a larger dataset, with this regional subset being

used to construct the boundary of the anatomical model. Commercial packages, such as MIMICS (Materialise, Plymouth, MI), provide an integrated environment of segmentation methods and processing tools to develop refined anatomical models. With an abundance of work on this topic, there are many choices of software or published algorithms to accomplish the task [42–45]. Cardiovascular-specific image segmentation tools are also available, and may trace lumen boundaries better than other packages that are more orthopedic focused [46]. Most packages will deliver an STL model, either surface or solid, of the extracted volume of interest. This model type is discrete; the geometry surface is a mesh of facets and vertices. Interpolation of the boundary between two vertices, and across a facet, is linear. This is governed by the principle that all segments between vertices must be straight, which enforces that the facets are all triangles. The base resolution of many segmentation routines is constrained by the medical imaging resolution, which may suffice for many applications. When the features of the anatomy approach the size scaling of the resolution, or the model will be used in analyses where the interaction (e.g. fluid, sliding contacts) is greatly affected by roughness, processing the rough model becomes necessary.

Commensurate with the options to extract the geometry, there are many options to post-process the model. The refinement of an anatomical model typically involves three routines; removal of artifacts, smoothing the mesh profile, and facet count modification. These processes are used recursively with no stated dependency of order; however, the listed sequence is the best course for many models. As previously mentioned, some segmentation software packages include post processing tools. There are many standalone options as well, such as Blender or MeshLab, for post processing CAD models [47,48]. The result of many of these post processing

packages is a more refined discrete STL model, with the same linear interpolation between the points on its surfaces.

An alternative to the discrete STL model structure is a surface described method; a lofted geometry based on non-uniform rational basis splines (NURBS). In this case, the free surfaces of the model are defined by fitted nonlinear interpolations that seek to match the segmented geometry. A lattice of splines provide an open framework that defines the shape of the model. The splines are closely matched to the curvature of the model, allowing for the surfaces that are created from this lattice of guide curves to closely approximate the models surfaces. The advantage of this method is that the surface is inherently smooth, due to the continuous curvature of the underlying splines. Work based off this continuously interpolated surface (e.g. FEA mesh, machining paths) is simplified, as opposed to a patchwork surface of triangles found in STL based models.

1.5.2 Fabrication Methods

The fabrication method chosen to deliver anatomical models is largely dependent on the investigation of interest. For the purpose of optically based measurement in experimental fluid dynamics, the optical clarity and the accuracy of the model are the most important. When using PIV or PTV methods, the refractive index of the material must match that of the system fluid. This typically necessitates the use of salt solutions to increase the refractive index of the fluid to that of the material used. This limits the materials that can be used to those with a refractive index that can be matched with a salt solution. The accuracy of the fabricated piece is typically regulated by the quality of the CAD model and the material choice (rigid or flexible). The fabrication method used is based on these material and accuracy choices.

Additive manufacturing methods are the simplest form of producing an accurate model. There are limitations with the material type, and the cost of optically clear models can be high [49]. Rigid models have been used by directly using the printed part to represent a variety of geometries [50]. Alternatively, the printed parts can be used as the molds for distensible models applied to fluid structure interaction (FSI) studies [51]. There have also been experiments into directly printing distensible material, removing the need for a mold making step to deliver FSI models [52,53]. Considerations for additive manufacturing methods should include the strength of the desired part, the quality of the printed surfaces, and the optical clarity of the implemented piece.

Subtractive manufacturing has been the primary means of producing parts from CAD models, until the recent accessibility of additive methods. This class of fabrication is typically termed machining, and in the context of producing parts from complex CAD designs, is constrained to CNC implementations of this method. To produce a part with a CNC machine, the geometry of the CAD model forms the basis for cutting paths that are programmed through the use of CAD/CAM software [54]. The capabilities of the machine being used greatly affect the type of part that can be produced; more operating axes enable more complex parts to be generated [55]. This manufacturing method can be used to deliver rigid models destined for direct implementation as investigational pieces, molds for dip-spin techniques [56], and classic pour molds [57]. The advantages of subtractive machining are the ability to utilize a wide range of materials for the investigation (e.g. metals, plastics, composites) and the relatively low cost of material per part.

1.6 Area of Research

As the primary aspect of function in cardiac devices involves mechanical interaction with blood, hydraulic evaluation systems have been implemented as bench top research tools. These systems have been termed mock circulatory loops, as their function provides an in vitro analog to the human circulatory system. The historical examples discussed have been confined to mock circulatory loops utilizing the lumped parameter approach to modeling the systemic and/or total circulatory system. Pulsatile bioreactors, hemolysis testing systems, and other systems tasked with investigation on material reactions will not be presented. Typically, groups that have developed in vitro tools have computational models that represent their systems. The embodiments of these systems and computational models are varied; the focus of the group is typically represented in the design choices made.

1.6.1 Early Work

Hydraulic analogs of the human circulatory system started to be developed once the cardiovascular tissues structure-function relationship was identified. The early works centered mostly on providing rudimentary preload and afterload on hearts being studied by Otto Frank, Ernest Starling, and Dario Maestrini [4,58]. With the technological advancements in engineering and materials science garnered from World War II development, artificial organs concepts became feasible. Federal support of the artificial heart initiative is exemplified by the NIH starting the Artificial Heart Program in 1964, with the objective to have an implanted device serving as an artificial heart within the decade [59]. The emergence of mock circulatory loops, as focused bodies of work, began in the late 1960's when cardiac valve and total artificial heart development began to accelerate [60,61]. Efforts at that time were made to develop lumped

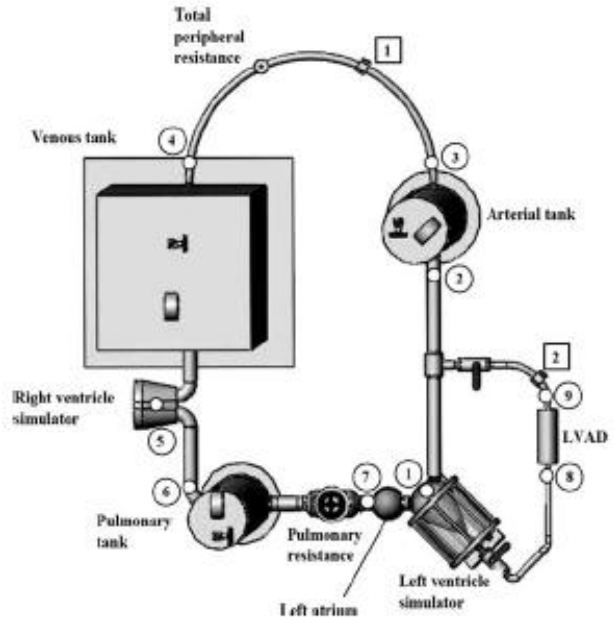

Figure 3: Mock circulatory loop design presented by Liu (2006).

parameter computational models of the human circulation on analog computers to address the need for early stage investigatory tools [62].

1.6.2 Virginia Artificial Heart Institute

Developing a mock circulatory loop for the purpose of evaluating a left ventricular assist device necessitates appropriate design choices for the hardware in order to achieve the performance needed. The work published by the Virginia Artificial Heart Institute provides a well communicated roadmap for researchers tasked with developing a mock circulatory loop [27]. Figure 3 provides an excellent illustration of that system's layout and design. The design exemplifies the dual loop design with the implementation of a systemic venous reservoir.

The ventricles are pneumatically driven sac-type pumps for both the right and left ventricles. These pumps utilize the Utah Heart Controller (Symbion, Inc., Salt Lake City, UT). as the means of pumping actuation and control. This is the same controller that is used for some pneumatically driven total artificial hearts. The right ventricle uses the feed from the venous

reservoir; effectively a constant supply pressure source. The left ventricle has a slightly elastic spherical piece that serves as the left atrium; this assists with the simulation of the left atrial filling effects.

The compliance chambers are fluid column towers with air space headers that allow for the hydraulic system to expand in volume under pressure. The compliance of the system is governed by Boyle's Law; the linear relationship of pressure and volume for an isothermic sealed chamber of gas. Changing the amount of air volume in the compliance chamber at rest affects the compliance of the system; less air space results in a lower compliance and vice versa. The compliance cannot be changed to another known setting in runtime for this system, as the determination of compliance is based on the resting settings.

The resistance in the system is controlled via proportional valves. There is a total peripheral resistor simulating the systemic resistance and a pulmonary resistor. The former is actuated by a tuning clamp and the latter via a gate valve. The difference in design choice for these resistors is not made clear. Literature sources show that these two flow control methods match the respective resistance needs of these different circulations [31]. Both of these devices are manual, and do not have the ability to be changed in runtime.

The venous tank used in the design is quite large; it effectively dampens the return perturbations from the systemic circulation section. The tank is sealed and pressurized slightly to simulate the near atmosphere pressure that exists in the systemic veins. The feed from this tank supplies the right ventricle simulator, and due to its size, allows for a near constant pressure head.

The inclusion of a left ventricular assist device in the system design, with appropriate ventricular and aortic connections, allows for studies on assisted circulation [63]. The

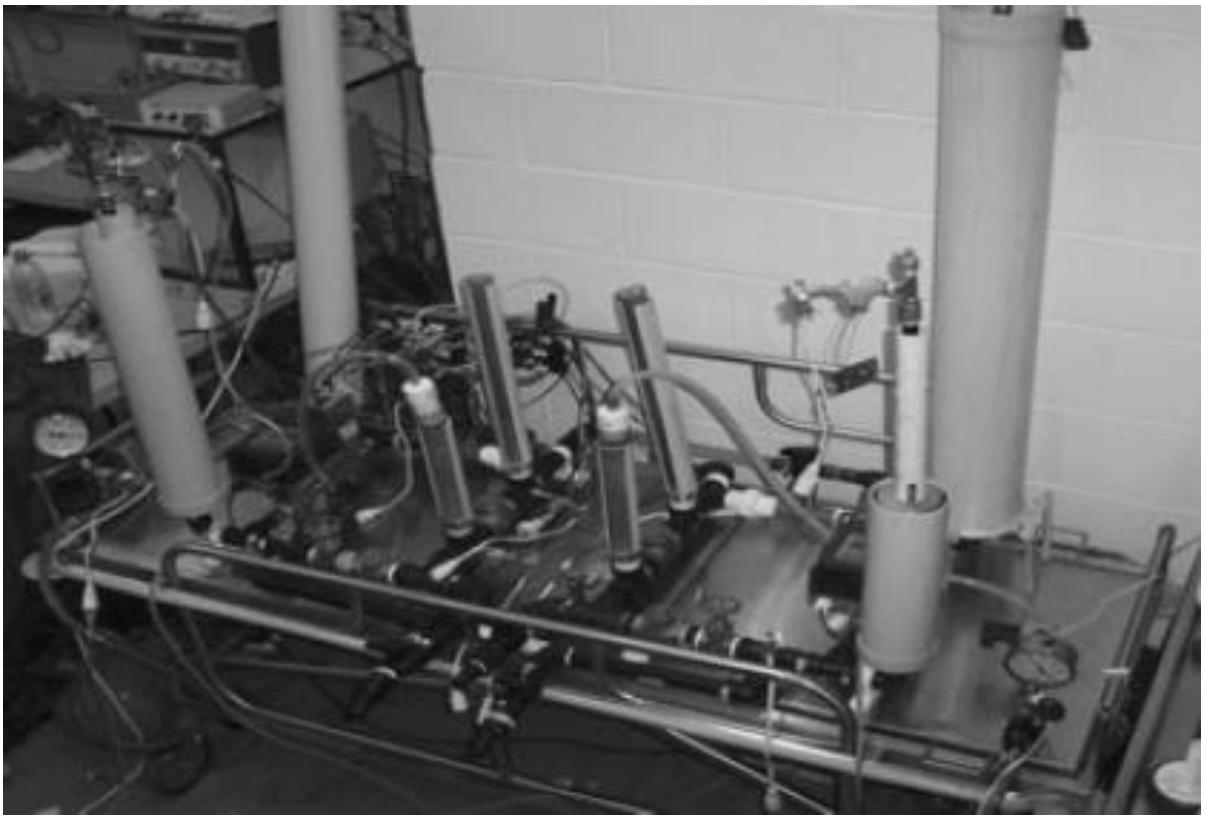

Figure 4: Mock circulatory loop design presented by Timms (2005).

ventricular cannulation is correctly apical and the aortic connection is a 90-degree end to side anastomosis. The length of inlet conduit leading to the pump and the outlet line to the anastomosis are longer than that of an implanted arrangement. However, for a continuous flow assist evaluation, this is an acceptable arrangement.

1.6.3 Queensland University of Technology

The work by the Queensland University of Technology has produced a mock circulatory loop that extensively represents the various compartments of the cardiovascular system (Figure 4). This system has the ability to set a wide range of circulatory parameters; arterial and venous compliance, pulmonary and systemic resistance, left and right atrial preloads, left and right

ventricular contraction. The system has been the subject of numerous publications on its design and functionality [28,64,65].

The ventricles are pneumatically actuated with custom code developed for this application. The ventricles were originally hydraulic chambers. The pneumatic system would control the air space pressure to enacted systole and diastole in the ventricles. There have been studies published by this group where silicone phantoms have been used to represent anatomically shaped ventricles [51]. Pneumatic pressure control was utilized as the means of pumping the silicone phantom.

The compliance chambers were liquid columns with variable resting air space pressure. The control of compliance could only be achieved via stopping the pumping of the loop. However, work was published on a membrane based method of changing compliance [33]. Compliance was changed by modifying the air space pressure, but the new value of the compliance was not determined in runtime. The compliance was not maintained by a controller, and was an open loop control.

Inclusion of ventricular assist device connections supports the investigation of circulatory support devices [66]. With the widely adaptable settings this system provides, robust in vitro assessment of assist pump technology and controllers can be conducted. Numerical modeling efforts have also been pursued to investigate performance enhancements and conditions assessments prior to running them in the mock circulatory loop [67].

1.6.4 University of Louisville, Kentucky

The most widely cited mock circulatory loop is that of the University of Louisville group [68,69]. This loop is a systemic mock circulatory loop that utilizes a four chamber design to evaluate left ventricle and ventricular assist device function (

Figure 5). The published work from this system provides an excellent source of settings and values for mock circulation simulations. The basis for the settings used in the work has been sourced from clinical patient data, the sources of which are well cited. The structure of the components in the loop are based on earlier designs used to develop total artificial hearts [37,70].

The ventricle employed in this design is a distensible phantom of a left ventricle that is driven by a pneumatic system. The ventricle is cannulated at the apex for connection to a left ventricular assist device, and there is a subsequent cannulation in the outflow conduit for the pump outlet. This system uses a pressure-volume catheter to monitor the aortic pressure, ventricular pressure, and the ventricular volume. The volume measurements are inferred from the curvature of the cannula as the walls of the ventricle change the chambers shape. Thus, it is an approximation of the ventricular volume. Upstream of the ventricle is a left atrium; a polyurethane sac that provides the proximal compliance needed during ventricular diastole. The atrium has a catheter that is used to monitor the preload pressure of the ventricle.

There are two compliance chambers in use; one for the systemic arterial compliance and the other for the venous compliance that feeds the left atrium (Figure 6). The compliance chambers in this design are spring loaded pistons. The compliance of the system is changed by adjusting the force generated by the spring; adjust the deformation range of the spring or use a spring with a different constant. The pistons do not use a sliding seal; instead, there is a membrane that is attached to the casing and the piston that they term a "roll sock diaphragm." This gap between the casing and the membrane is wide enough for the membrane to stretch and relax as the piston moves. This design is preferable due to its lack of friction; the breakaway friction of translating seals can cause discontinuities and nonlinearities in the compliance.

Figure 5: Mock circulatory loop design presented by Pantalos (2004).

.

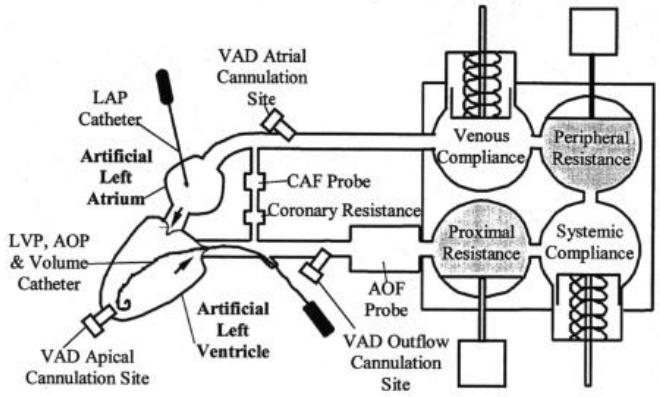

Figure 6: Diagram of the University of Louisville, Kentucky mock circulatory loop.

The resistors are chambers of open cell foam that is compressed by a piston to reduce the pore size and adjust the resistance to flow. There are two resistors in use; a proximal resistor and a peripheral resistor. This use of resistors is due to this groups use of a four element Windkessel model as the design basis for this system. The four element Windkessel model utilized in this design has a parallel resistance and inertia that are in series with the systemic compliance. The proximal resistance will have a much lower value than that of the peripheral resistor, and would have less dense foam in this design.

The system has been utilized as a pump evaluation rig for both hydraulic testing and control assessment [71–73]. With the different cannulation sites for the LVAD, both atrial and ventricular, the ability to assess various configurations is possible. This loop has also been used a clinical training tool for physicians to illustrate function of the circulatory system under

different types of assistance; extracorporeal mechanical oxygenation, left ventricular assist, cardiopulmonary assist, and intra-aortic balloon pump [74].

1.7 Research Objectives

Advanced in vitro methods for left ventricular assist device and prosthetic valve assessments have been identified as catalysts for more successful device designs, resulting in better clinical outcomes [75]. Research groups that have implantable device projects employ mock circulatory loops as their means for evaluation, but mainly rely on traditional designs. Steady state cardiovascular conditions and highly idealized simulation of cardiovascular system function have been the mainstay of device assessment in these traditional systems [76]. Clinical studies have shown that current limitations in quality of life with implanted patients arise from changes in cardiovascular conditions (e.g. postural changes, sudden exertion) [2]. It is necessary to test the emerging technologies against the challenging conditions witnessed in everyday life in order to address these issues.

Translating these physiological conditions into an early stage in vitro environment necessitates a reflective analog of the cardiovascular system. This analog must have the functional capacity to have runtime parameter control, recursiveness, and flow field similarity at the interfaces to the devices being tested. Although the cardiovascular system can be functionally represented in a lumped parameter model, embodied as a mock circulatory loop, the capability of executing changes in the parameters without stopping the system is key for constructing complex events [25]. Additionally, simulating dynamics enables the analysis at a multitude of stationary settings in a battery testing method; this could screen a device against a large set of conditions each representative of a target patient population. The second point of functionality, recursiveness, is integral to the closed loop circulation of the cardiovascular

system. Designing the appropriate system to correctly provide the recursive response can be challenging; it has many dependencies and is highly dynamic. Inclusion of anatomical geometries at interfaces of the mock circulatory loop and the devices being tested is crucial. The accuracy of these local flow fields have been shown to have a strong effect on heart valve function and pump efficiencies [77,78].

Robust in vitro testing has been identified by regulatory agencies, and governing scientific bodies, as integral to the safety assessment of devices in this field [11]. This investigator has identified key software designs and completed hardware developments that satisfy these agency initiatives and provide the requisite testing solution. Experimental condition design tools based on software packages being used for system modeling are readily adaptable to satisfying this proposed work. Use of PhysioBank patient databases as in vitro condition sources connects this work with current clinical efforts, and can only be achieved with updating the current mock circulatory loop technology [79]. Applying Visible Human Project data as the basis for anatomical models continues the effort to utilize pre-existing government databases, which enables the comparative analysis by other researchers [41]. The strategies chosen highlight the value of using currently funded databases and commercial engineering tools to produce high functioning investigational tools and establish design paths for continued development in this field.

Applying these strategies to the development of a new mock circulatory loop model addresses the limitations of presently implemented systems. The restrictions of current models fall primarily in the insufficient automation and anatomical irrelevancy of the systems. Developing a robust experimental system, with supporting computational tools, would advance research in this field through the following:

Illustrate the application of sophisticated physical modeling software in the construction of mock circulatory loop computational models (Aim 1). Computational models have been developed concurrently with mock circulatory loops by other groups [27,65]. However, the precision of these models has not provided the fidelity that is required for constructing precision control systems or design of experiments with dynamic conditions. The construction of a model through a method that is not based on hydraulic first principles (e.g. adaptation of electrical modeling packages) is typically the culprit of poor performance [80]. Physical modeling packages that are built for the systems they are representing (hydraulic, mechanical, etc.) produce exceptional performance in these models [81,82]. The goal of translating the application of these modeling methods into biomedical engineering, specifically the medical device field, has large ramifications in the design efficiency by adopters of these tools.

Application of embedded control techniques to solve current limitations in mock circulatory loop performance (Aim 2). Control of particular mock circulatory loop parameters has not been successfully implemented by other groups in this field. Attempts at controlling arterial compliance with traditional sensors and hardware have not been effective, until implementation of a novel control strategy was deployed by this investigator [33]. Inertial effects within the system are another area of difficulty for many designs, especially when trying to correctly model the cardiovascular recursiveness [68]. The commercial applications utilized in efficiently constructing the embedded control systems and novel hardware has been of particular interest to the in vitro groups of this field.

Free anatomical CAD model development path with low cost fabrication method (Aim 3). Development of anatomical structures for investigations is a resource intensive task;

dataset acquisition, cost of modeling software, and cost of model fabrication [49]. This proposal seeks to illustrate a method for utilizing the Visible Human Project data in the construction of anatomical CAD models through open source software. The fabrication method chosen for these models requires resources typically available to engineering groups; a CNC mill as opposed to stereo lithography (SLA) systems. The basis of this work on a publicly available dataset seeks to cut the cost of model development and homogenize the models used by research groups.

Supplying this field with a robust and accurate testing system enables many of the pressing clinical concerns to be effectively investigated. Advancing the state of preclinical evaluation tools will have a sizeable impact on the investigational quality and technological advancement of the devices developed with this platform. This project not only proposes this completed system, but publication of the workflows applied (Figure 7) in the achievement of this objective may enhance research capabilities in this field through the following:

- **Aim 1:** Modeling process for constructing the plant model of the mock circulatory loop can be extended to device computational models. Ventricular assist device and total artificial heart developers working with multi-domain modeling will greatly benefit from the deliverables of this project. Providing this field with these cutting edge methods accelerates development efforts on other funded projects currently burdened with the computational modeling of these complex systems.
- **Aim 2:** Embedded control systems have an increasing role in device development in this field. Introducing development tools that assist in the translation of complex control architecture onto the target hardware is beneficial to many groups still utilizing manual coding techniques. Implementing code generation tools that were developed for regulated environments addresses future compliance issues with the FDA in this area

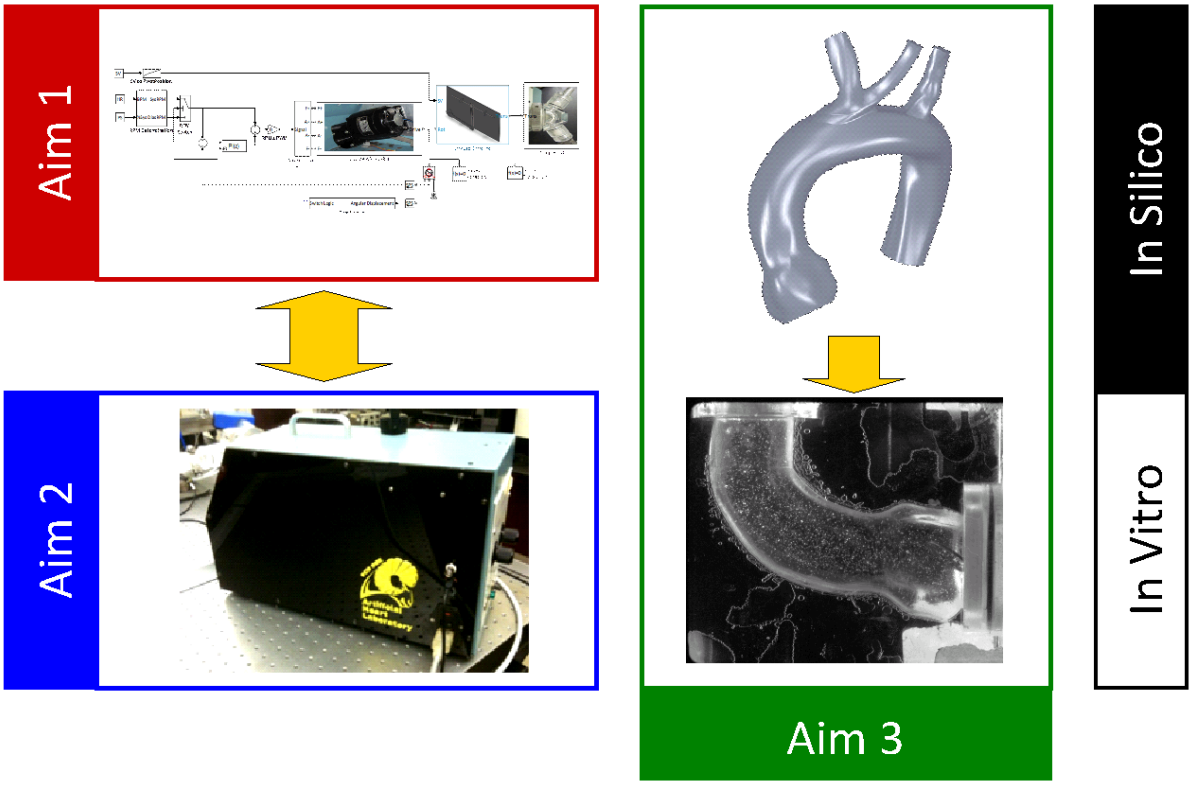

Figure 7: Diagram of the dissertation objectives and how the work is encompassed by the respective aims. In silico work is grouped in the upper half of the illustration, with the in vitro analogues for each presented in the lower half. Computational model work on the subsystems representing the elements of the mock circulatory loop is delivered by Aim 1 (red outline). Fabrication of the hardware and incorporating the subsystems into a mock circulatory loop is presented in Aim 2 (blue outline). The development of the anatomical CAD models and production of the in vitro pieces is presented in Aim 3 (green outline).

[83]. Increasing the code deployment throughput synergizes the research return for the device projects and streamlines the development process.

- **Aim 3:** Anatomical geometry inclusion is crucial to many biomedical engineering projects. The use of cryoslice data in this project and open source software are novel, with a broad spectrum of applications in this field. The promotion of this data source, and software packages, will hopefully enable research that was previously cost prohibitive without these resources.

This proposal promotes the solutions an automated mock circulatory loop will provide, but it also illustrates multiple design tools that have significant implications on applied biomedical research. This modernization of design tools is crucial to successfully implementing high fidelity testing tools and technological development of devices in this field.

The utilization of public datasets for both the anatomical geometry (Visible Human Project) and conditions (PhysioBank) were deliberately chosen so that other researchers could apply the work of this proposal more easily. In following this open source data model, contact has been made with the administrators of both databases to procure resources for data publication. Publishing the simulated event data (in silico and in vitro) in the PhysioBank, delivers on one of the missions of this database being a repository for cardiovascular conditions data. Submission of the anatomical CAD files to the Visible Human Project seeks to establish a forum in this database for geometries that are based on the imaging data. These data sharing initiatives are crucial to this investigators vision of common data sources in this field and higher utilization of previously funded repositories.

The deployment of the automated mock circulatory loop, with inclusion of the anatomical sections, is crucial to the advancement of this platform as a modern approach to circulatory device assessment. The broader implication of this work lies in the methods and data sources employed. Accelerating development with these approaches has the ability to impact a wide range of research. Enabling this research base with these cutting edge methods has the potential to increase the momentum in other funded projects and accelerate progress towards the public health solutions they are pursuing.

1.7.1 Specific Aims

This project proposes a high performance mock circulatory loop, inclusive of correct anatomical geometries, and accompanying computational tools for state of the art solutions to cardiac device assessment. A combination of novel hardware and application of industrial software solutions will be used to produce a system with a level of functionality that is currently not available in the field, allowing for previously unachievable simulations to be performed through the following aims:

Aim 1: Develop computational plant model of the mock circulatory loop inclusive of process control logic

Challenge: Develop an in silico physical system model that is capable of accurately simulating an analogous in vitro platform; it must also include the monitoring algorithms and control logic governing the actuators.

Approach: Utilize commercially available physical modeling tools to rapidly develop the computational models. Parameter estimation functions and control design tools will be used to tune the model components to experimental performance data and develop the appropriate controller methods, respectively.

Impact: Utilization of industrial engineering tools in developing these computational resources, and executing the control design, illustrates an application of this software technique not widely applied in this field.

Aim 2: Deploy a fully automated mock circulatory loop

Challenge: Fabricate an in vitro embodiment of the computational model that represents the performance bandwidth and control acuity seen in silico.

Approach: Construct the following subsystems of the mock circulatory loop: ventricular simulator, arterial compliance chamber, peripheral resistor, and pulmonary simulator. Utilize commercial code translation products to deploy the computational control elements onto the embedded control systems hardware.

Impact: This system will provide a robust testing platform with functionality that is currently not available in this field; nonlinear arterial compliance and change of all controlled set points in runtime.

Aim 3: Critical anatomical geometries; left atrium and ascending aortic root.

Challenge: Develop anatomical geometry models of the left atrium and the ascending aortic root, which need to be based off a publicly available patent data set.

Approach: Extract the geometry from the Visible Human Project, process the results into a model capable of fabrication.

Impact: Inclusion of these anatomically correct sections develops the local flow field characteristics that have been shown to have significant impact on device performance.

This integrated multi scale research tool approach provides an investigator with the (a) in silico tools that allow for effective experimental design, (b) in vitro performance that enables a wide range of cardiovascular parameters to be simulated, and (c) accurate local flow conditions in the regions of the devices being evaluated. These deliverables provide the functionality that has been in increasing demand as the need for experimental acuity has risen.

2 Methods

The workflows that were executed to achieve this project's objectives crossed many development environments and utilized a wide range of tools. Brief introductions to the key software packages will be made, followed by detailed design paths for the individual subsystems, and overviews of the software programs that were designed to assist the experimental execution of the studies with this mock circulatory loop.

2.1 Development Tools

The principle success of creating accurate computational models that drove the control design responsible for the performance of the mock circulatory loop rests on MathWorks software tools and the embedded code implementation. Only brief discussions will be made on these products, as the support for true application of these tools is best sourced from MathWorks. This section seeks to inform the readership of the options available, and to communicate the high return on investment by using these tools.

2.1.1 Simulink Simscape

The goal to develop accurate computational models was reached with the Simscape® (The MathWorks, Natick, MA) block set for Simulink™ (The MathWorks, Natick, MA). The Simscape® blocks allow the modeling of physical systems with computational components based on physical parts used in these assemblies, with tunable parameters relating to values typically available in data sheets for these parts [84]. Figure 8 illustrates the relation of the physical component, the Simscape block, and the block parameters that characterize the physical component. The blocks utilized in the computational models were taken from the hydraulics foundation library for Simscape®, the mechanical foundation library for Simscape®, and the SimHydraulics® (The MathWorks, Natick, MA) toolbox.

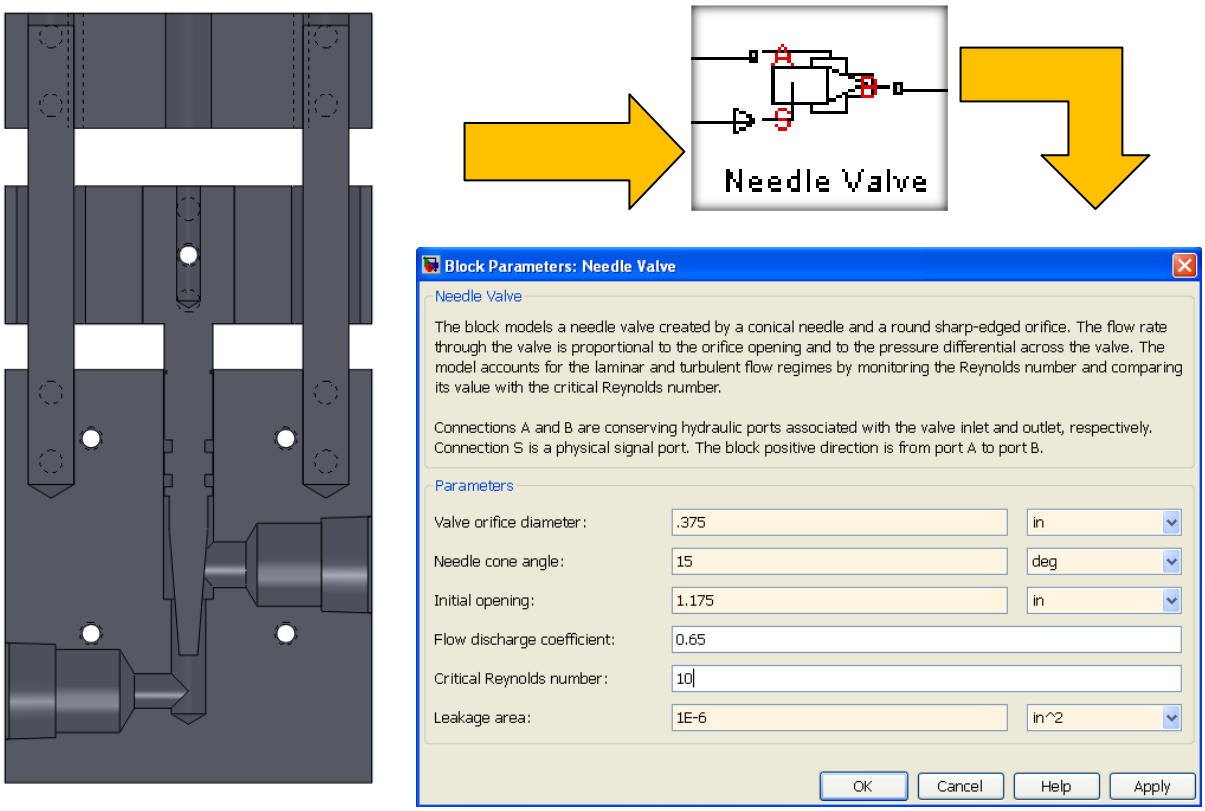

Figure 8: Illustration of Simscape physical model tools; CAD drawing of physical assembly, Simscape physical modeling block, and parameter dialogue box for Simscape block. Description of block connections is presented in the dialogue box.

The advantage of this method is the specificity of the model elements to the physical components that are being modeled. This is a departure from previous methods, such as the use of electrical elements, to represent physical components in computational models [63,85]. The items that are available in the Simscape® toolboxes limit the number of assumptions needed for simpler modeling methods, and they supplant the need for the inordinate amount of programming otherwise required to achieve higher fidelity representation of complex elements. The establishment of a Simulink™ model furnishes the control designer with the availability of the numerous libraries associated with Simulink™ and Matlab® (The MathWorks, Natick, MA).

2.1.2 Parameter Estimation

If a device is custom, and lacks the data sheet reference for parameters required in the corresponding computational block, a Parameter Estimation™ task can be performed to identify possible values. This estimation requires an experimental dataset to tune the computational model parameters; minimal error between the model simulation and experimental data occurs with parameters that correctly describe the components of the model [86,87]. This estimation process necessitates the use of Simulink™ Design Optimization™ (The MathWorks, Natick, MA), Simulink™ Control Design™ (The MathWorks, Natick, MA), Matlab Control System Toolbox™ (The MathWorks, Natick, MA) and Matlab® Optimization Toolbox™ (The MathWorks, Natick, MA). The physical configuration should reflect the Simulink™ model as closely as possible, especially with respect to sensor placement. The fidelity of the reflection of the physical system in the computational model correlates to the accuracy of the determined parameters.

2.1.3 Process Controller Design

Deploying stable and well performing process controllers has become increasingly easy with the advent of physical modeling and tuning software. Developing a control architecture, tuning the process controllers to a plant model, and verifying the performance used to be time intensive tasks [88]. Using the aforementioned physical models of the plants generated using the Simscape toolboxes and fine tuning the model values using Parameter Estimation produces a high fidelity model against which an accurate process controller can be developed. The use of Simulink Control Design and Design Optimization toolboxes allows a user to insert a PID controller into the model and design the controller through a series of user interfaces. This

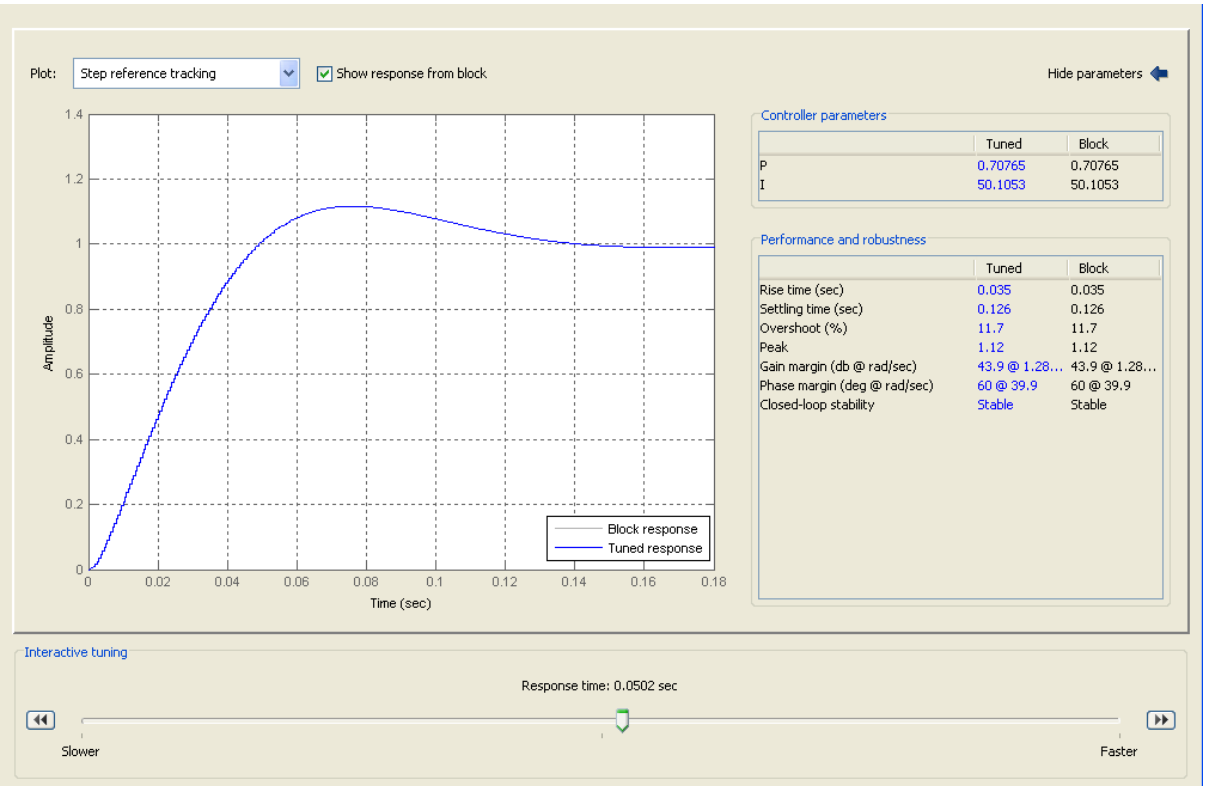

Figure 9: Simulink Control Design tool for tuning a PID controller. The plot can be set to a variety of time response plots, Nichols plot or Bode plot. Metrics for the controller are presented in the right pane and the user selectable response time slider is at the bottom of the user interface.

workflow enables users that may not have the expertise of process control design, but need a control architecture in their model.

The process begins by inserting a PID controller into the model, connecting the signal error (set point minus actual value), and connecting the controller output to the actuator port of the system. Double clicking on the icon opens an interface that allows the architecture and features of the controller to be selected; discrete versus continuous, saturation conditions, etc. Once the controller architecture has been selected, there is a tune button that initiates the tuning of the controller to the plant that it is attached to.

The first step of the tuning is the linearization of the plant. The controller will linearize the plant at its initial conditions. If this is not the point of linearization that is desired, there are

options for circumventing this action. The plant can be linearized at a particular time point in the simulation of the model or a linearization can be imported from other MathWorks tools. Once the plant model has been processed, and the controller values computed, the user interface in Figure 9 is presented. Here the user can make the appropriate selections that best fit the application of the controller.

The tuning of the controllers in the scope of this project was conducted with two objectives in mind; appropriate time response and stability. Time response for many of the systems was simply chosen by selecting a time response on the slider that was not near the instability limit. Subsequent simulation of the entire model would confirm if the response was appropriate. If it was not, then a faster response was chosen. If the controller was unstable in the simulation, possibly due to the operating point used for linearization being near a nonlinear region of the plant, then a longer response time was selected. Minimizing the oscillations of the controllers was important; overshoot was minimized as well as settling time.

2.1.4 Controller code architecture

The microcontrollers code that was developed for this project was designed specifically for this application. The code was tasked with three objectives; precise process control of the subsystem, communication with a host conductor that was coordinating the subsystems, and the ability to maintain safe subsystem operation in the event communications failed. A template controller code architecture was developed, with the specific functionality of the target system populated into the template sections.

The code was developed in the MPLAB IDE using the student C compiler provided by Microchip. Code was originally developed manually for the controller sections, by transcribing the values obtained in the Simulink Control Design tools to a controller code segment. When

training had been received on Simulink Embedded Coder, the controllers that were developed in Simulink could have their C code equivalent code generated. These code sections were then imported into the MPLAB IDE environment as source and header files to be included in the project for that particular controller. Simulink Embedded Coder has the capability to deploy code directly from the MathWorks environment to the target hardware. The choice of the PIC18 architecture for the microcontrollers prevented using the MathWorks supplied software tools, and no custom alternative could be successfully implemented.

Appendix A is provided as a reference for the microcontroller construction and programming tasks completed during this project. It contains illustrations of the code architecture and the Eagle diagrams of the circuits.

2.2 System Design

The bulk of this project was spent developing the subsystems and delivering high performance components that could deliver the operating bandwidth needed. Many design choices and considerations were made during the development process. Communicating the research leading to the implementation of these products is crucial to understanding the capabilities inherent in the final system.

2.2.1 Peripheral Resistor

The resistor design is comprised of a flow path passing through a block with a piston mounted perpendicular to the flow path that provides resistance to flow through occlusion. There are four main mechanical elements of the design; the block, piston, frame, and linear actuator. The electrical system is comprised of the linear actuator driver board and a linear potentiometer used for operational limit control. The software controlling the system is a Virtual Instrument (VI) programmed in LabVIEW (National Instruments Corporation, Austin, TX).

The piston design allowed for simplicity of actuation and fabrication, as well as a design that would be relatively simple to model numerically. The resistor block is aluminum with a 2.301cm bore through the block for the flow path; this dimension was dictated by the tap drill size for the ¾-14 NPT female threading on each end of the block. The piston chamber is a cylindrical bore that is 3.823cm in diameter and perpendicular to the flow path. The bore extends past the lower edge of the flow path to allow for complete occlusion by the piston. The frame for the linear actuator serves the purposes of a guide to prevent the rotation of the piston during actuation, and a mounting point for the linear potentiometer.

The motion of the piston is delivered by a commercially available linear actuator. The actuator was chosen for its high force capability as this is integral to actuating a piston with o-rings against a pressurized flow. The driver board for this motor was selected for its RS-232 communication interface, ability to execute absolute position commands, and capability of providing positional feedback during movement. Additional capabilities of the driver board are: acceleration manipulation, holding torque adjustment, and motion limits derived from a linear potentiometer. These settings are programmed through a RS-232 communication link, and can be manipulated for desired speed or force performance. The effects of these settings were not investigated in this particular testing cycle. The end speed and acceleration settings were programmed low to allow for a greater generation of force, and reduced the possibility of missed motor steps. The latter would contribute to lower precision in movement and reduced accuracy in the control of orifice size.

The use of motor steps in positioning was complemented with the use of a linear potentiometer to prevent movement out of the limits of operation. A single motor step was found to have an equivalent linear actuator movement of 25μm. The movement of the linear

actuator is checked by the motor driver board against the potentiometer readings. The potentiometer values for the operational limits can be changed via the serial interface to the control board, which was seen as preferable to contact limit switches.

Characterizing a valve's performance is important in constructing a computational model for the device. The primary means of describing a proportional valve are in terms of orifice size at particular settings, coefficient of discharge, and critical Reynolds number for flow within the valve [89,90]. These parameters provide for an objective description of the valve's performance, and should be derived from experimental data.

Determining the geometrical flow path profile at various valve settings allows for the calculation of a hydraulic diameter at those settings. This calculation is presented in various hydraulic textbooks, and is typically employed for multi-orifice valves [89]. The equation provides the area of the orifice that is perpendicular to the flow. An effective hydraulic diameter is constructed by normalizing the orifice area to that of the perimeter. Equation 1 and Equation 2 are presented to determine orifice area.

Equation 1

$$A = \left(\frac{\theta}{\pi} - \frac{\sin(2\theta)}{2\pi}\right)\left(\pi\left(\frac{D}{2}\right)^2\right)$$

$$D = Diameter\ of\ flowpath$$

Equation 2

$$\theta = \cos^{-1}\left(1 - 2\frac{h}{D}\right)$$

$$h = Distance\ of\ piston\ from\ bottom\ of\ flowpath$$

The coefficient of discharge is a correction coefficient that links the experimental results and the ideal computed performance (Equation 3). This correction is provided by constructing an experimental setup that allows for isolation of the valve's performance in terms of pressure

differential across the valve for a particular flow rate at a particular orifice size [90]. Connecting this data with the ideal calculations, a discrepancy is typically observed. This error is proportional to the flow rate, which provides that the discharge coefficient is a scaling factor and not an offset [89]. Equation 3 represents the general valve flow rate determination [89,90].

Equation 3

$$\dot{Q} = C_D A \sqrt{\frac{2(P_1 - P_2)^n}{\rho}}$$

$$P_1 = Upstream\ \ [of\ valve]\ pressure$$

$$P_2 = Downstream\ pressure$$

$$\rho = Density$$

$$A = Area\ of\ orifice$$

$$C_D = Discharge\ coefficeint$$

$$\dot{Q} = Flow\ rate\ through$$

$$n = 1\ for\ laminar\ flow$$

$$n = 0.5\ for\ turbulent\ flow$$

The critical Reynolds number for a valve is dependent on the geometry of the orifice and the flow rates involved. The geometry considerations can be derived from the hydraulic diameter. Values for certain orifice shapes can be taken from tabulated sections found in hydraulics literature [90]. This critical value provides whether laminar or turbulent equations should be employed for a particular flow rate through the valve. The Reynolds number for the flow through the valve is determined by Equation 4 and Equation 5 [89].

Equation 4

$$Re_{valve} = \frac{U_{avg} D_{hyd}}{v}$$

$$U_{avg} = Average\ fluid\ velcocity\ through\ orifice$$

$$v = kinematic\ viscosity$$

Equation 5

$$D_{hyd} = D\frac{[2\theta - \sin(2\theta)]}{[2\theta + \sin(2\theta)]}$$

Determination of the orifice size is integral to the modeling and control of the resistance device. The orifice size is determined by the area in a plane perpendicular to the axis of flow that the fluid is able to flow through [89,91]. The orifice area is provided by the integration of the area in the circle defining the flow path (Equation 1) from the base of the flow path to the lower edge of the plunger. The diametrical difference between the bore of the block and the piston is 0.127mm; this gap is assumed to be negligible in the orifice area consideration.

The position of the piston is provided by initialization to a particular distance in reference to the frame of the device, and tracking of the absolute position reported as motor steps by the control board. With the dimensions of the piston and the block from the CAD model of the device, it was possible to identify the corresponding piston position in the flow path from an initial position. This initialization position was set as 3.35cm from the top of the resistor guide to the top edge of the frame element on which the motor is mounted. Distance per motor step is given in the data sheet for the linear actuator; it was verified by measurement of the piston top to the frame over a range of positions with digital calipers. With the integration of position read back and orifice size, the determination of orifice size at any time during the simulation is possible.

In characterizing the performance of the resistor, it was important to isolate its function as much as possible. The circulation system that was constructed to evaluate the resistor is a permutation of a mock circulatory loop currently deployed. The mock circulatory loop used in this analysis is consistent with mock circulatory loops utilized in this field [27,28]. The segment of the loop containing the resistor is consistent with the design outlined in ANSI/ISA-S75.02-

1988, which is a method utilized for identifying the parameters of a valve this experiment sought to determine [90]. One deviation from the ISA standard was the placement of the flow sensor downstream of the valve; this was consistent with The MathWorks method for valve characterization and was seen as an acceptable change [92].

The following changes were made to the existing system to assist in the isolation of the resistor function from other components and simplify the function of the loop to increase fidelity in the computational model. The pumping mechanism was a Flotec R2B1-1100V (Flotec Corporation, Delavan, WA) continuous flow pump; the ISA standard specifies a continuous flow source. The two throttling valves specified in the ISA method are indicated in Figure 4. The upstream valve serves as a flow regulator and the downstream provides a higher downstream pressure for the analysis.

The connections between the components of the loop are made by Tygon® (Saint-Gobain SA, Courbevoie, France) tubing and acrylic piping. The Tygon® tubing is 1.905cm (0.75 in) ID and 3.175cm (1.25in) OD; distention under the pressures investigated (<34 kPa) is negligible in the analysis. The choice of these dimensions was to prevent nonlinearities caused by compliance of the tubing. The piping and fittings that comprise the remainder of the conduits between the devices are all within the range of 1.778cm ID and 1.905cm ID.

Viscosity measurements of the solution were made using a Cannon-Fenske Calibrated Viscometer (Cannon Instrument Company, State College, PA) of size 75 [93]. The density of the system fluid was determined by weighing a known volume of the fluid on a Mettler-Toledo scale [94]. 4 liters of system volume fluid was prepared; the system has a minimum capacity of 2.85 liters and a maximum of 4.5 liters. The fluid was pumped through the loop for 15 minutes prior to physical property determination to ensure that it was adequately mixed and degassed.

Pressure and flow measurements were taken from imbedded sensors in the loop (Figure 4). The flow measurement was taken with a H20-XL (Transonic Systems Corporation, Ithaca, NY) sensor placed downstream of the resistor. The analyzer for the flow sensor was a T110 (Transonic Systems Corporation, Ithaca, NY) unit with an analog voltage output. The pressure transducer models utilized were Entran EPX-V01-5P's (Measurement Specialties Corporation, Hampton, VA) with an excitation voltage from an Agilent 3630A (Agilent Technologies Corporation, Santa Clara, CA) power supply. Amplification of these transducers was achieved through custom amplification boards. Each sensor is calibrated at every system start to an Omega PX202-15G5V (Omega Corporation, Stamford, CT) transducer being amplified by an Omega DP25-S (Omega Corporation, Stamford, CT).

The measurements of pressure, flow, and piston position were received by a LabView VI. The pressure and flow measurements were converted with a NI-6025E (National Instruments Corporation, Austin, TX) data acquisition board interfaced with a NI-SCB-68 (National Instruments Corporation, Austin, TX) connector block. The respective voltage inputs were interpreted to physical units using DAQmx scales. The pressure transducers were calibrated using the LabVIEW DAQ Assistant, which provides calibration report generation to allow for traceability. The position read back and control of the linear actuator was achieved through a custom serial communication driver developed for the motor driver board using LabVIEW. The pressure and flow measurements were taken at 512Hz, while position read backs from the linear actuator were taken at 16Hz. The lower data rate for position read back is due to the data rate limit of 9600 bps for the motor driver board. These data streams were written to an experimental log file, and were analyzed using Matlab® and Simulink™.

2.2.2 Compliance Chamber

The compliance chamber is a cylindrical chamber with a hydraulic and a pneumatic compartment divided by a transverse circular membrane (Figure 10). This design allows for forces to be transmitted through the membrane while maintaining separate liquid and air environments. The only distensible boundary in the hydraulic system is at the membrane, which ensures the volumetric expansion in the entire mock circulatory loop occurs only at this surface and therefore allows the compliance in this chamber to be that of the entire mock circulatory loop. The past control of pneumatic compliance chambers has involved stopping the circulation of the mock loop to change the header air pressure, or changing the air pressure during operation and inferring the compliance from pressure waveforms [33,95]. In this system, a laser displacement sensor monitors the center displacement of the membrane through a window into the pneumatic chamber. By controlling the expansion of the membrane from pressure developed in the hydraulic compartment, the compliance enacted by this device can be accurately controlled. The hydraulic compartment of the device has an inlet and an outlet radially oriented to produce a transverse flow path through the chamber. The inlet and outlet are 3/4" ID acrylic pipe conduits with sharp edged circular orifices into the hydraulic compartment. The inner diameter of the cylinder is 5.75" and the height from the base of the hydraulic compartment to the membrane is 2.75". The inlet and outlet conduit centerlines are 1.5" from the bottom of the compartment. This geometry allows for the incoming and exiting flow to have minimal effects from surrounding walls. A bleed port was installed near the membrane interface to allow for air to be released from this compartment when a membrane is installed. During installation, the membrane is pressurized such that it distends into the hydraulic compartment. This causes any

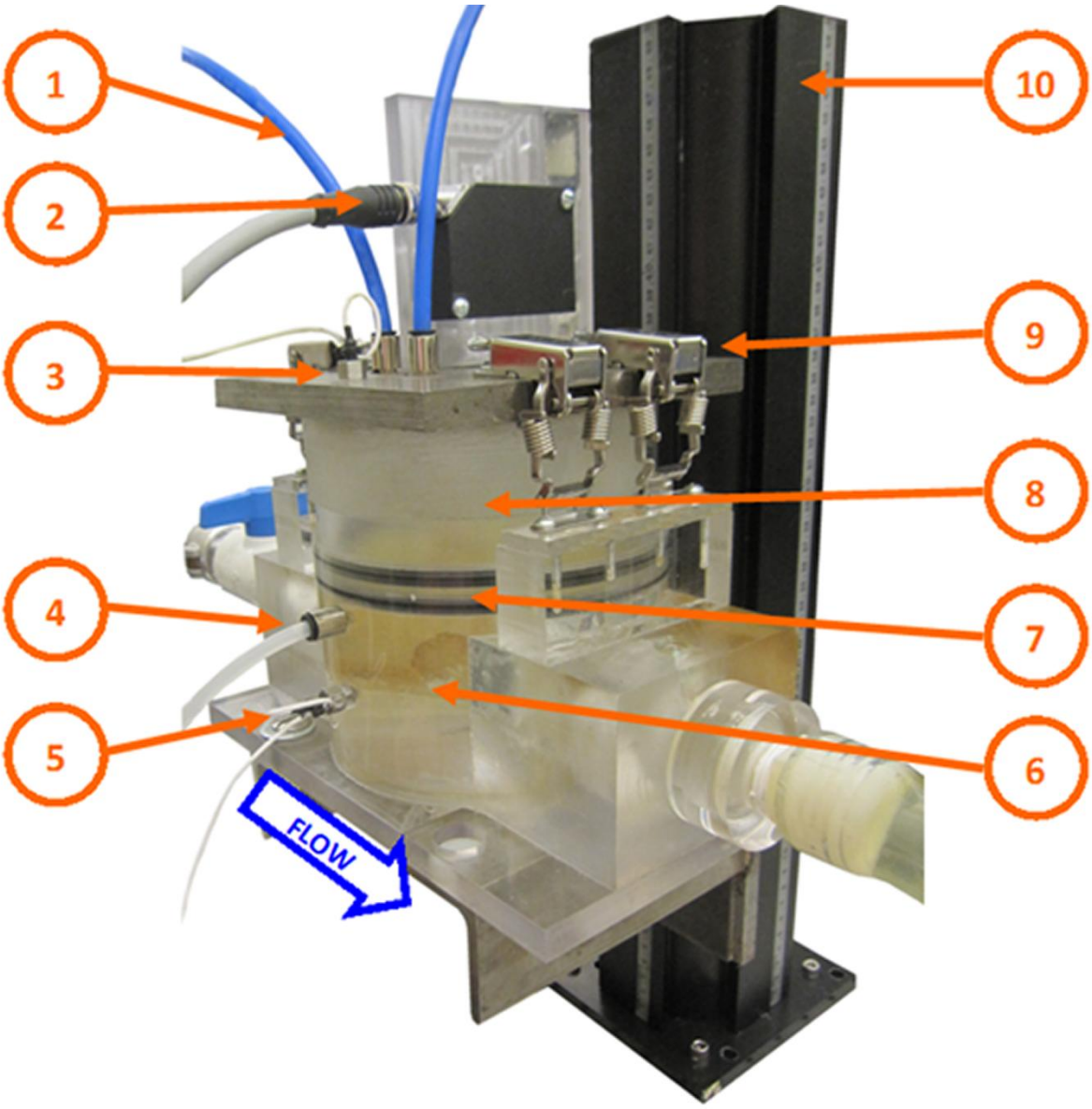

Figure 10: The compliance chamber design illustrating the various components utilized; pneumatic lines respectively connected to the pressure regulation block and the emergency pressure relief valve (1), laser displacement sensor monitoring the membrane center deflection (2), pneumatic pressure sensor (3), air bleed line (4), hydraulic pressure sensor (5), hydraulic chamber (6), membrane cartridge between two black o-rings (7), air chamber (8), clamps used to create a hermetic seal between the compartments(9), and the mounting rail for the assembly (10). The blue arrow indicates the direction of flow through the chamber. Not shown are the pneumatic pressure regulation block and the amplifier boards for the pressure sensors.

air to aggregate at the edge of the chamber. The bleed valve is opened to allow the air to escape and is closed when the hydraulic chamber has been purged of air. The air chamber is bled to allow the membrane to revert to its operational state, distended into the air chamber.

The membrane is comprised of natural latex rubber with a thickness of 0.006" and a Young's Modulus of 130 PSI. This highly elastic material is ideal for this cyclic loading application, and will not have a large force contribution range of strain during use [96]. This lack of force development for the range of distention provides that the pneumatic control over the compliance will be more exacting without having to account for the membrane contributions. The latex material is adhered to an acrylic ring under a no load state, creating a cartridge to be inserted into the compliance chamber (Figure 11). These cartridges prevent the membrane from having to be stretched when installed and provide an efficient means of replacing membranes. The cylindrical housing of the hydraulic compartment has a pedestal cut on the inner surface that holds the rubber gaskets and membrane cartridge.

The mechanical behavior of the membrane at the interface of the hydraulic system and pneumatic system in this design is a classic deformable material problem. The expansion of a clamped circular plate with large deflections is a problem that has been analytically proven, which allows for an accurate numerical model to be developed in this application [97]. The plate in this application is 0.006" thick, has a radius of 2.375”, and will have deflections up to 2.000"; thus, only membrane stresses should be considered in the problem statement [98]. The bending moment forces can be neglected due to the small cross-sectional area of the membrane, and the highly elastic properties of the natural latex rubber used in the design. The elastic nature of the material chosen for this design provides that even with the large deflections, the material should not undergo plastic deformation. The numerical model for this solution includes deflection in

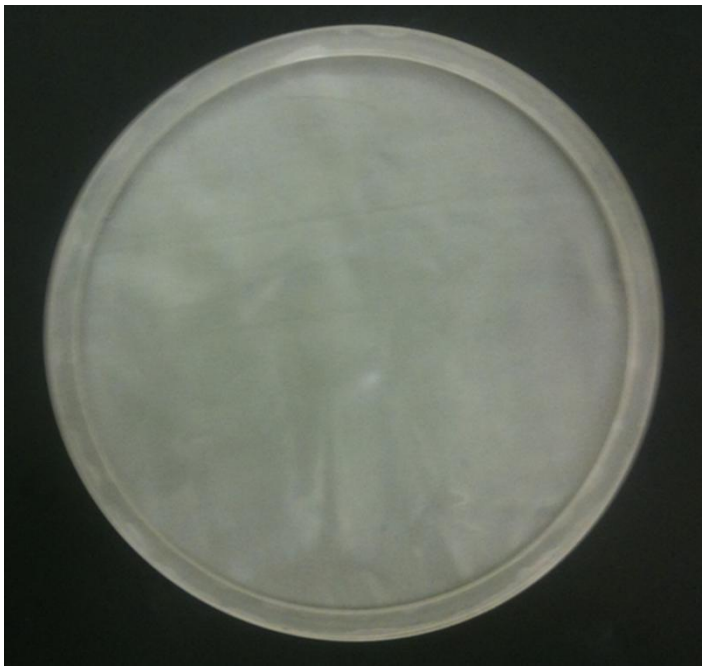

Figure 11: Membrane cartridge developed for the compliance chamber. The latex sheet is adhered to acrylic rings and cut to size. These cartridges allow for ease of replacement in the membranes, tracking of membrane use to ensure they are replaced after appropriate durations of use and prevention of pre-stretch during installation into the compliance chamber.

the longitudinal and radial directions due to the large deformations of the plate. Axial symmetry and the assumption of material continuity maintain that the circumferential deflections are zero.

The method used to develop the numerical model for this membrane was a strain energy equation [97]. A strain energy method defines a summated global potential energy (scalar) in a structure at particular deformations. A minimum in strain energy is reached at a steady state of loading from a force balance of the stress in the structure. This minimum is dependent on the material properties and geometry of the structure. The potential strain energy for a clamped circular membrane is defined by the following equation with the variable definitions in Table 4:

Equation 6

$$U_m = \frac{\pi E t}{1-\gamma^2}\int_0^a \left[\left(\frac{du}{dr}\right)^2 + \frac{du}{dr}\left(\frac{dw}{dr}\right) + \frac{u^2}{r} + \frac{2\gamma u}{r}\frac{du}{dr} + \frac{\gamma u}{r}\left(\frac{dw}{dr}\right)^2 + \frac{1}{4}\left(\frac{dw}{dr}\right)^4\right] r\,dr$$

Table 4: Definitions of circular membrane distension variables.

Variable	Definition
U_m	Total membrane strain energy
E	Young's Modulus of the membrane material
t	Thickness of the membrane
γ	Poissons ratio
a	Radius of membrane
u	Radial displacement
r	Radius
w	Vertical displacement
w_{max}	Largest vertical displacement
c_1	Coefficient for radial displacement
c_2	Coefficient for radial displacement

The axial and radial displacements are respectively defined by the following two equations (see Table 4 for variable definitions):

Equation 7

$$w(r) = w_{max}\left(1 - \frac{r^2}{a^2}\right)^2$$

Equation 8

$$u(r) = r(a - r)(c_1 + c_2 r)$$

The coefficients of the radial displacement (c_1, c_2) are determined from a minimization of the potential strain energy equation for a particular radius of the circular plate and Poisson's ratio of the material. The Young's modulus is a global scalar to the potential energy minima, and has no regional effects in the strain field as it is not in the integral. If the w_{max} is known, the displacement profile of the membrane can be determined. From axial symmetry, the revolved profile can be integrated to determine a volume displacement of the circular plate. This provides the w_{max} to volume distention relationship needed to implement a w_{max}-to-volume conversion method for use in the calculation of instantaneous system compliance.

The pneumatic chamber is comprised of a cylinder that has been machined to insert into the hydraulic counterpart. The housing of the pneumatic chamber is compressed downward via

spring loaded clamps on the side of the assembly. With the upper and lower gaskets on the membrane cartridge, both the hydraulic and pneumatic chambers are hermetically sealed. The pneumatic chamber has two ports on the cap to the cylinder; one interface to the pneumatic proportional valve controlling the pressure and another to a safety valve that is set to release at 7PSI to prevent overpressure. The measurement limit of the pressure sensors in the mock circulatory loop is 5PSI, which governs the safety pressure limit for the pneumatic system.

The laser displacement sensor is mounted on the cylinder cap, with a clear acrylic window to allow its monitoring of the membrane center displacement. The device chosen was a Micro-Epsilon (Raleigh, NC) OptoNCDT 1402-50. The displacement sensor has a range +/-60 micron measurement accuracy in a measurement range of 50-95mm. This equates to a sub-milliliter accuracy determination in the volume distention of the membrane, and is capable of 1.5 KHz sampling rates. Equation 6 through Equation 8 provide the center deflection distance to volume relationship through revolute integration of the deformed profile. This relationship is verified periodically through a calibration of volume distention by closing the upstream and downstream hydraulic ball valves to the compliance chamber and injecting known volumes of system fluid into the chamber via the air bleed line. This calibration accounts for any strain irregularities in the material that may have been present during the fabrication of the cartridges and provides a suitability check of the membrane to indicate if a replacement is needed.

The pneumatic valve utilized in this design is a voice coil actuator (VCA) based LS-V15s (Enfield® Technologies, Trumbull, CT) 5/3 bi-directional proportional valve with a normally closed center. The valve is being driven by a LS-C27 (Enfield® Technologies, Trumbull, CT) pulse-width modulation based electronics board with an integrated closed loop current control. This pneumatic assembly is capable of 2.5 ms shifting time and high flow rate, which are both

crucial to the response necessitated by this application. With the controller operating at 500 Hz, a fast valve response is necessary for acute control of the membrane deflection. The inlet has a source pressure of 25PSI and the outlet is connected to atmosphere. Thus, the high flow rating would provide the flow capacity for the chamber's vent to atmosphere. Previous work with solenoid proportional valves did not provide the flow rate and fast response time at the low differential pressures existing in this system. VCA based valves do not rely on the differential pressure across the valve spool to supplement the force needed for actuation, and can generate force rapidly. These characteristics provide VCA based valves with the fast switching times and pressure independent operation, which were both desirable in this application.

Pressure sensors are mounted on the cylindrical wall of the hydraulic compartment and the top of the pneumatic compartment. The hydraulic compartment sensor is used for the control of the compliance, and is the measurement point for the fluid pressure used by the process controller. The pneumatic pressure sensor is used as a process monitoring point, and is not used in the control algorithm of the airspace pressure. The pressure transducer models utilized were Entran EPX-V01-5P's (Measurement Specialties Corporation, Hampton, VA), with amplification of these transducers achieved through custom amplification boards. Each sensor is calibrated at every system start to a PX202-15G5V (Omega® Corporation, Stamford, CT) transducer being amplified by a DP25-S (Omega® Corporation, Stamford, CT). The data acquisition of the pressure and displacement data was performed with a National Instruments™ Corporation (Austin, TX) PCI-6024E DAQ card, which is capable of 16-bit analog to digital (A/D) conversion and 200 KS/s. The sampling rate used to log the experimental data is 512 Hz. LabVIEW (National Instruments™ Corp., Austin, TX) was used to construct an interface to the compliance chamber controller and log the experimental data.

2.2.3 Harvard Pump

The Harvard Apparatus (Holliston, MA) pulsatile blood pump (model 1423) is a piston pump capable of single ventricle simulation in cardiovascular research. This model is capable of reproducing left ventricular output similar to humans, and provides manipulation of specific pumping parameters. The positive displacement design and integration of check valves in the pump head creates a close approximation to the left ventricle pumping mechanism. The ability to independently manipulate the heart rate, stroke volume and percent systole positions this design as a favorable means of constructing flow conditions within a mock circulatory loop. This products established usage in ventricular simulations was a deciding factor in the choice to include this pump in the mock circulatory loop being developed by this laboratory [99–101]. It has been proven through these previous works to be a suitable reference standard for a pulsatile pump source in the course of evaluating cardiac assist technologies.

The design developed by Harvard Apparatus involves the use of manual controls mounted on the case of the pump to control the performance parameters (Figure 12). This design requires the operator to manually adjust each parameter at the pump, with no ability for remote operation (Table 5). The heart rate and percent systole settings are assumed to be the operating conditions of the device, after the appropriate correction factors are applied from the manual [102]. There is no ability to obtain confirmation and performance read back from the device.

The supplied control mechanisms for the heart rate and percent systole are potentiometers which are interfaced to the electrical board controlling the motor that actuates the hydraulic piston. The generalized electrical schematic that applies to the model 1423 pump is identical to that of the model 665 Intermediate Ventilator produced by Harvard Apparatus; this schematic is presented in the ventilators user's manual [103]. What is presented in this ventilator schematic is

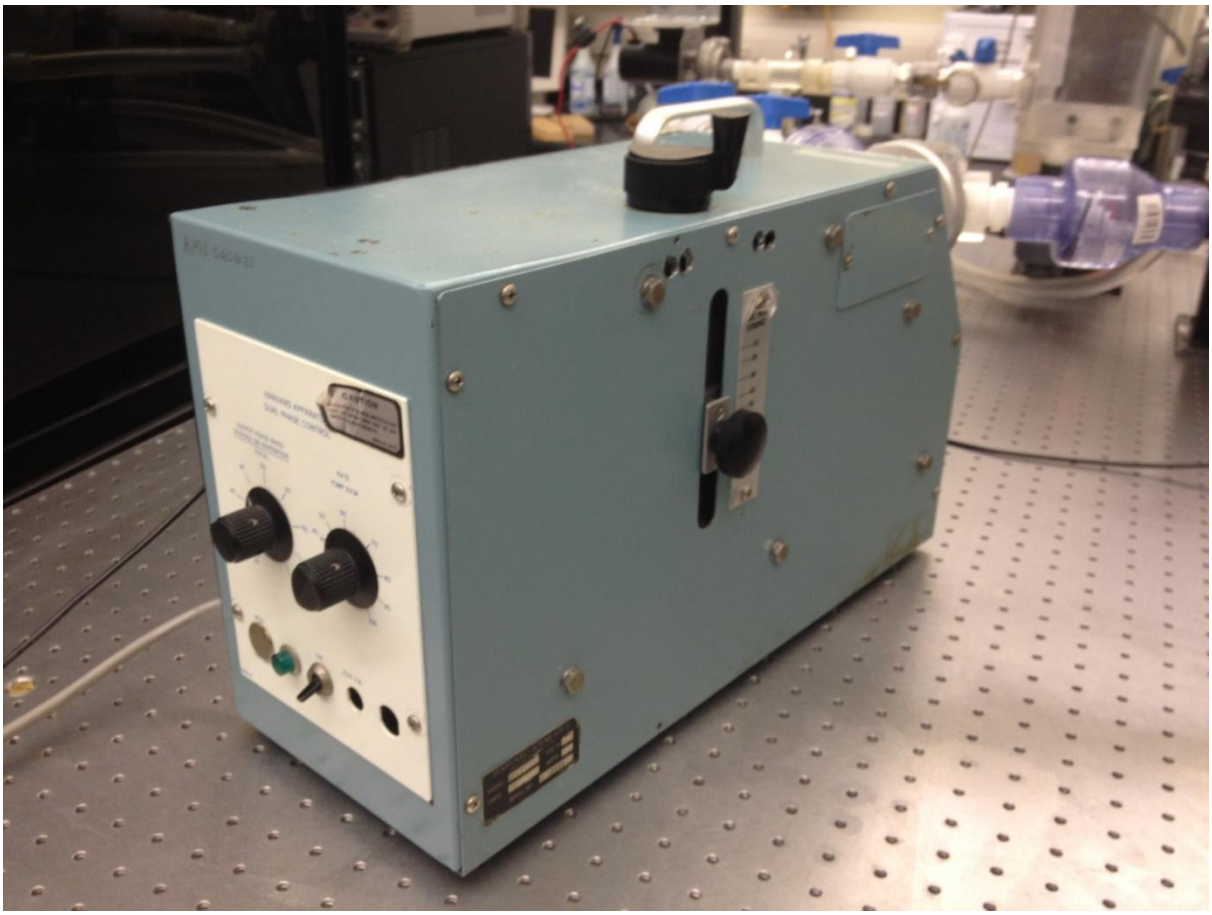

Figure 12: Harvard Apparatus Model 1423 Pulsatile Blood Pump. Turn knob potentiometers are shown on the back to control heart rate and percent systole. The turn knob on top adjusts the stroke volume, with an indicator scale on the side of the pump.

a connection to a "cam switch," an element that detects when the pump is filling (diastole) or ejecting (systole). This switch provides a mechanical feedback on the position of the piston, which in turn changes the speed in that particular phase to meet the settings for percent systole and heart rate.

The piston of the pump is actuated by translational motion achieved by converting the rotational motion of an electric motor's driveshaft by means of a bar linkage, shown in Figure 13 [104]. The third link is a class 1 lever with a sliding collar as the fulcrum; this changes the mechanical advantage with position of the piston. The fulcrum for the third link can also be translated along the longitudinal axis of the link. This is the mechanism for changing the

Table 5: Comparison of factory model Harvard Pump and automated version.

Setting	Factory Model	Automated Model
Heart Rate		
Actuation	On unit dial	Remote control via USB
Set point control	Open Loop	Feed-forward PI control
Percent Systole		
Actuation	On unit dial	Remote control via USB
Set point control	Closed Loop Proportional Control	Feed-forward PI control
Stroke Volume		
Actuation	Hand crank	Remote control via USB
Set point control	Set screw	Closed loop control
Setting data logging	Not available	USB communication

magnitude of displacement in the fourth link per revolution of the first link, affecting the stroke volume in the piston. This translation of the fulcrum is achieved via a worm gear, with a hand crank mounted on the top of the device. A position indicator and equivalent stroke volume scale are included on the side of the device. The fourth link is constrained by roller bearings to only allow translation along the longitudinal axis, and is interfaced to the hydraulic piston. The piston is constrained in the casing by two O-rings with Christo-Lube ® (Lubrication Technology Inc., Franklin Furnace, OH) applied to reduce friction. This mechanical driveline provides for an angular torque change, and with the friction of the piston, can provide significant motor loading.

Previous modifications to this pump have been focused on retrofitting the hydraulic pump head. Two previous studies investigated the use of distensible membranes to create a physiological fluid-structure relationship in various forms [100,101]. Replacement of the ball check valves with prosthetic valves for the purpose of flow field visualization has also been investigated [99]. This present study encompasses the design modification to automate a commercially available pump (Harvard Apparatus Model 1423) to achieve a remotely-operated design capable of producing accurate ventricular pumping profiles. The modification requirements prescribed that the heart rate, percent systole and stroke volume must be

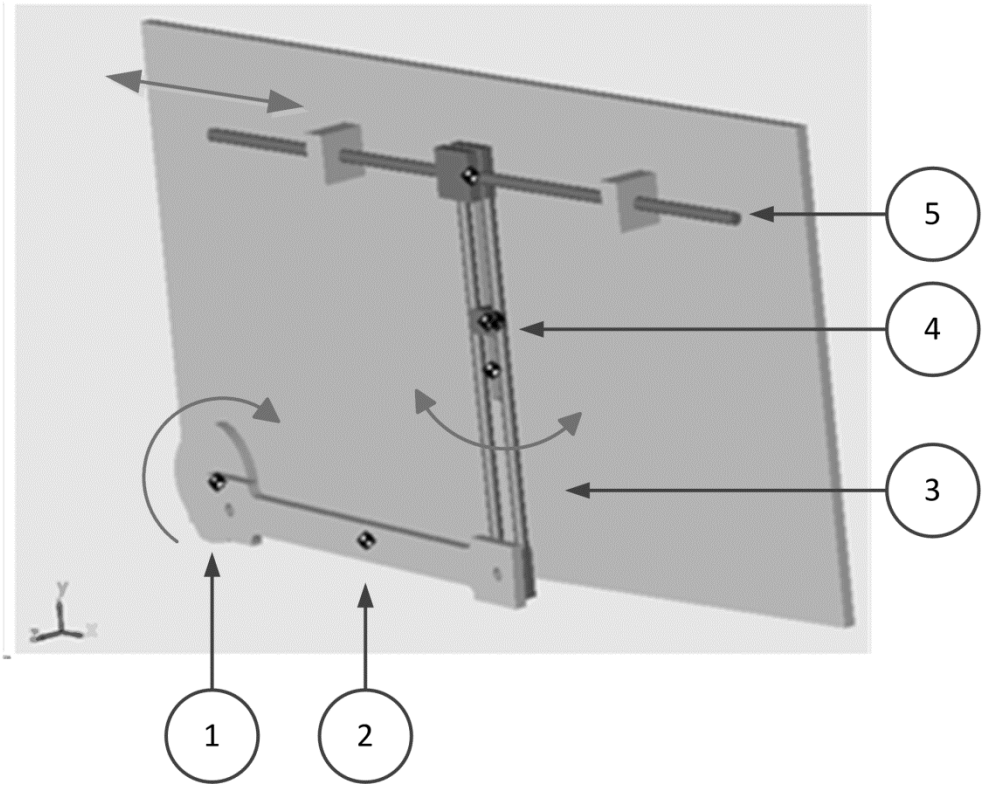

Figure 13: A CAD model of the Harvard Pump drivetrain, designed in SolidWorks, and later imported into Simulink™ via the SimMechanics™ Link tool. The arrows indicate the movement of the respective linkages. The elements of the drivetrain are the (1) CAM connected to the driveshaft of the motor, (2) swing arm, (3) third linkage acting as a class 1 lever, (4) fulcrum of lever, and (5) translating linkage that attached to the hydraulic piston.

changeable from a LabVIEW (National Instruments Corporation, Austin, TX) interface with real-time determination of the pumps performance for each of those parameters.

The motor supplied in the Harvard Apparatus Pulsatile Blood Pump Model 1423 modified in this publication is a Bodine Electric Company (Northfield, IL) NSH-34RH shunt-wound motor. From the information on the plate attached to the motor, it is seen that this motor is capable of 86 RPM at 29 lbf-in of torque while being driven with the specified 115VDC. The horsepower rating is 1/15 and the current drawn at peak load is 1 A. The gearbox has a ratio of 1:20. The motor mechanical properties of inertia and damping could not be determined through

available product literature, and would have to be determined through parameter estimation using the computational model of the system.

The motor has two operating conditions; steady RPM for 50% systolic ratio and switching RPM for non-50% systolic ratios settings. In the case of the non-50% systolic ratios, the motor must operate at a particular RPM for systole and another for diastole to produce differing duration times for filling and ejection. Each turn of the driveshaft on the pump motor corresponds to a fill/eject cycle on the piston; revolutions of the driveshaft per minute is equivalent to simulated beats per minute (BPM). Time in systole and diastole is determined purely by the speed of the motor in that phase, as the mechanical linkage constrains half the revolution (180°) to each phase. The angular velocity determination during each phase of pumping for a particular heart rate and percent systole setting is determined by the following equations:

Equation 9

$$RPM_{systole} = \frac{BPM}{(\%\, Systole)} \frac{180°}{360°} = \frac{BPM}{2(\%\, Systole)}$$

Equation 10

$$\therefore \text{RPM}_{\text{diastole}} = \frac{\text{BPM}}{2(\text{1-\% Systole})}$$

Using the equations for equivalent RPM in each phase, the maximum RPM at a particular setting can be determined. RPM values above the rated speed of the motor elucidates the origin of the correction factors in the user's manual for the Model 1423 pertaining to heart rate corrections for percent systole settings [102]. This design update includes a higher driving voltage of 145VDC, allowing for a broader range of operation than the base Harvard Apparatus design. A higher voltage was not tested, as the 145VDC represented 126% of the rating for the motor, which was as far out of specification as was deemed safe. The upgraded design is capable

of reaching a maximum speed of 105 RPM, which precludes simultaneously high heart rate and highly asymmetrical systolic ratios, but provides an operational range that was deemed sufficient for most applications. The regions that cannot be simulated are indicated by the yellow to red range of Figure 14.

The pump performance was validated in a mock circulatory loop (MCL) used to simulate systemic circulation conditions. The MCL utilized was able to change left ventricular performance parameters, arterial compliance, and peripheral resistance. The system fluid employed in this test was 40% glycerin in water at a temperature of 23 degrees celsius. The

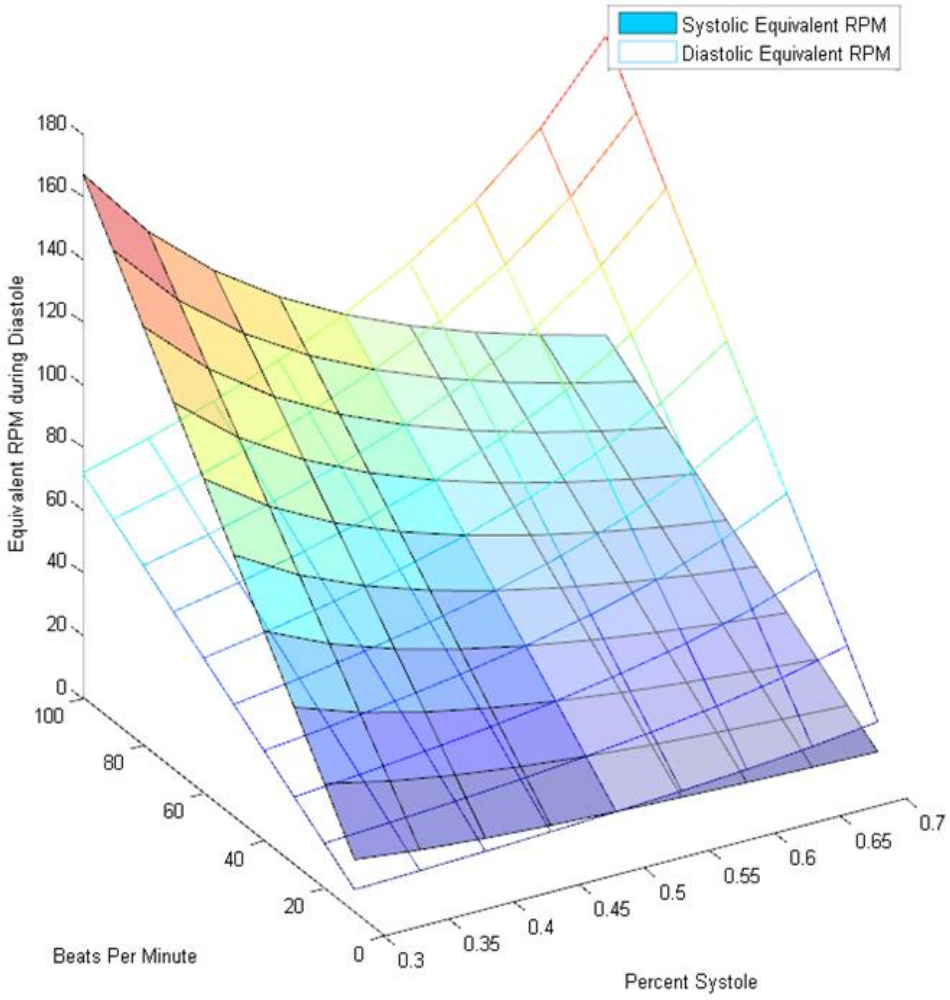

Figure 14: Harvard Pump RPM speeds for different settings.

viscosity of the fluid was verified at time of testing to be 3.707 cSt and the density was confirmed to be 1.1047 g/mL. Both of these values are consistent with published physical property information on this solution [93,94,105]. Compliance was maintained at 0.8 mL/mmHg throughout the performance evaluation, the low value was chosen to keep the pressure values safely under 150mmHg throughout the various conditions tested. The peripheral resistance was kept constant throughout the trials at an effective flow path diameter of 0.081 in^2. These conditions sought to replicate the pumping loads the pump would experience with the system fluid, and isolate the pump performance by maintaining constant set points in the other MCL components.

The sensors utilized in the MCL were an M20XL (Transonic Systems Inc. , Ithaca, NY) ultrasonic flow rate sensor downstream of the pump outlet, and a EPX-V015P (Measurement Specialties, Hampton, VA) pressure sensor monitoring the fluid pressure of the compliance chamber. There was no interest in monitoring the inlet pressure of the pump, as this portion of the system is not utilized in systemic circulation condition simulation. Previous investigations have been conducted on the upstream pressure effects of this pump, which further negated the need for pressure sensors in this region [106].

2.2.4 Anatomical modeling

The development of anatomical models for this project had the stated objective of using open source data and software to deliver the needed geometry. Developing models with cost free tools was seen as highly advantageous, as this workflow could be adopted by any lab that needed anatomical models for their work and could not afford the commercial options. The challenge was to indentify a public high resolution data set. The Visible Human Project, through the National Library of Medicine, provides medical image datasets of different modalities.

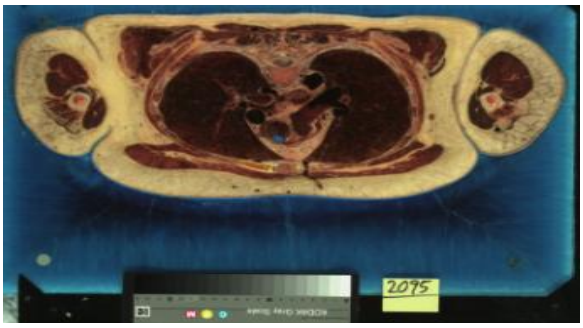

Figure 15: Visible human project cryoslice image. This image is part of the female image set. The image presented is a transverse plane taken near the aortic valve plane.

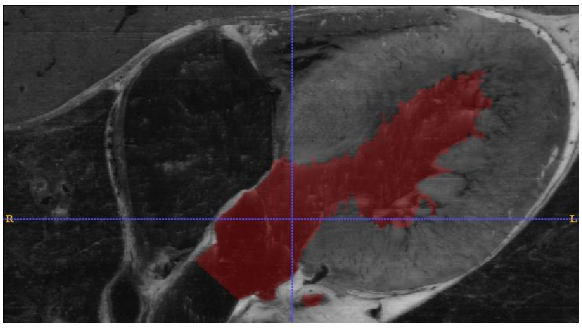

Figure 16: Screenshot of the ITK-SNAP tracing environment. The red section is the region being traced, in this case the left ventricle. The view is of a sagittal plane through the ventricle.

However, the CT and MRI data does not have the resolution that is needed for the smaller geometries and less defined boundaries of the cardiovascular system. Interestingly, the cryoslice data that is included in the Visible Human dataset is high resolution; the female dataset has 0.3mm square voxels (Figure 15). This was chosen as the modality to use in the tracing; the resolution was excellent and the boundaries were very clearly defined.

A process for constructing patient specific models of failing hearts was adopted for the work in this project [107]. This presented workflow enabled the generating of the models of interest through the use of open source software; ITK-SNAP for geometrical extraction and Blender to post process the mesh. The cryoslice images were converted to DICOM format using a program that was published to a user forum; the images were converted to a grayscale format based on the luminosity of the color cryoslice pixel. An example of this image conversion is seen in Figure 16. Adjustment of the RGB weighting in the conversion could be used to increase the contrast between certain tissue types. The DICOM format was necessary, as the ITK-SNAP program was designed to handle radiography data types.

Tracing within ITK-SNAP was performed using the auto-segmentation routines first and capturing the more detailed boundaries manually with the watershed tools. Due to the non-

radiological nature of the dataset, it was determined that the completely automated segmentation of the data would not be a time effective route. Once the tracing of the volume of interest was complete the model was made ready for export as an STL file. Extraneous geometry captured was cut from the solid model to reduce the file size when exported.

The STL generated from the model in ITK-SNAP was imported into Blender for post-processing. The goals of the processing should be to remove any errors that SolidWorks may have with the mesh and reduce the mesh size to a number that is capable of being imported to SolidWorks. The mesh that is imported into SolidWorks needs to be a continuous surface mesh that does not have any holes. These holes in the manifold can be created when smoothing and removing tracing artifacts from the STL file generated by ITK-SNAP. Patching the holes involves manually stitching the facets from the free vertices and edges of the holes. The STL file that is imported into SolidWorks should be a roughly 15E3 facet mesh. Larger meshes can be imported if the "Scan to 3D" toolbox is used, which was not available for this work.

To generate the lofted models, the work by other cardiovascular researchers was adapted to the tools available within SolidWorks [108]. The imported STL file provides the basis for the spline traces that will be used to create the lofted geometry. The splines that need to be generated are cross-sectional traces of the lumen boundary and guide curve splines that are parallel to the centerline of the vessels. The latter allow for more accurate interpolation of the geometry between the cross section splines. Each intersection of two splines should have a coincident constraint placed on that point, as SolidWorks lofting tools mandate this relationship when lofting. Consultation of the SolidWorks manual is highly recommended, along with completing the tutorials on surface modeling and lofting prior to initiating an anatomical geometry lofting.

Once the swept model is created, the code that is needed by the CNC to cut the model from the bulk material needs to be completed. The use of the "MasterCAM for SolidWorks™" plugin allows these machining paths to be generated from within the SolidWorks environment. Prior to generating the machine tool paths, the swept model must be negated from a rectangular block to produce the hollowed lumen that embodies what the machined model will resemble. Any geometry that needs to be added to the part for connections of the model to the other experimental hardware needs to be completed at this step. Then the part must be split in two, using a split line, to allow for separate pieces to be machined and glued together to form the final model. With each of these pieces, each representing one half of the cut lumen in a rectangular block, the machine paths are generated. First, roughing passes must be programmed for bulk material removal. Subsequent passes with sequentially smaller tools are used to finish mill the material to a smoother surface roughness. When all desired machine tool paths have been created, the g-code that is used by the milling machine is generated using a "post file" containing the settings specific to the machine being used. Once the model parts have been fabricated, they are adhered together to form the final piece.

The model piece must be validated for strength and compatibility with imaging systems. Pressure testing the model to the upper mock circulatory loop limit of 250 mmHg, and achieving no leaks, ensures the model is sound. Conducting an imaging experiment with a particle doped flow, and producing PIV vectors, confirms the ability of the model to be used for those investigations. The PIV validation is contracted to another investigator, who will ultimately be using the models. The requested data for this validation of the model is an image used to create PIV vectors and a contour plot of the flow through the model.

2.2.5 Mock circulatory loop layout

The final embodiment of this mock circulatory loop is shown in Figure 17. It is a systemic mock circulatory loop with a modified Harvard Apparatus pulsatile blood pump attached. This system has been designed to investigate dynamic cardiac conditions, conduct robustness testing of cardiac devices, and act as a conditions generator for flow studies involving PIV techniques. The arrangement of the previously described subsystems creates a uniquely adaptable system that enables efficient use of this system for a wide array of investigation types.

The hardware responsible for the pulmonary and systemic effects are mount on respective pylons. This was done to allow for configuration of the mock circulatory loop to suit the investigative needs. The optical table (Newport Corporation, Irvine, CA) on which the mock circulatory loop is mounted, has a 1" hole pattern that enables flexibility in the placement of the components. The vertical green pylons at the connections to the mock circulatory loop support the conduits, and prevent damage to the components when reconfiguration is being performed. The systemic hardware is comprised of the compliance chamber and the peripheral resistor. These two subsystems are able to construct the appropriate impedance of the systemic arterial circulation. The arrangement, with respect to the flow into the mock circulatory loop, is the compliance chamber and followed by the resistor. A return line from the resistor channels the system fluid to the venous reservoir. This reservoir and the centrifugal pump comprise hardware simulating the pulmonary venous supply. These four components, segregated into two subgroups, comprise the systemic mock circulatory loop embodied in Figure 17.

The Harvard Pump in Figure 17 is providing the cardiac function simulation for the experiments. As previously described, this pump has been modified from its factory standard to a fully automated version. This pump is a piston pump that is based on a displacement and

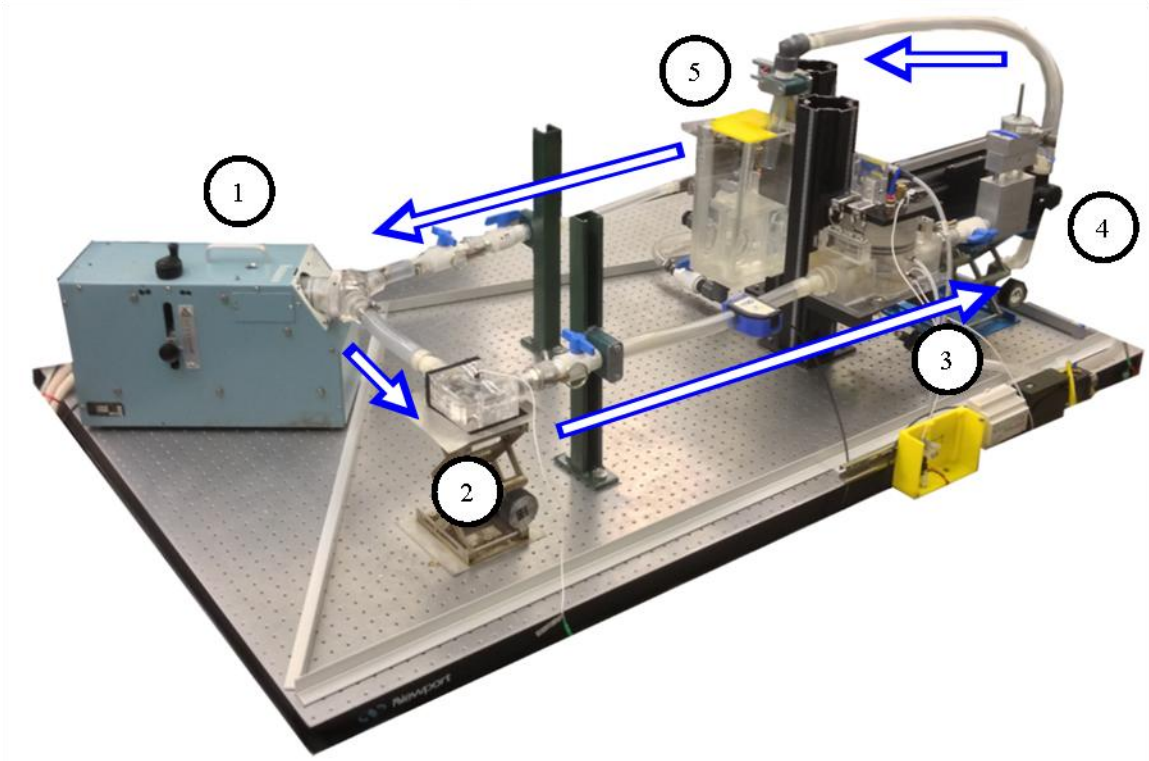

Figure 17: Photograph of the mock circulatory loop. The cardiac function is simulated by the Harvard Apparatus pulsatile blood pump in the upper left corner (1). The aortic model is present in the lower left (2). The outflow of the aortic model passes through the flow meter (blue case) and enters the compliance chamber (3). The peripheral resistor (4) is downstream of the compliance chamber, with a tube that extends vertically to empty into the venous reservoir (5). The reservoir has a return line that feeds the Harvard Pump inlet. The blue arrows indicate the net direction of flow through the loop.

timing profile; heart rate, percent of time in systole, and stroke volume. Considering the pressure ranges and impedances being simulated in this system, this pump can be considered afterload and preload insensitive. The point of simulation when using this pump is the outflow, which is analogous to the ascending aorta conditions.

The aortic model is connected to the Harvard Pump outlet, as seen in Figure 17. The distance between the outlet check valve of the pump and the model has been minimized; the placement is considered acceptable for the purpose of evaluating this models function. The main objective was to align the exit of the aortic model with the inlet to the mock circulatory loop, which was met.

The system fluid used for the operation of the mock circulatory loop is the 40% glycerine in water (by weight) that was used for the subsystem validations. This solution has a similar asymptotic viscosity and density with that of human blood. This same fluid was used in the PIV experiments, even though the refractive index does not match that of the plastics used for the anatomical models. This optical distortion is not an issue for the purposes of validating the optical clarity of the models; quantitative measurements would necessitate matching the refractive indexes to minimize error from distortion.

Control of the Harvard Pump and the mock circulatory loop is enacted through a central control computer. This computer communicates with the controller of the Harvard Pump and the controllers of the subsystems in the mock circulatory loop to enact set point changes. This central conductor is able to be run in manual or automatic mode; a dashboard interface enables the selection of settings or the ability to run a precompiled experiment file with scheduled settings changes. This dashboard also records the sensor readings to log files, which can be viewed through a software package designed to analyze the data from this loop.

2.3 Software tools

To assist research being conducted with this system, software development was undertaken to deliver solutions for the three stages of experimentation; design, execution and analysis. Three separate programs were developed and deployed to handle each phase.

2.3.1 Conditions Designer

A software program was developed to design the condition files that would be used in the mock circulatory loop. This software program allows a user to select the parameters of interest, or tune for a set of parameters from a PhysioNet patient file, and add those settings to list. The software user interface is arranged to guide the user through the stages of creating an

experimental file for the mock circulatory loop. This program was designed for standalone use from the mock circulatory loop to allow for multiple users to develop testing protocol. It was developed in the Matlab environment using the GUIDE tool to design the user interface.

The connection of this program to the PhysioNet database was an integral part of this projects ability to simulate realistic conditions. Establishing PhysioNet as the conditions source for experiments, this system takes advantage of a growing database with a wide array of possible conditions and disease states to simulate. The software program utilized the well developed UI of the PhysioBank ATM, which is embedded in the UI of the program (Figure 18). This was achieved by utilizing the Matlab web browser as a java object in the UI. When a patient record that contains an arterial blood pressure trace is located, and a time segment of interest is identified, the "capture study" button records the time window being viewed. This record is added to a list that is saved for the "Parameter Fit" pane.

The Parameter Fit pane provides the ability for the user to construct the settings files that the mock circulatory loop uses to run the automated experiments (Figure 19). This pane allows a user to manually select the settings of interest, or use parameter estimation routines that seek to identify the settings needed to replicate the waveforms of interest. This parameter estimation is achieved through the same tools used to identify component values in the Simscape models. The values being tuned in this case are the settings in the computational model of the mock circulatory loop, with the pressure trace in the model being tuned to the patient records arterial blood pressure waveform. Once a setting is reached, either manually or through the parameter estimation, the values can be added to the conditions list in the right panel. The items in the panel can then be exported as an experimental conditions list formatted as a tab-delimited text file.

Figure 18: Conditions Designer UI for PhysioBank conditions capture.

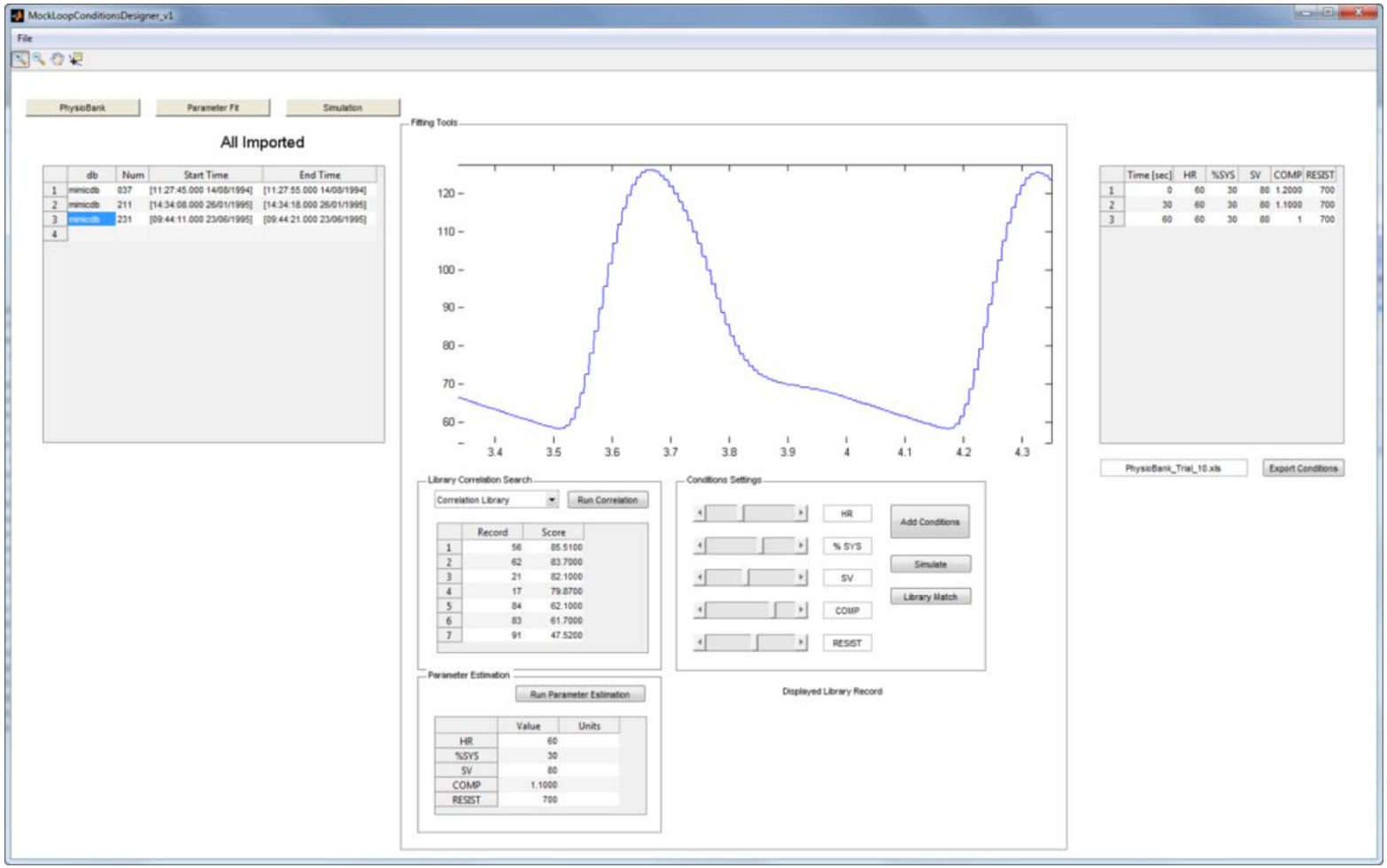

Figure 19: Conditions Designer UI for parameter estimation.

2.3.2 LabView control interface

The dashboard for the mock circulatory loop allows for the monitoring and control of the hardware in the loop through an interactive user interface (Figure 20). This dashboard was developed in LabView due to the ease of implementing graphical controls and indicators in this environment. The block diagram that drives this front panel is available in Appendix B. The architecture of this program centers around the front panel design; graphs, file I/O, and control panels for each of the subsystems.

The graphs on the left hand side display the sensor data being collected in the loop. The top trace represents the pressure sensor data from the compliance chamber. The middle trace is that of the flowmeter that is measuring the aortic outflow. The bottom trace contains the pressure of the hydraulic section of the compliance chamber and the volume displacement of the membrane. The blue vertical bands indicate 1 second intervals in the traces.

The control panels contain the setting controls and read backs that are specific to the subsystems they represent. Each of these panels is being updated at the 8Hz rate that the subsystem microcontrollers communicate their settings to this dashboard program; the updates are propagated at the same refresh rate. The File Import panel indicates the progress in simulating the conditions from the experimental file that have been loaded.

At the top of the screen, there are two file path boxes. These represent the location of the experimental file to be run (top with white background) and the output log file of the data collected (bottom with gray background). The switches to the right of the file path boxes indicate where to run the experimental conditions file and whether to record the data being collected.

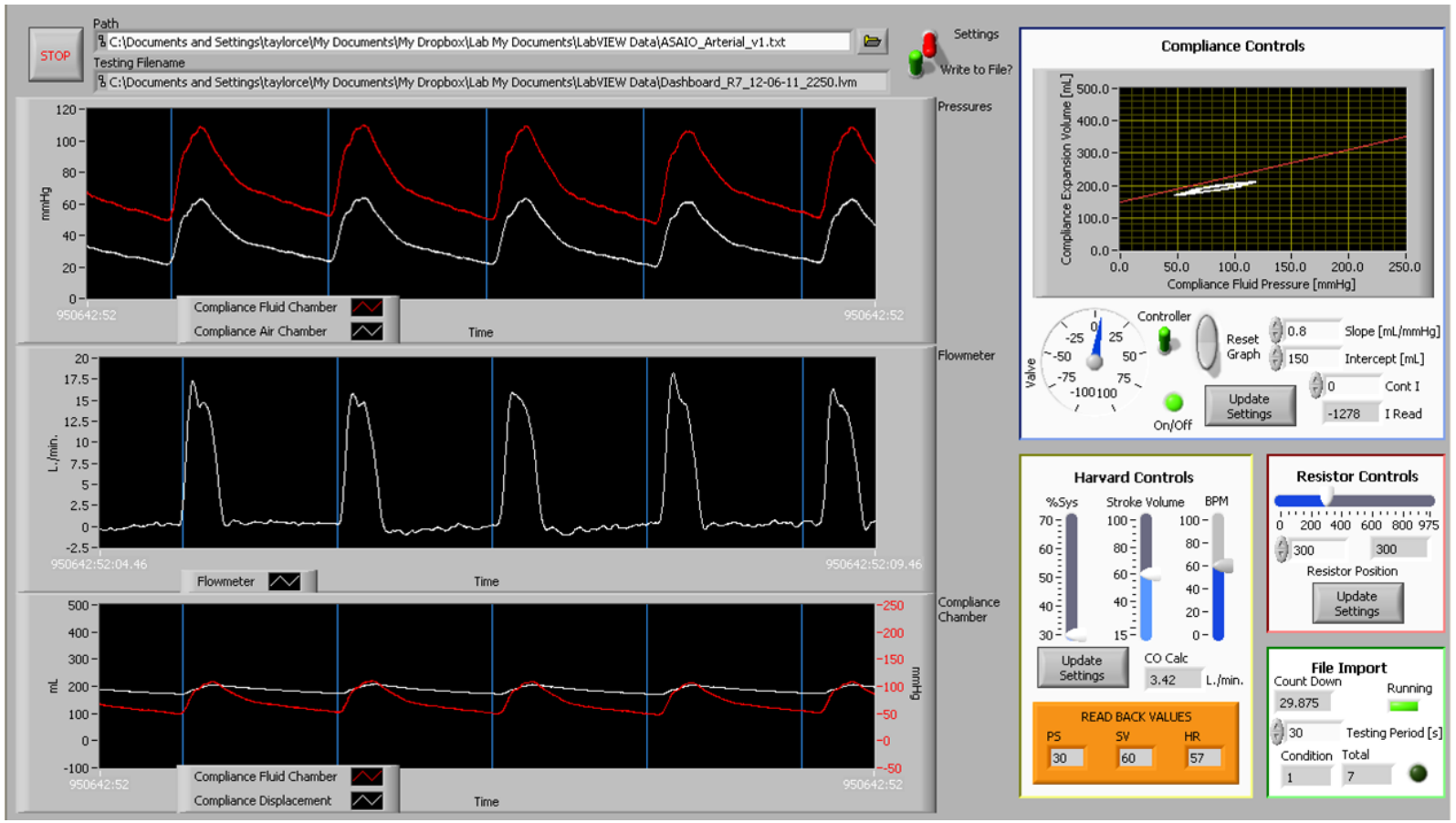

Figure 20: Mock loop control LabView control dashboard.

2.3.3 Data Viewer

To handle the volume of data from the mock circulatory loop, it became necessary to develop a data viewer to process and display the data. The software program that was developed is shown in Figure 21. This program accepts the log files that are generated from the control dashboard, parses the data, analyzes the data to compute various metrics, and displays the results. The program was developed in the Matlab environment using the GUIDE tool to develop the user interface. It was designed to be a standalone program so that multiple users could utilize the program.

The import settings and capture details panels in the upper right of the user interface indicate the file that is being imported and the nature of the data contained, respectively. The dropdown menu in the import settings panel indicates what parsing routine to use when analyzing the data. Different control dashboard development versions required different parsing routines. The capture details panel indicates what the pressure and flow meter sensor sampling rates were, as well as the update rate of the subsystems. The length of the captured data is presented as well.

The top two traces on the left hand side of the user interface display the compliance chamber (top) and flow meter data (second from top). The compliance chamber data shown in Figure 21 has the pressure sensor data in blue and the volume of the membrane in green. The flow meter sensor data is in blue, with other calculated values displayed and annotated in the legend. The "Actual CO" is the integration of the flow meter data between heart beats; providing the cardiac output. The "Calc CO" is the heart rate of the Harvard Pump multiplied by the stroke volume.

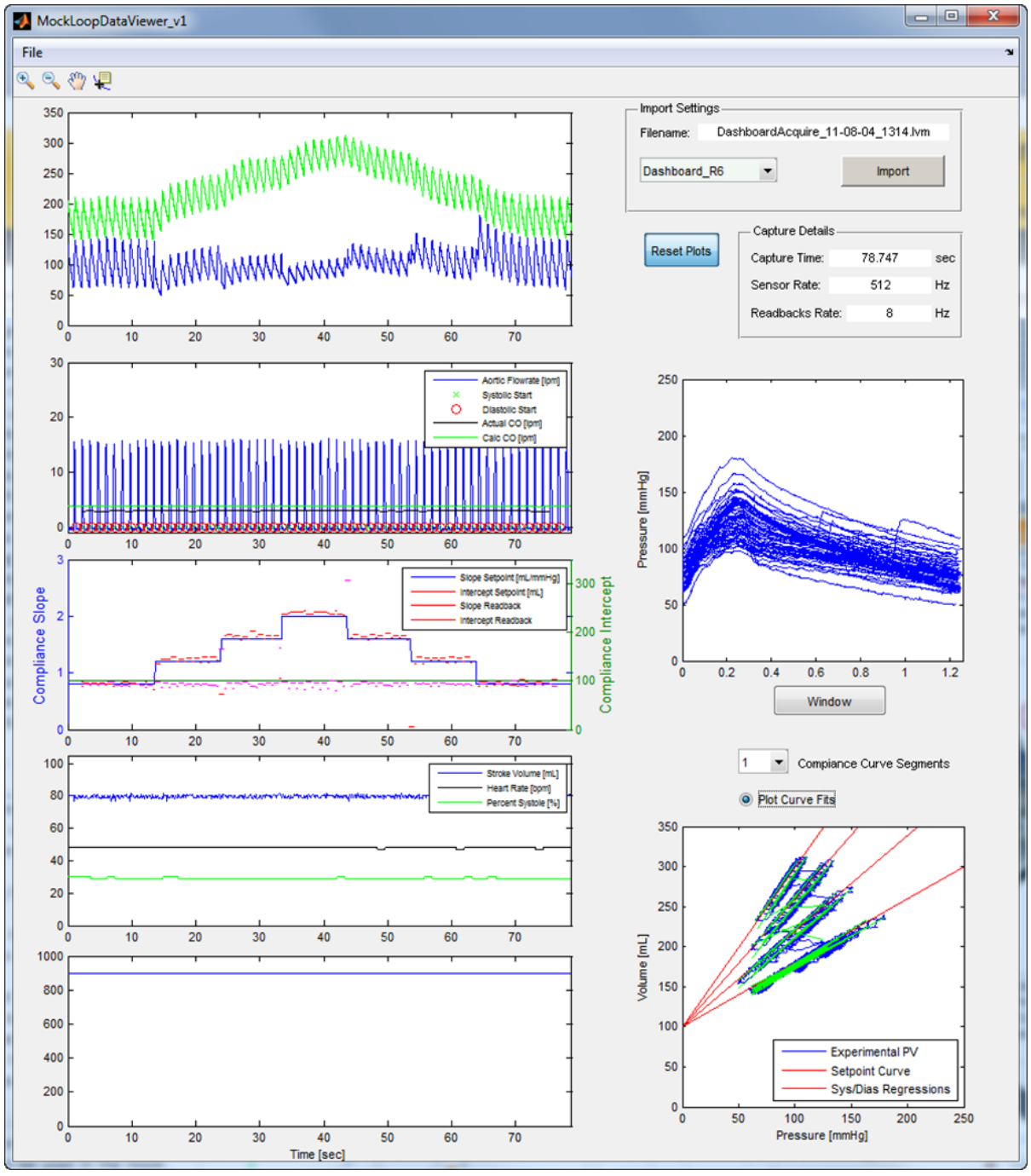

Figure 21: Mock circulatory loop data viewer interface.

The bottom three traces in the data viewer are graphical representations of the read backs from the subsystems (from top to bottom): compliance chamber, Harvard Pump, and resistor. The compliance chamber has the settings for the compliance, slope and intercept of the compliance curve, and the determined compliance. The determined compliance is derived from linear regressions of the volume versus pressure for the compliance chamber. The linear regressions are performed separately for the compliance in systole and that in diastole. The Harvard Pump trace plots all three parameters as indicated by the legend. The resistor trace plots the resistor position in number of motor steps from zero.

The two graphs in the lower right are overlays of the data encapsulated by the time window shown in the compliance chamber plot in the upper left of the user interface. The first overlay graph, second from the bottom on the lower right, is the pressure waveforms of the compliance chamber pressure sensor for each heart beat. The second overlay graph, in the lower right, plots the volume versus pressure for the compliance chamber. The sensor data is presented in blue, with the green representing the linear regressions that were performed for each of the systolic and diastolic periods. The red lines indicate the set point curves for the compliance chamber. This provides a succinct presentation of the set point, the performance of the system, and verification of the compliance.

3 Results

The experimental evidence in support of this projects successful achievement of the research objectives is based on the subsystem validations, the anatomical modeling achievements, the acuity of the computational model, and the performance of the mock circulatory loop. Presentation of the results in each of these categories will be made, with the understanding that the subsystems validations support much of the final mock circulatory loop performance assessments.

3.1 Subsystem Performance and Validation

Due to the incremental development of this mock circulatory loop, it was necessary to validate each subsystems function as a standalone device. The work progressed from the simplest device (resistor) to the most complex (Harvard Pump). Each subsystem was designed, prototypes fabricated, and components characterized for the computational model. Discussion of these standalone verifications is critical to communicate the thoroughness of the design and assessment given to these devices.

3.1.1 Peripheral Resistor

The Simulink™ model of the experimental setup utilizing the Simscape™ block set, which includes mathematic model elements similar to the physical bodies used to construct the test loop, is shown in Figure 22. The accurate depiction of the experimental configuration is essential for an accurate model and proper characterization of the resistor. The elements included in the model depict major sections of the experimental loop. Due to the consistent inner diameter of the fittings in the loop to that of the conduits, the connector elements were not given their own blocks.

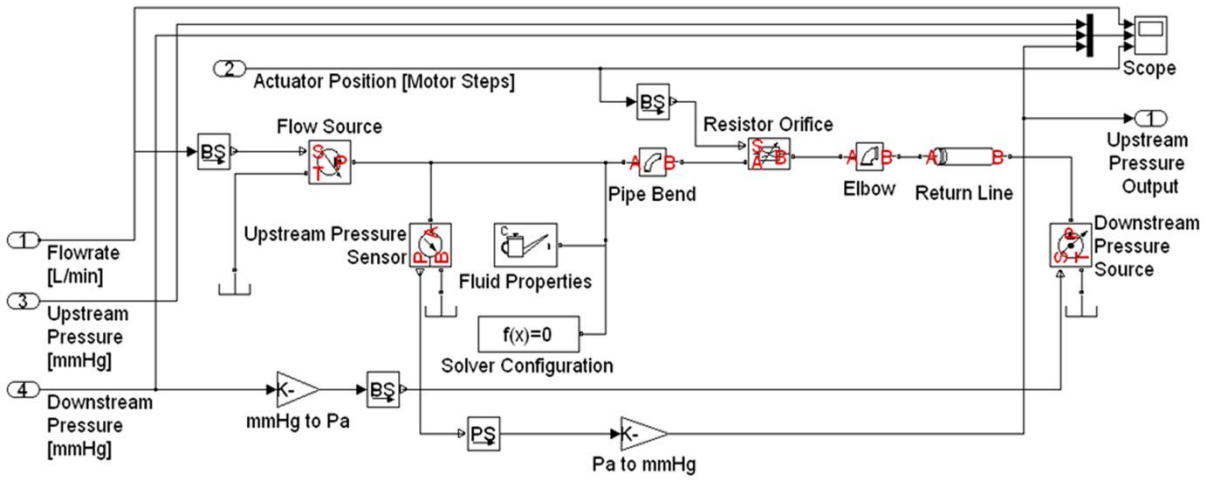

Figure 22: Simulink™ model of the resistor characterization system utilizing Simscape blocks to model the physical components of the mock circulatory loop. The simulated flow is from left to right, with components similar to those described in the experimental setup. The experimental flow sensor data is permuted as a flow source in the computational model; the model needs a volume source. The downstream pressure sensor experimental data is represented as a pressure source in the model, as there needs to be an exit condition for the simulated flow.

The resistance device was modeled as a variable orifice element, with orifice area correlated to a characteristic opening. Orifice areas per linear actuator position, at 10 position value increments, were supplied in the vectors to the block settings page. Conduits between the various components were modeled with low pressure hydraulic pipelines, pipe bends and elbows. The geometrical parameters were defined by dimensions of their physical counterpart in the experimental loop; all inner diameters were defined as 1.905 cm. The hydraulic blocks used were defined as rigid sections, with no distention under pressure.

Differential pressure across the valve was taken from two gauge pressure sensors; one upstream and one downstream. The model is tuned to the upstream pressure, which is represented as a sensor. The downstream pressure is represented as a source, as the model needs to have an exit flow condition. The flow rate from the sensor downstream of the resistor in the experimental data is permuted as a flow rate source feeding the model elements. This is

acceptable as the fluid is incompressible, and there are no losses in volume in the segment of the loop investigated. It is represented as an ideal flow rate source that is referenced to atmosphere.

The hydraulic fluid block and the solver configuration block are responsible for model-wide parameters. The kinematic viscosity and density for the system fluid should be determined experimentally, and confirmed against literature values for the desired composition [93,94,105,109]. The values utilized in the computational model were those determined experimentally when validating the system fluid.

The experimental data connections to the model were defined by an input to the ideal flow rate source, an input to the variable orifice position, an input to the downstream pressure source and an output from the upstream pressure sensor. With these connections established, the model could be tested with experimental data or artificially constructed values as inputs to the system. The input and output connections also provide the handles necessary for the Parameter Estimation Tool.

With the Simulink™ model of the experimental loop completed using the Simscape™ toolbox, the task of constructing an accurate model was undertaken. The goal of the model building in this particular investigation was twofold: to identify objective characterization parameters for the custom resistance device and to construct an accurate numerical depiction of the device for future imbedding in larger models. The former is important, as it allows for comparison to other devices currently in practice and substantiation for the current design in this application.

The parameter estimation for this particular model sought to identify variables in the model that could not be determined by direct measurement. These variables included: discharge coefficient of the resistor, the critical Reynolds number for the valve, and offset factor for the

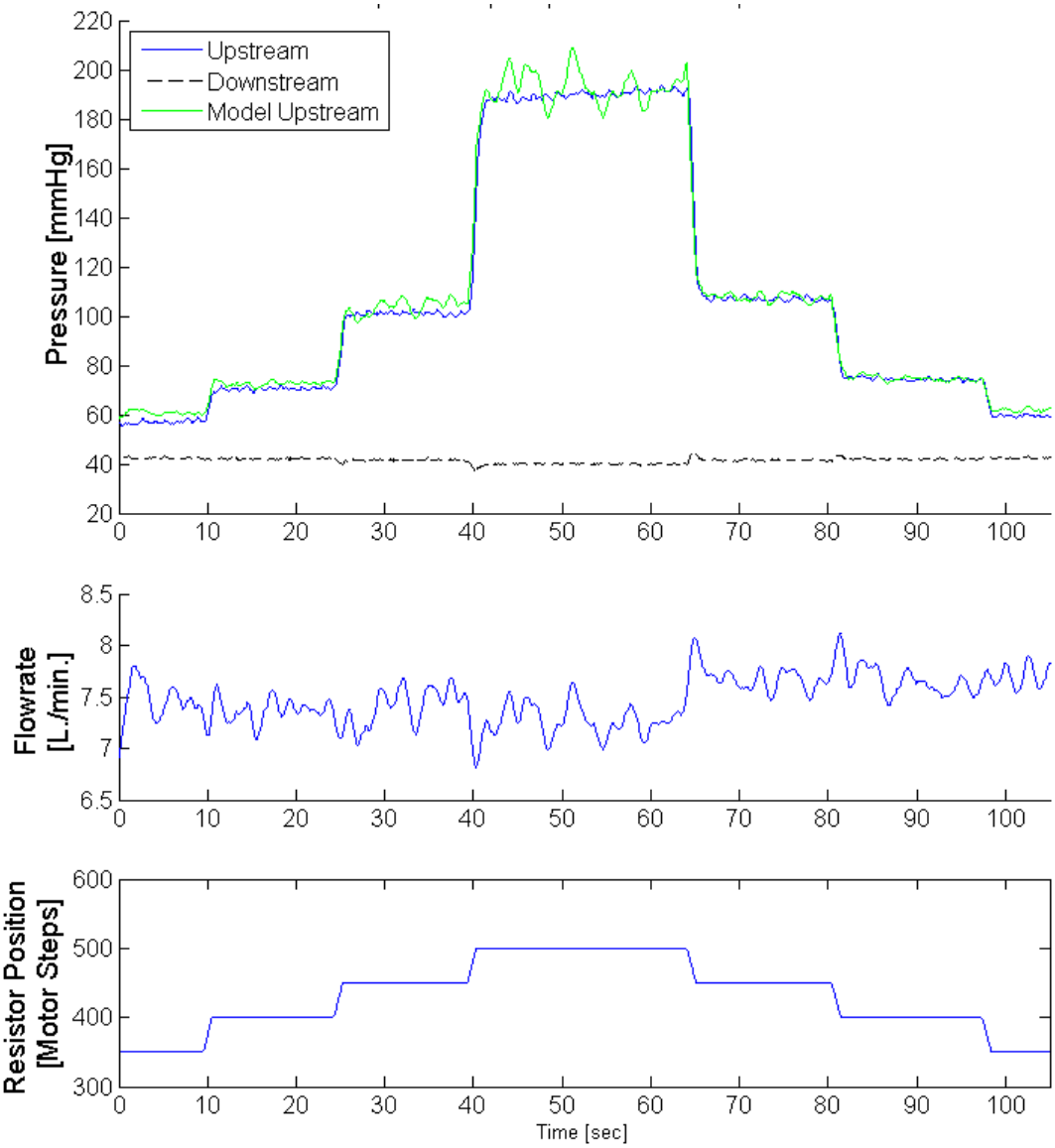

Figure 23: High flow performance of the peripheral resistor. The top graph depicts the tuning dataset with the result of the model using the tuned values to that of the experimental dataset for the upstream resistor. The flow rate graph (middle graph) indicates that an approximately constant flow was maintained.

orifice area determination (Table 6). The offset factor for the orifice area is to correct for possible lack of precision in the determination of the initialization position.

The dataset for the tuning of the parameters was an experimental set of corresponding linear actuator positions, flow rates and upstream pressures of the resistor (Figure 23). This dataset provided the necessary inputs to the model, and a pressure output that the optimization

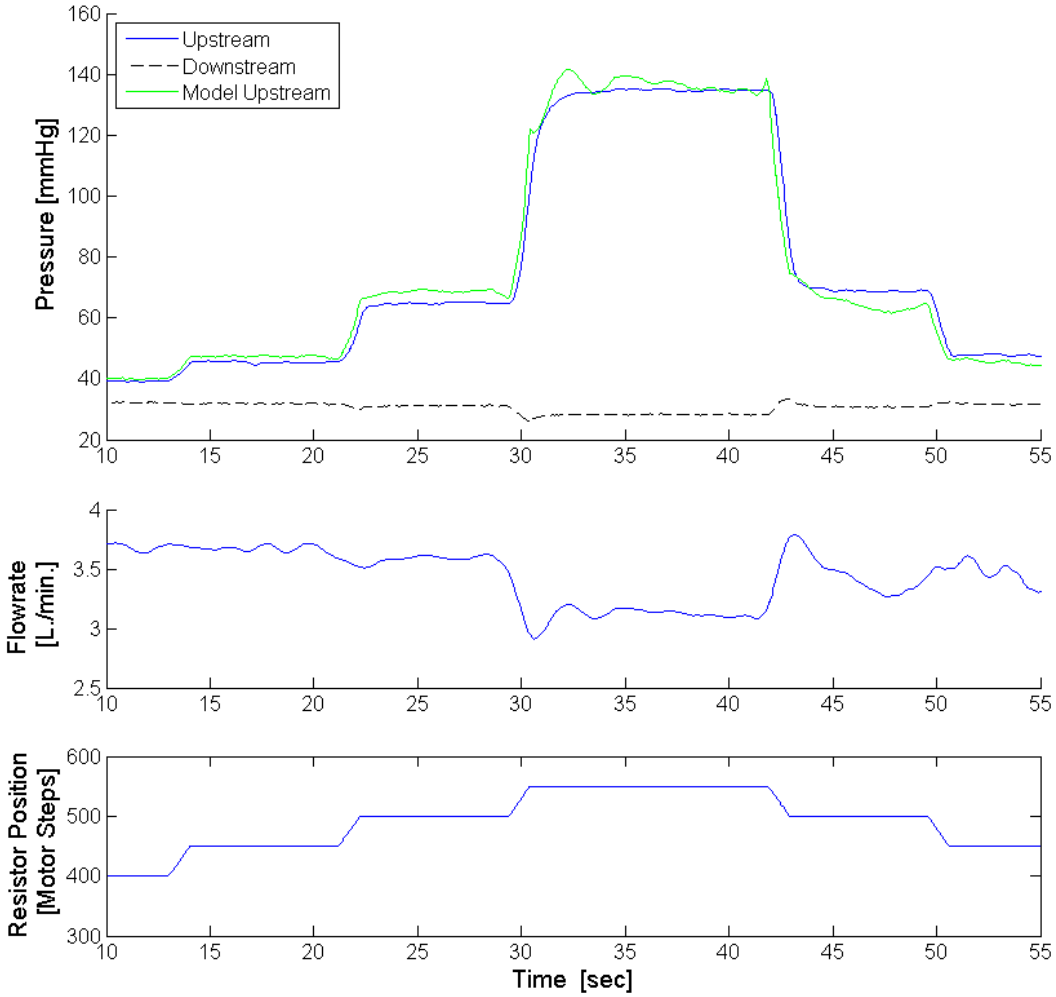

Figure 24: Low flow performance of the peripheral resistor. Performance of the tuned Simulink™ model using input data with different conditions to that of the tuning data. The model simulation at the lower flowrate showed signs of sensitivity to the fluctuations in flow, which was seen in the tuning data as well. The similarity of the simulation to experimental data provides that the parameter estimation was a success.

algorithm needed to tune the model with. The dataset utilized was a staircase of actuator positions, under a constant flow rate that would be indicative of a midrange flow rate experienced in the mock loop (~7 L/min). There were a series of three staircases in the dataset utilized for the estimation of the parameters.

A validation dataset was obtained experimentally to verify the performance of the model (Figure 24). It deviated in conditions from the estimation dataset in order to test the robustness of values of the parameters estimated. This validation dataset was comprised of three staircases

conducted for a lower flow rate. The validation dataset was used as a performance indicator for the estimation and was not utilized in the parameter estimation process.

The parameter estimation solver that was chosen was ODE15s. The precision of this solver was acceptable due to the stiffness of Simscape models [84]. The speed it provided, coupled with the low level of noise in the data, was more desirable considering the number of iterations that must be run during the estimation routine. The time interval used for evaluation bracketed the staircase movement on the piston.

The acquisition of the datasets utilized in the analysis were obtained after stopping the flow in the system, in order to provide similar starting points for each dataset. The experimental data yielded appropriate pressure levels and response to change in piston extension and was therefore deemed to satisfy the criteria for the parameter estimation. The initialization position was found to be consistent, with no missed motor steps that would provide erroneous position read backs during the acquisition. The physical property determination for the glycerin/water solution was a viscosity of 5.45 +/- 0.15 cSt and a density of 1.12 +/- 0.02 g/cm^3; these values were used in the computational analysis. The viscosity and density were consistent with published values for a 50% glycerin in water solution [93,94,105,109].

The dataset employed in the parameter estimation was acquired within a flow rate range of 7 to 8 L/min (Figure 23). During the acquisition, the resistor piston was positioned in a staircase fashion from absolute position 350 motor steps to absolute position 500 motor steps.

Table 6: Peripheral resistor values obtained from Parameter Estimation.

Parameter	**Applicable Range**	**Final Value**	**Unit**
Discharge Coefficient	0.5-1.5	0.8492	n/a
Orifice Size Offset	-0.1-0.1	0.0162	cm^2
Critical Reynolds Number	1-3000	71.58	n/a

This was repeated three times during the capture. The length at each particular step was not timed, and the position was controlled through LabView. The validation dataset employed a flow rate of 2.5-4 L/min and has a resistor position staircase from 350 to 525 repeated three times (Figure 24). If the parameter estimation was correct, the values should produce a model that performs accurately across a range of flow rates. The validation dataset confirms this by showing the fidelity of the model at a much lower flow rate.

The noise in the flow sensor is indicative of an undeveloped flow profile. The flow rate sensor is proximal to the outlet of the resistor, as compared to the pressure transducer. The flow at the sensor may have not developed a fully laminar flow profile causing undulations in the measured flow rate. This noise is reflected in the pressure sensitivity of the computational model to flow rate fluctuations, as shown by the relationship of the two in Equation 3. The equation dictates that the pressure differential is proportional to the square of the flow rate for laminar and the power of 4 if the flow is turbulent. This relationship exacerbates the noise of the flow rate data when computing pressure values.

The flow rate data in the parameter estimation and validation datasets exhibit a rise after the peak of the staircase and a depression at the peak resistance, respectively. Both of these deviations in the flow rate are accounted for by pressure changes, which satisfy the constitutive equations and ensure the computational model's fidelity. The rise in pressure on the descending stairs of the parameter estimation data set result in a slight rise in upstream pressure, as opposed to the values seen on the ascending limb. The depression of the flow rate in the validation dataset is accounted for by the drop in downstream pressure. The accuracy of the computational model, through the governing equations, validates that these deviations in flow rate were correctly expressed in the pressure data.

The movement pattern of the resistor illustrated linear position change with time and no breaks in the read back data. This verified that the piston was moving with constant speed, and that the driver board could consistently update on piston position during movement. The successful performance of the resistor with pressure up to 200mmHg indicated that device is capable of working within the limits of operation for the mock circulatory loop.

The parameter estimation returned the values reported in Table 6, and provided a model with acceptable approximation to that of the physical system (Figure 24). The discharge coefficient value and critical Reynolds number were within ranges reported for valves, and are indicative of this type of valve [89,90]. The orifice area offset was determined to be very small, compared to the orifice areas determined by Equation 1. This indicates that the estimation of the orifice areas by piston position and setting of the initialization position are accurate. The comparison of the model with the estimated values to that of the validation dataset proved that the values obtained were robust, and produced an accurate characterization of the resistor.

3.1.2 Compliance Chamber

The Simulink™ model developed for this system illustrates the multiple domain elements that were used to produce a high fidelity simulation of the physical system (Figure 25). The pneumatic, hydraulic and mechanical sections contain elements that are generalized numerical models for that particular functional component in that domain. Sensor elements in the model replicate the sensor data being acquired in the physical system. The PI controller is shown in the model, with connections from the sensors to the actuators. This computational model provides a robust control design tool, which allows for controller parameters to be accurately determined in silica to reduce experimental tuning time.

The elements used in the hydraulic section were taken from the Simscape® Foundation Library and SimHydraulics® toolboxes. The hydraulic section of the model contains an inlet connection, a pipe conduit into the chamber, a hydro-mechanical converter, an outlet conduit, and the outlet connection. The hydro-mechanical converter element transmits the hydraulic force into a mechanical force which interacts with the membrane mechanical element and the pneumatic piston. The displacement of the mechanical section of the converter represents volumetric change in the fluid section. This element represents the hydraulic volume change in the space under the membrane, and the transmission of mechanical force at the membrane.

The mechanical elements were taken from the Simscape® Foundation Library toolbox. The membrane element is modeled by a linear spring. The highly elastic natural latex rubber produces minimal pressure development with distention, and this spring element would analogously have a low spring constant [97]. The spring strength is minimal, and the need for a nonlinear spring was not necessary in the range of use for this membrane. The force produced by this element represents the normal projection of force in the membrane due to the tension from expansion. The arrangement of the element in parallel with the pneumatic piston provides that the bulk of the force from the hydro-mechanical converter will be transmitted directly to the pneumatic section, with the membrane contributing only a slight mechanical response.

Pneumatic elements were taken from the Simscape® Foundation Library toolbox. The pneumatic section consists of a piston that is able to produce mechanical force from pressurization of its air chamber. The piston is connected to the proportional valve elements via a pneumatic tube. The pneumatic manifold subsystem in Figure 3 is comprised of the pneumatic valve model representing the 5/3 bi-directional proportional valve, the electronic valve driver board, the inlet pressure source of 15 PSI, and the outlet connection to atmosphere. Actuation of

this valve is delivered by a control signal originating from the PI controller, which is converted into a scaled response signal through a lookup table. This table represents the orifice opening to control signal calibration curve; the analogous voltage level to percent opening in the physical system. The valve response time, denoted as a 2.5 ms shifting time in the datasheet, was modeled as a first order system in the Pneumatic Manifold subsystem.

A displacement sensor on the membrane spring element is reflective of the measurement by the laser displacement sensor on the center displacement of the membrane. The output of this displacement sensor is passed through the Volume Determination block to provide the equivalent volume distention. A pressure sensor in the hydraulic chamber is routed through a compliance curve lookup table which denotes what the volume distention should be at that particular hydraulic pressure. This value is the set point for the controller, the calculated volume from the displacement sensor value is the read back. The error is passed to a discrete PI controller block with a sample time of 0.002 sec, analogous to the 500Hz process control loop on the microcontroller. The output of this controller is then actuated in the pneumatic manifold. Floating point calculations are not used on the hardware controlling the compliance chamber, which necessitates the use of specific data types in the computational model for fidelity purposes. The computational model enforces the bit precision utilized on the physical hardware in terms of analog to digital conversion (ADC), mathematical calculation rounding errors, and precision of the output controlling the pneumatic valve.

Mandatory blocks for the simulation of this system are presented in Figure 25; the Solver Configuration block establishes the handle for the ODE solver and is required for every

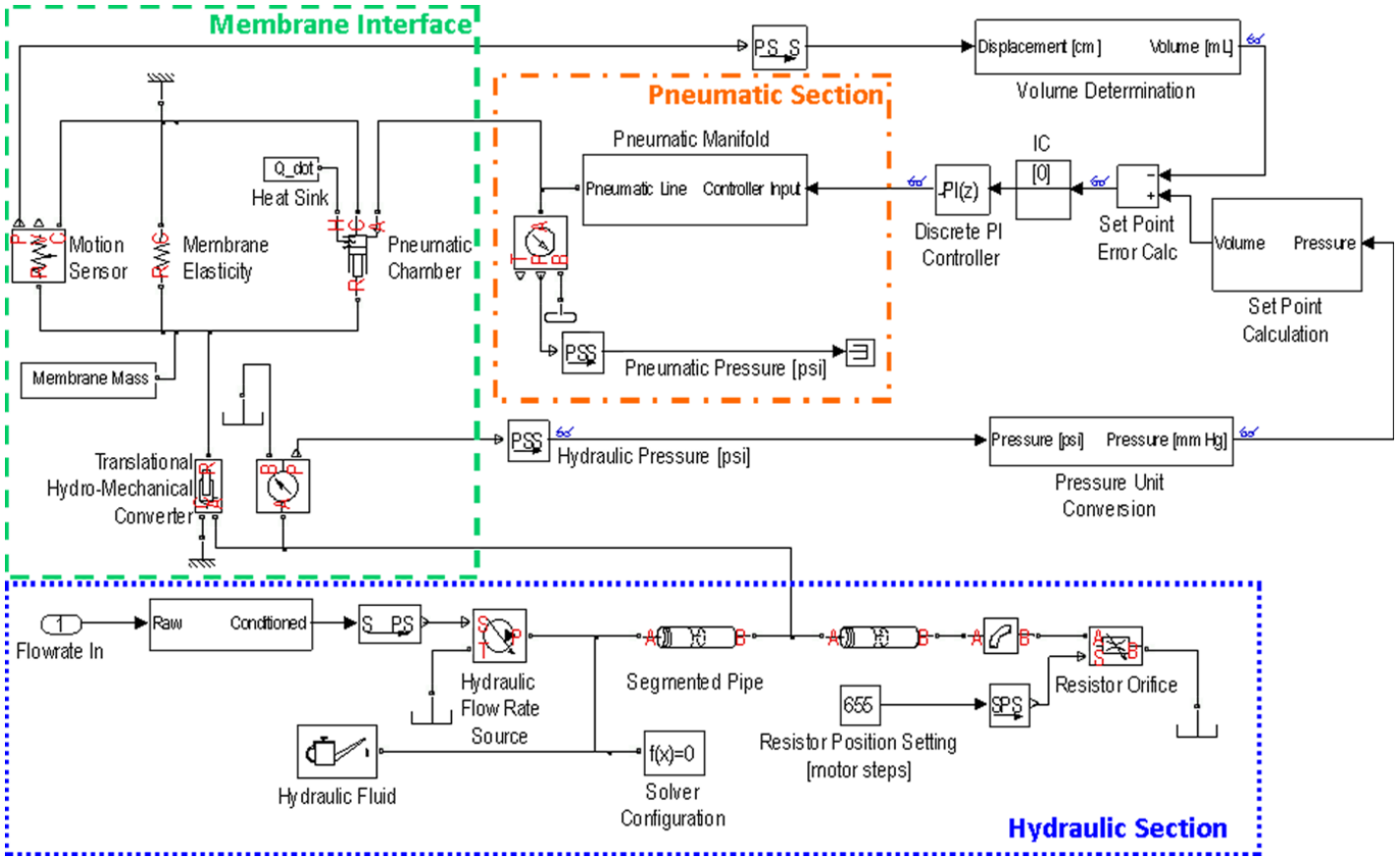

Figure 25: Simulink™ model of the compliance chamber indicating the three different domains the model is able to simulate. The hydraulic section is comprised of a flowrate source with pipe sections leading to and one exiting from the hydraulic chamber. The resistor creates the backpressure to the flow, with the 655 value indicating the stepper motor position needed for a 0.022 in^2 equivalent hydraulic orifice. The membrane section illustrates the interface of the mechanical element of the membrane, the pneumatic contribution from the air pressure above the membrane, and the hydraulic pressure acting on the membrane. The motion sensor in this section provides the analogous reading of membrane deflection that the laser displacement sensor is providing in the physical system. The pneumatic section simulates the pressure regulation system that drives the air space pressure changes. Controller calculations are conducted in blocks located in the upper right of the model, which are interfaced with sensors connected to the appropriate domains of the system.

Simscape® system. The Hydraulic Fluid block contains the physical properties of the fluid being simulated; 40% glycerin in water at 22 degrees Celsius. The Membrane Mass represents the small mass contribution (50 mg) of membrane to the mechanical system, and is necessary when using the mechanical block elements. The Heat Sink is required for the pneumatic piston, and allows for ideal gas laws to be maintained in the solution of the pneumatic equations. The Gas Law block contains the gas properties for the pneumatic section.

Pressure sensors for the hydraulic and pneumatic points of the system were included. These were used in the parameter estimation process to determine values of parameters utilized in the blocks. The Parameter Estimation™ tools in Simulink™ utilize cost function analysis to determine the accuracy of the model to that of experimental data. Descriptive experimental data from the physical system is required, with accurate depiction of sensor placement in the computational model [92]. Multiple sensor data provides a more efficient parameter estimation task, as the system is able to delineate the effects of parameter changes in particular elements more acutely.

A Microchip (Chandler, AZ) PIC18F26K22 microcontroller unit (MCU) was used as the platform for the process controller governing the compliance chamber function. This MCU was chosen due to its processing power of 20 mega instructions per second (MIPS) and features that would allow it to handle the peripheral devices involved in the compliance chamber control. The C18 student compiler was utilized in conjunction with the MPLAB® IDE (Microchip, Chandler, AZ) to produce the code deployed in this application. A PICkit™ 2 (Microchip, Chandler, AZ) was used to program the MCU with the compiled code developed in MPLAB®. The use of a distributed process control design allows the compliance chamber subsystem to remain stable in the event the host computer goes offline. The use of a MCU, as opposed to a programmable

logic controller (PLC), was dictated by the relatively simple calculations needed for this application and the cost differential between an MCU and PLC.

The run-time loop involves two main processes; timer interrupt at a frequency of 500Hz and receive interrupt from the computer controlling the mock loop. The timer interrupt loop is tasked with taking measurements from the pressure sensors and laser displacement sensor; this is a low priority interrupt. The hydraulic pressure value is used to determine the compliance chamber membrane volume set point, and the stored value of the current membrane volume is retrieved to provide the PI controller with an input error. The PI controller output is directed to a digital to analog (DAC) IC, which drives the proportional valve electronics. The receive interrupt from the computer is high priority, as these commands should execute immediately. The connection with the computer is used to change the set points on the MCU and take read backs for the purpose of data logging in the experiments.

The fidelity of the computational model to the physical compliance chamber behavior was found to be high. This accurate model allowed the discrete PI controller to be tuned appropriately, with computational simulation of its performance indicating an effective control of the membrane distention through manipulation of the air pressure. Plotting the experimental and computational pressure data in the top graph of Figure 26 illustrates the fidelity of the computational model with the overlapping hydraulic pressure data. Initial conditions of the computational model prescribe a depressurized and stationary system; the experimental system as depicted in Figure 26 has been operating prior to 0 seconds. This accounts for the discrepancy seen between the two simulation modalities in the first 10 seconds of Figure 26. Nonetheless, the computational model effectively simulates the pressure response to compliance set point

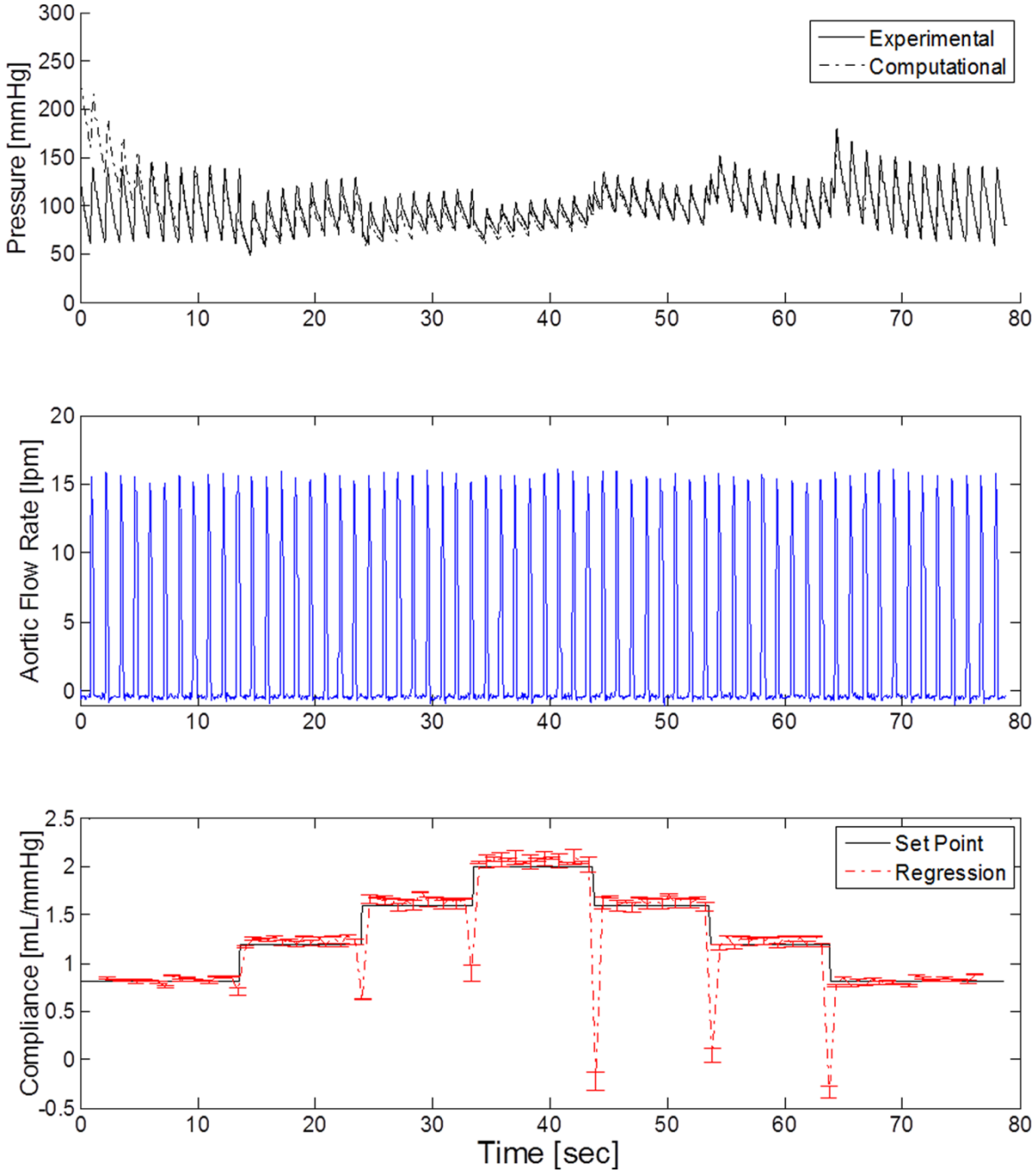

Figure 26: Experimental performance of the compliance chamber process controller. The pulsatile flow settings were 50 bpm, 30% systole and 80ml stroke volume. The peripheral resistance was simulated to be equivalent to a 0.022 in^2 hydraulic orifice. The first plot includes the fluid pressures of the experimental and computational models. The middle plot contains the flowmeter data, which is interpreted as left ventricular output. The bottom plot indicates the curve slope used to control the compliance and the determined slope from regression analysis. The calculation of the compliance through linear regression of the pressure-volume curves is plotted against the setpoints to illustrate the performance of this controller.

transitions and maintains an accurate representation of the physical systems performance.

The successful construction of the computational model was based in the parameter estimation of component values and the PI controller tuning. The estimation of the spring constant for the element modeling the membrane equivalent piston force contribution was found to be 0.01 lbf/in. This is consistent with the pressure produced by a circular membrane with a low elastic modulus. The pneumatic valve controller dead space was determined via parameter estimation, and was found to be in the control signal region of 2325 mV to 2490 mV. The PI controller values resulting from the tuning were -200.5 for the proportional gain and -24.8 for the integrator gain, in a parallel design [110]. A clamping method was found to be the best means of anti-windup for the integrator. The results of the parameter estimation and controller tuning aided in the construction of the high fidelity model and precise controller design, respectively.

The computational model was an excellent development tool with respect to system component selection and diagnosing experimental performance issues. The pneumatic valve selection was a direct consequence of diagnosing the inability of the solenoid based valves to perform in this system. The fidelity of the model allows for parameters of the computational network to be measured easily during the design phase. In the case of the valve selection, the flow rate could easily be determined in the computational model and identified as a crucial parameter in the selection of an appropriate valve. The computational model was important in determining the minimum controller update frequency, and gain values, for the range of cardiac conditions to be simulated. The final compliance chamber performance benefited directly from the in silica design testing achieved with this computational model.

The numerical model provided a precise PI controller design that proved successful at regulating the compliance in the model. The experimental results echoed this success, and

showed the same level of performance. The physical model implementation of the controller design exhibited the same characteristics of fast set point rise time and disturbance rejection in maintaining the set point. The response time in the physical model is a not as rapid as in the computational model, but the performance still positions this design as a success.

The results of the controller performance are shown in Figure 26, through the implementation of a staircase compliance curve set point change. Compliance curves with slopes ranging from 0.8 mL/mmHg to 2.0 mL/mmHg in 0.4 mL/mmHg steps were executed, all with an intercept of 100mL. Regressions of the pressure-volume curve were taken for the systolic and diastolic time segments. These regressions provide the analysis of the controller's ability to maintain the curve dictated by the set points. The slopes, which are the compliance from the regression analysis, are plotted against the set points in Figure 26. Error bars were included to illustrate the precision of the controller in maintaining that compliance. The outliers of seen in the regression analysis occur at set point changes, which were anticipated. The capability of the system to migrate to a new compliance in the duration of one heartbeat was seen as acceptable. This performance is reflected in bottom plot of Figure 26; the regression results quickly assimilate to the set point after one transition beat. It was found that the controller was able to maintain a set point curve slope appropriately, and rapidly adapt to set point changes.

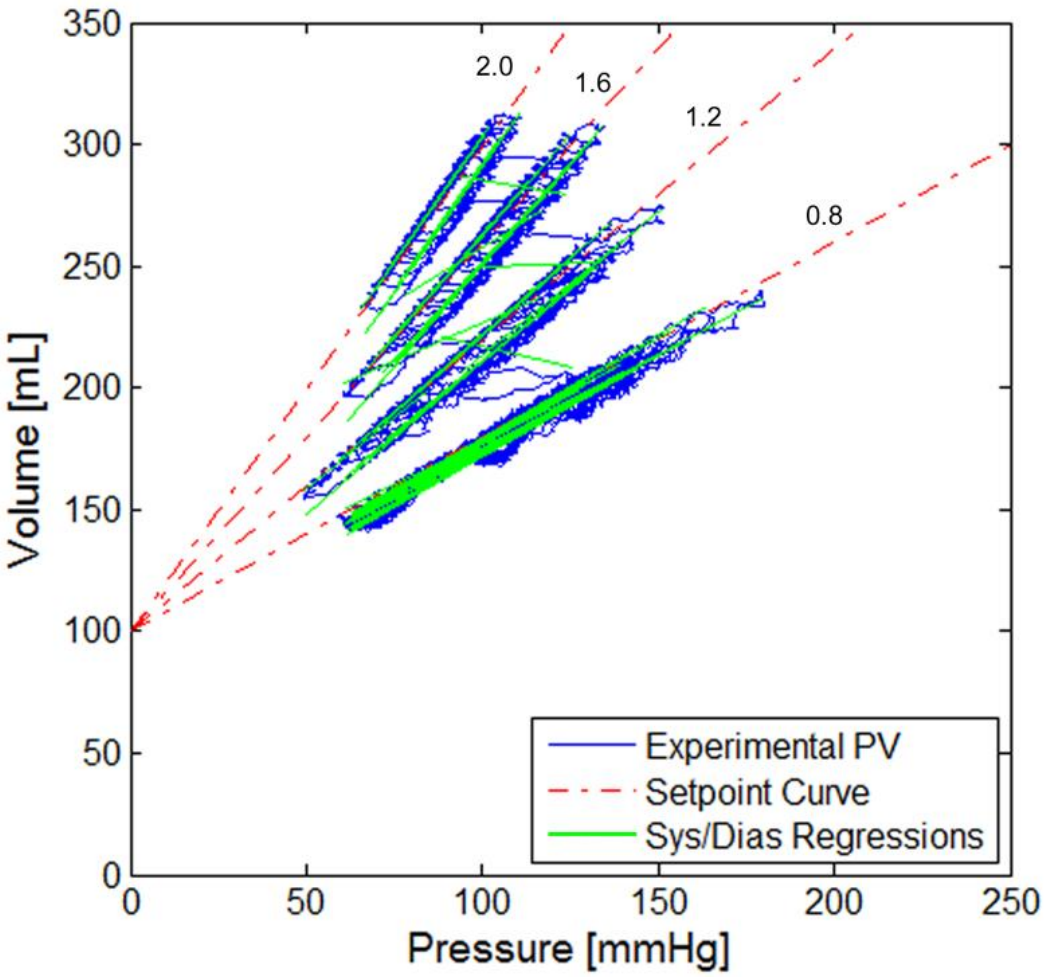

Figure 27: Compliance chamber pressure versus volume (PV) curves for the data presented in Figure 26. The dashed lines indicate the set point curves used to control the compliance. The black curves are the plots of the experimental PV. The light gray line segments represent the regression performed on the systolic and diastolic sections of the experimental PV curves. The numbers at the top of each set point curve indicate the slope of that setting. The black traces between the curves result from the controller'smigrating to a new curve. congruency of the set point, experimental and regression plots illustrate this control method's ability to accurately execute control of the system compliance using a curve-based set point method.

The pressure volume curves for the data presented in Figure 26 are shown in Figure 27 with overlays of the set point curves and the results of the regression analysis. This provides a clear representation of this control method's ability to effect system compliance changes and maintain a compliance curve during pulsatile flow. After the initial set point change, the system will operate on the new curve away from its steady state region. The assimilation of the system

to the steady state operating point for the new compliance is dependent on the pumping rate of the system, the peripheral resistance being simulated, and the compliance curve slope. The operating region for the volume distention has been determined to lie in the region of 50 to 250mmHg and 50 to 300mL. This region provides the appropriate driving pressure in the hydraulic region for volumetric expansion. The volume constraints maintain the shape of the membrane at the lower bound and a buffer region at the end of detection for the displacement sensor. Maintaining the system operation within this region provides the stability and control capability evident in the presented results.

The LabView interface developed for this application presents a user-friendly interface to the functionality delivered by this control design (Figure 28). The control panel for the compliance chamber includes a compliance curve read back panel that graphs the current volume of the membrane to the hydraulic pressure in the system, with an overlay of the set point curve currently in effect. A reset button allows the graph to be cleared when a new compliance curve is selected. Inclusion of read backs on the valve activity is presented in a dial gauge for reference, and detection of a failure in the controller. A process controller activation switch is included to provide a safety cutoff in the event that the controller becomes unstable. Inputs for the curve slope and intercept offer the option to change the compliance in real-time. The controller's integrator value is able to be set to a particular value, and is set to zero on the execution of a new curve to reduce the rise to set point time. The read back on the integrator value is available as a diagnostic tool for monitoring controller performance. The maximum update rate afforded by the script is 8Hz. This is also the rate at which the read backs on the valve activity and controller state are returned.

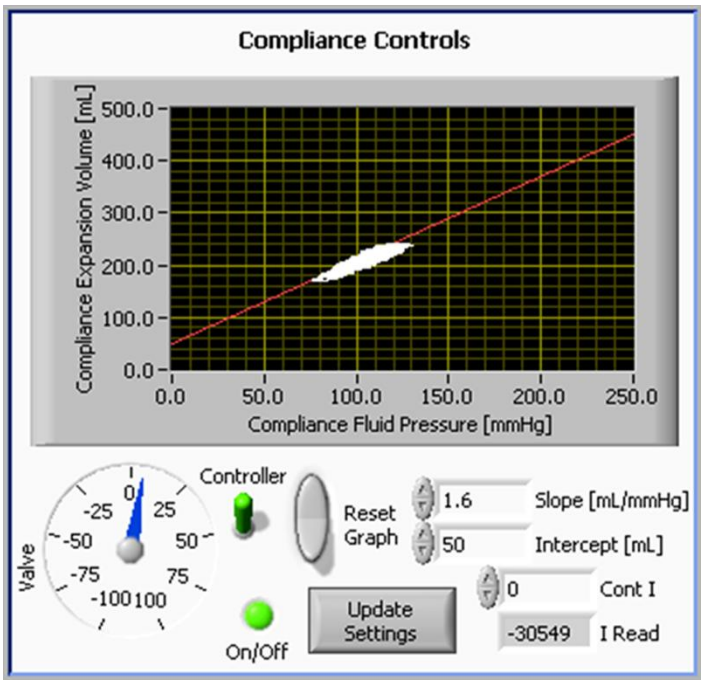

Figure 28: LabView control panel for the compliance chamber, during an experiment. The compliance graph presents the current volume-pressure value present in the chamber (white) with the set point curve overlaid (gray). The dial gauge indicates the valve opening in percentage; negative indicates venting and positive corresponds to positive pressure opening. A switch to activate or deactivate the controller is included for safety in the case of instability, or for investigations without compliance control. The led indicates that the controller is appropriately enabled or disabled. The reset graph button clears the compliance graph at the top, which is useful when a new compliance curve is actuated. The inputs in the lower right are for the compliance curve of interest; slope and intercept pertain to the volume-pressure curve that is to be followed by the controller. The ability to set and read the integrator value is useful in expediting controller response and monitoring controller performance, respectively. The update settings button communicates to the MCU the controller state and the curve values to be used.

3.1.3 Harvard Pump

The computational model of the design was utilized in the design process for both algorithm development and design validation (Figure 29). Simscape™ toolboxes were used extensively in the construction of the three physical domains present in this device; electrical, mechanical and hydraulic. Prototyping the design in this environment allowed for in silica evaluation prior to prototyping, and fine tuning the model with Parameter Estimation provided the high fidelity computational model for controller development.

The physical model contains the subsystems pertaining to the electrical voltage supply, motor model, driveline of the pump, and the hydro-mechanical interface of the pump head. The electrical voltage source was developed for this project using the SimElectronics® toolbox and the Foundation Library elements. Particular design work was performed on the inrush current limiters (ICL) used to regulate the initial current supplied to the smoothing capacitor. The desired performance was a fast charge of the capacitor, while preventing an overload on the outlet providing the AC voltage.

The model of the shunt wound model delivered in the Simscape™ package does not allow for the independent variation of the armature and field voltages. The motor model had to be developed from literature and basic elements of the Simscape™ Foundation Library [111]. The final model is presented in Figure 29, with the variables for the elements being determined directly through experimentation or by means of Parameter Estimation. This shunt wound numerical model provides the functionality of constant field voltage with the ability to change the armature voltage for speed control. It also models the nonlinear speed-torque curve that is characteristic of shunt wound motors.

SolidWorks (Dassault Systemes, Paris) was employed in the reverse engineering of the driveline (Figure 13). The SimMechanics™ Link allowed the SolidWorks geometry to be imported into Simulink™ as a SimMechanics™ body; interfaced between the mechanical elements of the motor driveshaft and the translating hydro-mechanical element representing the pump piston (Figure 30). This model allows the change of the pivot point location that dictates the stroke volume; creating an accurate working representation of this driveline. The pump head model was constructed with elements from the SimHydraulics toolbox to represent the geometries and fittings present. Included are sections of flow path size transition, ball valves and

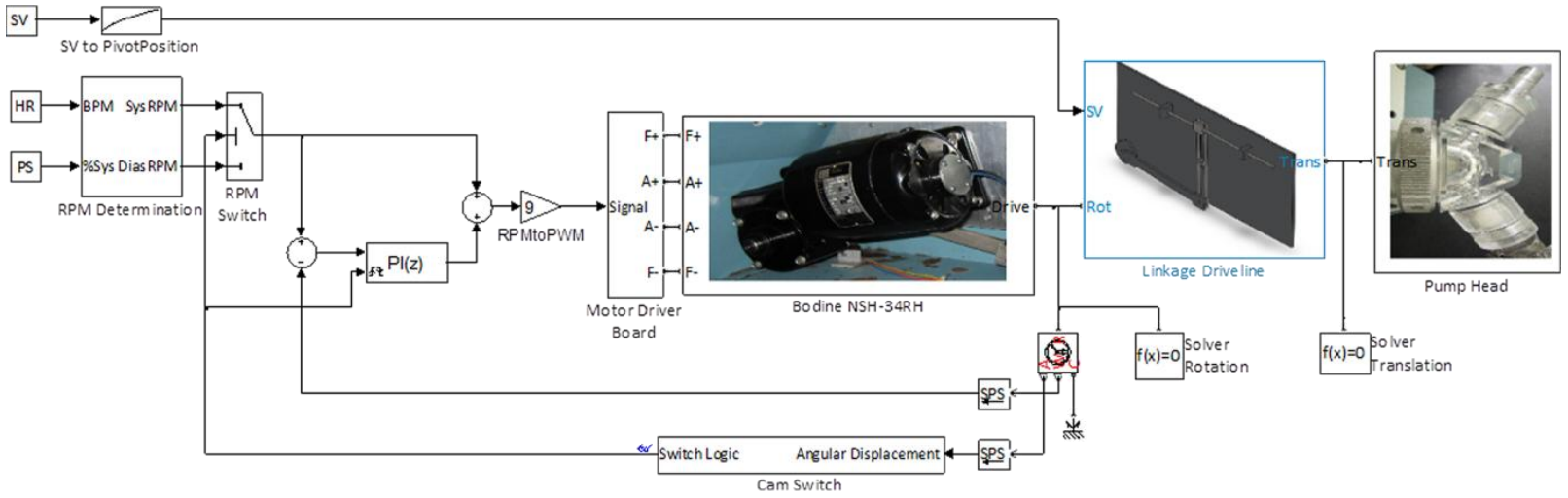

Figure 29: Simulink™ model of the Harvard Apparatus Pulsatile Blood Pump. The subsystems that comprise the larger model are presented with masks to illustrate the physical assembly they represent. Operating parameters are set on the left side of the model; stroke volume (SV), heart rate (HR), percent systole (PS), and the power switch ON/OFF logic. The RPM determination block uses Equation 1 and Equation 2 to produce the required RPM settings for each phase of pumping. The "SV to PivotPosition" lookup table in the upper left is an application of Equation 3, providing the setting position from the SV value. The cam switch block actuates the RPM switch to enact the correct RPM setting. The PI controller operates on the error of the setpoint delivered from the preceding RPM switch and the driveshaft speed read back from the rotary encoder. The controller reset (lower left of PI block) is enacted by a change in the cam switch state, allowing the feedfoward control from the RPM switch block to dominate the speed change in the motor. The model has no outputs as the hydrualic system this is connected to would need to be modeled. The pump head block represents the translation of the piston and the friction pertaining to that motion.

sudden flow path size changes. The values used in the model were derived from direct measurement of the pump head geometry to provide initial estimates, and Parameter Estimation was used to reach the final values.

The final model produced an accurate depiction of the updated Model 1423 operation. It allowed for sensors to be placed in the computational model to better understand the operation of the electrical and mechanical subsystems during operation to ensure their proper design. The input parameters for the model are power switch, stroke volume [mL] desired, heart rate [BPM], and percent systole. It was desired that the inputs for the model would be analogous to the device settings for ease of testing, and for future determination of operating points for prescribed conditions.

The Microchip Technology Inc. (Chandler, AZ) PIC18F2550 provided the features that were required in the design of the Model 1423 automation [112]. The MCU has a native capture, compare and PWM (CCP) module that was used for control of the pump motor [113]. The capture function of the CCP module was used to register the transition timing from an optical encoder attached to the pump motor driveshaft for the purpose of RPM measurement. The MCU also included onboard analog to digital converters (ADC), which were used to monitor position potentiometers and electrical board supply voltages. The key element to the controller was the universal asynchronous receiver/transmitter (UART) module. This interface provides the means of digital communication with the device, the primary objective in the automation of the Model 1423. A UART to USB converter was implemented to enhance the connectivity of the instrument to computer platforms, as RS-232 connections are not common on modern hardware. Multiple timer modules allowed for synchronizing events and sampling of data during the

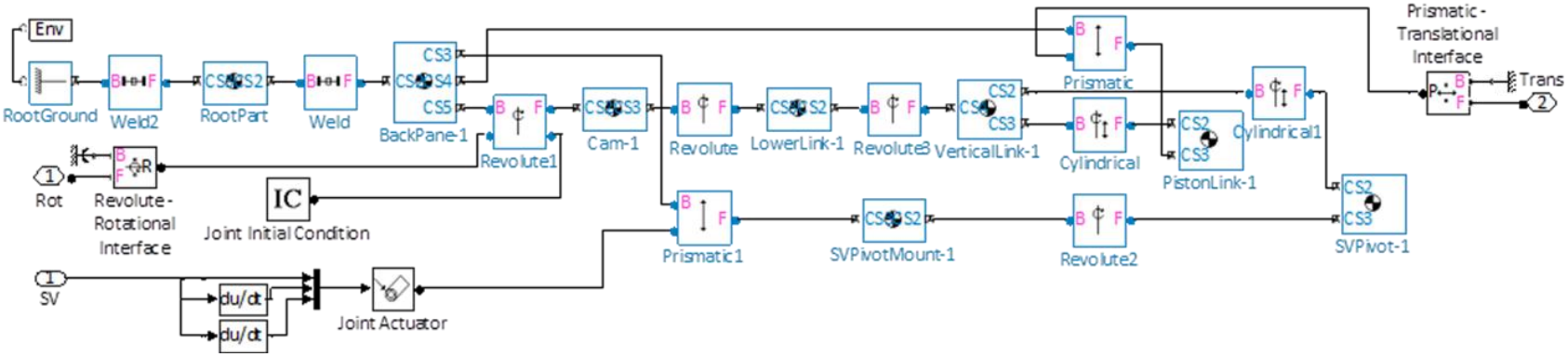

Figure 30: Simulink™ SimMechanics™ equivalent of the SolidWorks model presented in Figure 13. The light gray elements in this model were created and connected automatically from the SimMechanics™ Link. These blocks represent the rigid bodies and constraints equivalent to the SolidWorks parts and assembly; the rigid bodies can be identified as those containing the center of gravity symbol. The black elements were added to interface the SimMechanics™ blocks with the model, and provide an initial condition for the geometry. The "rot" connection on the left of the figure is interface of the motor driveshaft to the linkage and the "trans" connector on the right of the figure is where the hydraulic piston is connected. The joint actuator for the pivot point controlling the stroke volume (SV) necessitates the inputs of control parameter.

runtime program, which provide crucial stability to data processing and allow for consistently timed read back updates.

Speed control of the pump motor is enacted through a H-bridge PWM drive design. This method was chosen for its precision in motor speed actuation, compatibility with the MCU motor driving functionality, and ability to provide active braking. The H-bridge product employed was an ADVANCED Motion Controls® (Camarillo, CA) 25A20DD, driven by the CCP module on the PIC18F2550. A shunt regulator was employed with the power supply to prevent overcharging of the motor driver board supply voltage. Although the 25A20DD includes opto-isolation and gate drivers, the PIC18F2550 was not capable of sourcing the current needed to drive the device. The 50mA supply current requirement to drive the opto-isolators on the 25A20DD necessitated the use of low-side gate drivers between the MCU and the motor driver board. This implementation serves to provide adequate wattage for the application, and provides an additional level of isolation protection for the low voltage MCU.

The torque load on the driveshaft of the motor has a wide range of variability, which necessitates a control design that can provide the disturbance rejection to maintain the requisite RPM. A closed loop PI controller with a feed-forward section was implemented (Figure 29). This controller topology allows for low volatility set point maintenance with the PI section and fast adaptation with the feed-forward section. The feed-forward section takes advantage of the systems excellent open loop control potential, but needs the set point maintenance after the RPM change. At an RPM set point change, the PI controller is reset to prevent overshoot from rollover error.

The error signal feeding the PI controller is taken from the RPM determination using the CCP module's capture of the optical encoder data on the driveshaft, subtracted from the RPM

setting for that pumping phase. The optical encoder provides a quadrature-based data sequence created by the optical wheel motion through the sensors. In this application, only one channel is being monitored due to the unidirectional motion. The sensor has 1000 counts per revolution (CPR); allowing for adequate time resolution of speed change. The capture module interrupts at every 4^{th} pulse; a faster capture rate caused too many interrupt events at high RPMs that interfered with the MCU processing. This capture rate equates to a 1.44 degree resolution of movement on the driveshaft. This precise RPM feedback with a high refresh rate enables the PI controller to react appropriately to torque changes, providing excellent disturbance rejection.

The feed-forward section of the controller is driven by the cam switch and uses the RPM equations stated to predetermine what the RPM setting should be for that pumping phase. This set-point is added to the PI controller output and this sum is scaled to the 10-bit duty cycle input to the PWM module. Feed-forward topology was implemented due to the failure of classic PID architecture, even with gain scheduling, in accomplishing the rapid set point with minimal overshoot. This design takes advantage of the excellent open loop gain that this system exhibits, but adding the needed closed loop control to maintain the set points during changing shaft torque loads.

The equivalent BPM and percent systole of the pump is monitored by a timer module that tracks the transitions of the switch actuated by the cam mounted to the driveshaft of the motor. The rising edge of the switch pulse signals the start of systole, with the fall indicating the return to diastole. The following rising edge signals the beginning of the next systolic phase, and the conclusion of the previous cycle. The capture of these three times provides the values for calculations of BPM and percent systole. These values for heart rate and percent systole are those returned when the MCU is queried for performance values.

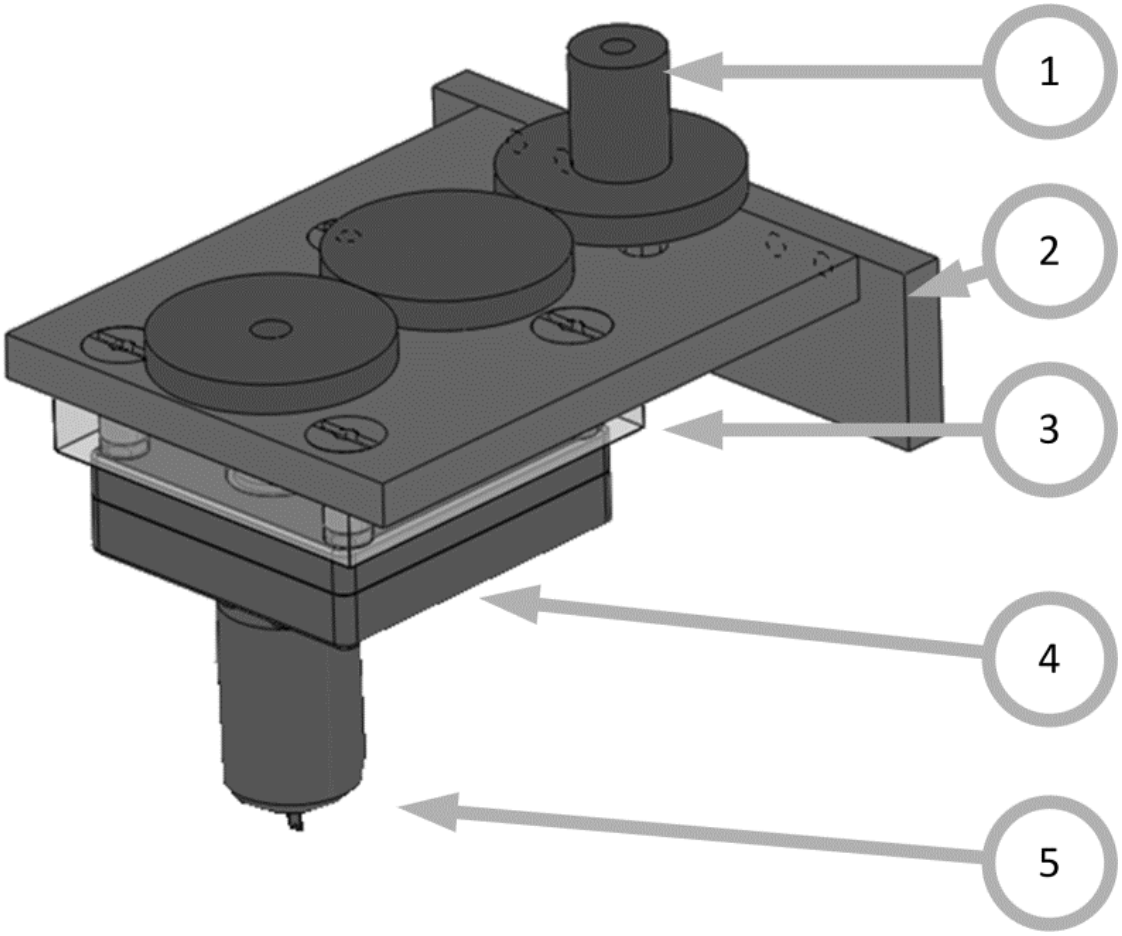

Figure 31: CAD model of the stroke volume actuator at an isometric view showing the top of the assembly. The gears are presented as cylinders with radial size equivalent to the pitch diameter. The interface of the actuator to the stroke volume lead screw (1). The backpane in this drawing (2) has been truncated to show only the section used for mounting the stroke volume actuator. The full backpane supports the drivetrain shown in Figure 2. The elements of actuator motor assembly are a mounting spacer (3), gear box (4), and DC motor (5).

This pump motor control design and sensor data created a platform capable of executing the precise shaft speeds needed to obtain the heart rate and percent systole performance needed. The confluence of updated motor driver board electronics and PI controller with feed-forward design produced a highly responsive electromechanical system capable of maintaining the set points through varying load conditions. This strong disturbance rejection and fast set point adaptation is critical to achieving the performance needed in this application, which was found to come only with the combination of the stated methods and hardware.

The stroke volume automation necessitated the addition of an electromechanical actuator to drive the lead screw assembly employed by Harvard Apparatus. The design of the stroke volume actuator sought to reduce invasiveness to the existing structure, and preserve the functionality present. It was also desired that the actuator and position sensors be contained within the case for aesthetics and splash guarding. The actuator design was chosen to be a geared DC motor with a gear train driving the post of the lead screw. Due to the internally mounted design feature, the interference of the assembly with the pumps linkage driveline and space constraints with the external case produced the cantilever mounting of the motor (Figure 31). The installation of the motor, gear train and bracket was achieved by removing the pump mounting pane from the case. No modifications were made to the linkage driveline; only clearance holes were drilled through the mounting pane. The DC motor chosen was a high torque (15 lbf-in) low speed (60 RPM) design, as the measurement of torque needed to drive the stroke volume change could not be measured. A gear train was chosen as the easiest means of working within the small clearance space provided. This design ensured that the torque of the motor would be adequately transmitted to the post. The ratio of the gear train is 1:1, due to the strength of the motor. The size of the gears is reflective of the distance from where there was room for motor in the case to the position of the lead screw post.

Stroke volume setting determination is achieved via a linear potentiometer connected to the pivot point of the driveline linkage. This potentiometer is monitored by one of the ADC channels on the MCU, with position updates every 100 ms. This update rate was chosen based on the determined speed of the stroke volume actuator and resolution needed for this information. The movement logic of the stroke volume is such that upon startup, the current position becomes the set point to eliminate initialization movement. The movement of the stroke

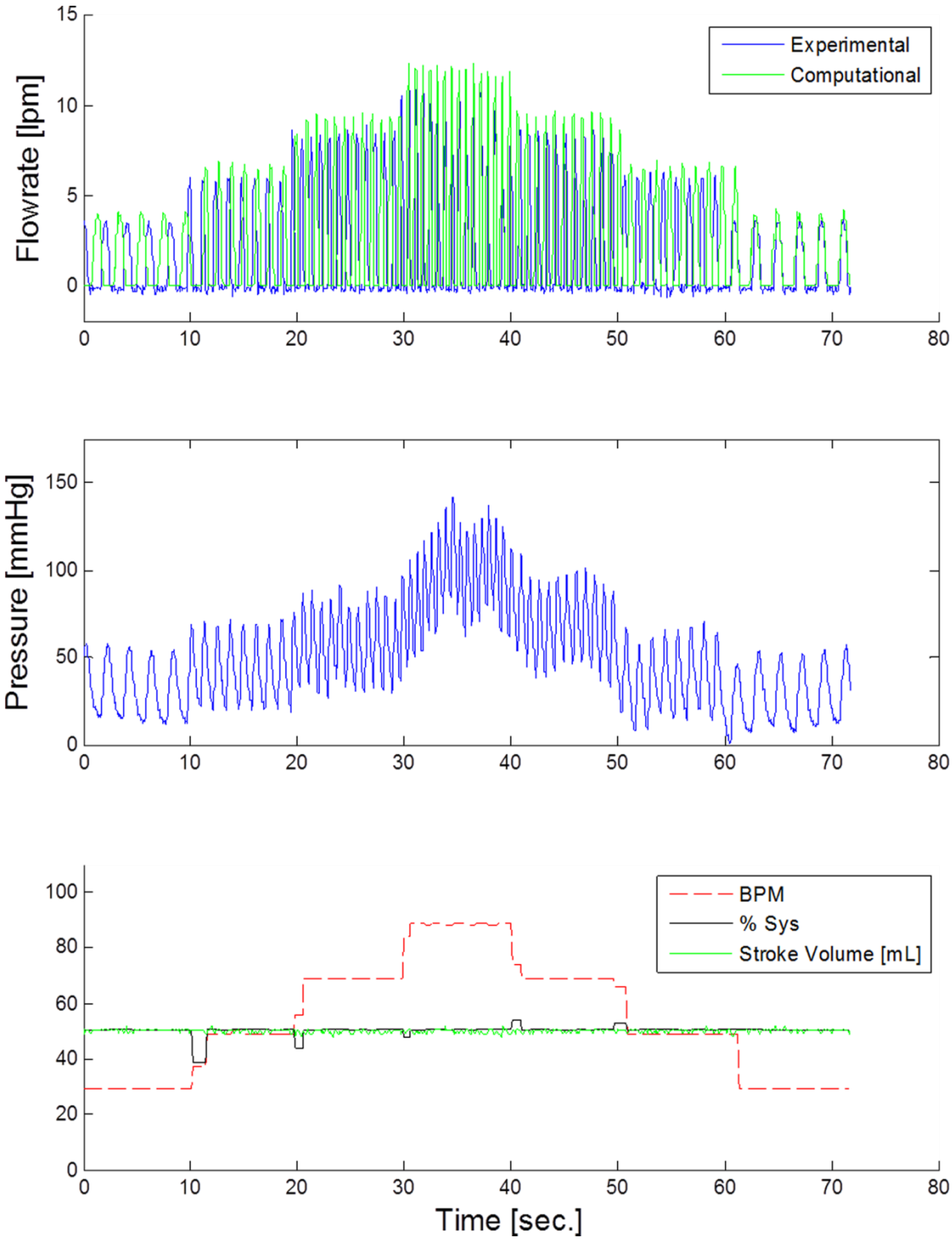

Figure 32: Harvard pump output with a staircase change in heart rate, while maintaining 50% systole and a stroke volume setting of 50mL. The lower trace indicates the read backs from each of the parameters, which were used as inputs to the computational model. The spurious values in percent systole and BPM at some of the transitions are due to the change to the new speed values mid pumping cycle.

volume actuator is monitored by a 10 Hz check on the value of the current position against the set point, with a test condition against an error limit. If the error is outside the prescribed limit, the motor moves in the appropriate direction until the error is within the limit. Communication update of the set point changes the error limit to zero, initiating movement. Upon a condition of zero error in the position to set point, the motor is stopped and the error limit is widened. This error limit window technique is in response to slight movement in the pivot point during pumping, and the lack of electronics shielding in the prototype design leading to spurious ADC values.

The heart rate control of the pump through the implementation of embedded control logic was successful. The ability of the MCU to control heart rates over a range of values is shown in Figure 32. The rapid change to a new heart rate set point and the maintenance of that value is clearly shown. Anomalies are present at set point changes, but are consistent with the effects of changing speed mid pumping cycle. The slight variation in the read back values indicates that the system is capable of detecting the natural variability of performance in this mechanical system.

The flow rate and pressure responses of the MCL to only a change in heart rate were consistent with this parameters effect. The flow rate peaks increased in frequency and magnitude, which validate the increased pumping frequency and rate of ejection. The average hydraulic pressure rose proportionally to the change in the heart rate, as would be expected with a change in cardiac output against a constant compliance and peripheral resistance. However, the pulse pressure remained consistent due to the maintenance of the percent systole, constant stroke volume, and constant arterial compliance value. This sensor data independently confirms

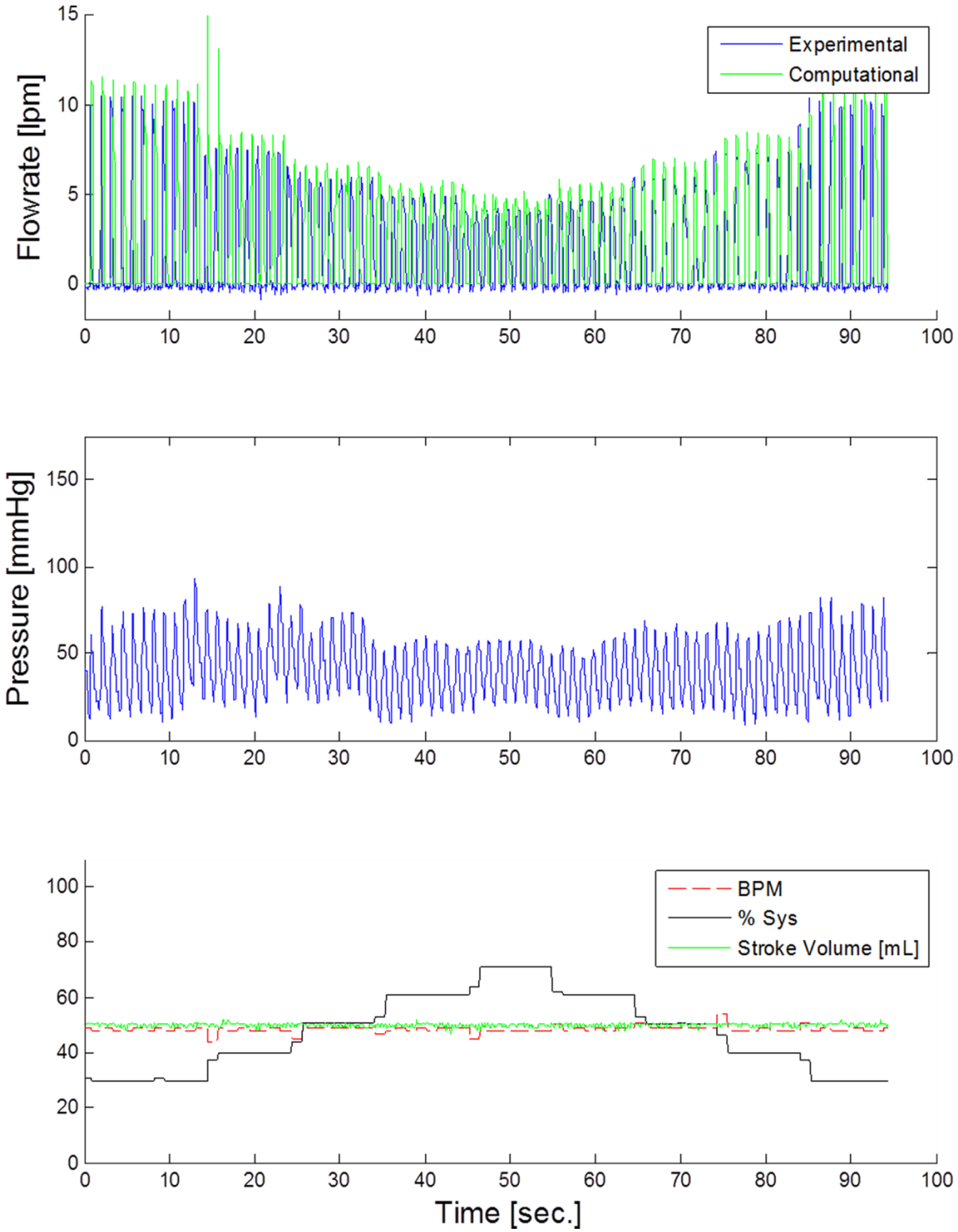

Figure 33: Harvard pump performance percent systole performance. 10% changes in percent systole from 30% to 70%, and back, with constant heart rate and stroke volume were performed. The spurious read backs at the transitions are due to the speed changes mid stroke. These events are exacerbated in the computational model due to the simulated system response to these perceived rapid changes.

the performance of the pump to that of the performance data returned from the pump MCU.

The speed set point maintenance in each phase of pumping needed for accurate percent systole control was achieved, with the performance illustrated in Figure 33. The rapid adaption from the feed forward control utilized in the shaft speed control allows the rapid change in RPM needed for each phase transition, while ensuring the speed is maintained through that phase. This process control is shown to have a successful implementation for this application, and is capable of ensuring the performance of the pump within the percent systole settings region of interest.

The sensor data gathered from the MCL confirms the percent systole change performance. The flow rate peaks increase in magnitude, but not frequency, which is consistent with the faster ejection rate and maintained heart rate. The pulse pressure is reduced when nearing 70% systole; pressure development in the system is impacted due to the low systolic flow rate. This is consistent with the constant compliance, unchanged stroke volume, and constant resistance. This confirmation of performance in MCL ensures that the read backs from the pump MCU are consistent with the hydraulic sensor data.

The stroke volume actuation and control was confirmed by the results in Figure 34. This performance validation illustrates the ability to achieve stroke volume values across the broad range provided by the mechanical design of this pump. The seamless return of stroke volume values in this illustration indicates the resolution in position, even during movement of the actuator, which is able to be achieved. The characterization of the stroke volume mechanism was integral to this precise control. It was found that a second order polynomial fit ($R^2 > 0.99$) provided a sufficient means of correlating the distance travelled from the 15mL stroke volume position to the stroke volume setting.

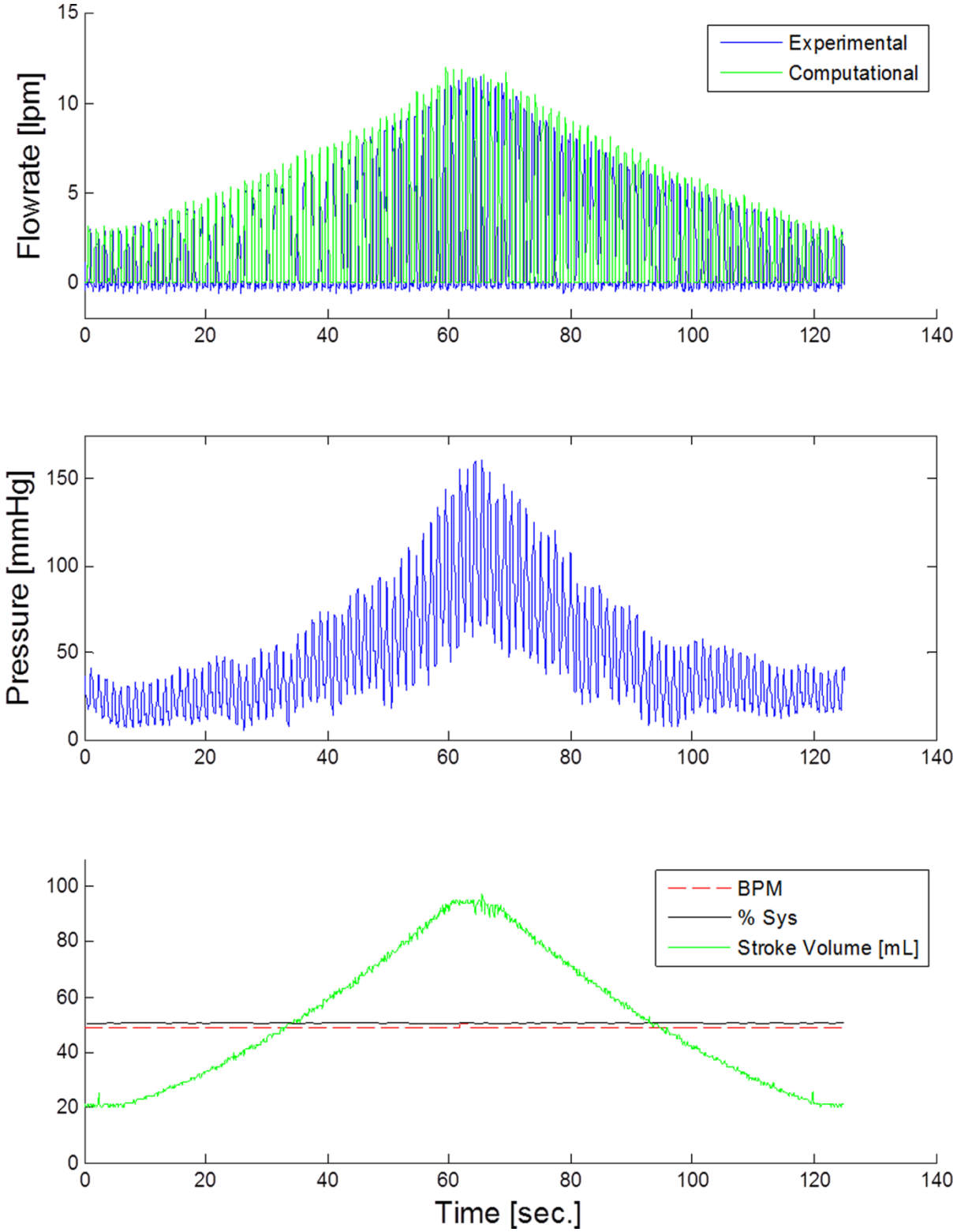

Figure 34: Harvard pump functionality of the stroke volume change is illustrated by the continuous change from 20mL to 95mL, with heart rate and percent systole remaining unchanged.

Equation 11

$$Stroke\ Volume\ [mL] = 8.875\,x^2 + 14.192x + 15.523$$

$$x = distance\ of\ indicator\ in\ inches\ from\ 15mL\ mark$$

The change of stroke volume in the MCL was consistent with this parameters effect in the system. The flow rate peaks increased in magnitude proportionally to the change in stroke volume. The average pressure and pulse pressure increased due to the change in cardiac output and ejection rate. The nonlinear change in the conditions coincides with the shape of the stroke volume curve, which in turn is effected by Equation 11 and the constant speed of the stroke volume motor. The equivalent translational speed of the stroke volume pivot point determined from the motor speed and gear ratio was 3.21 in/min. The unimpeded movement of the stroke volume movement during pumping validates that the stroke volume can be changed in real-time and that the actuation method is not underpowered. Stroke volume actuation is integral to simulating changes in cardiac output; the illustrated results from this validation indicate this modified designs capability in performing those simulations.

The computational model developed in the design of the process control of this pump was found to have a high agreement with reference to the physical system. Utilizing the read back information from the pump recorded from the in vitro experiments, these data traces provided the input settings time course for the computational model. The model was able to accurately simulate the changes in heart rate (Figure 32), percent systole (Figure 33), and stroke volume (Figure 34) conducted by the pump. The spurious read back values present at the settings changes, due to the change mid heart beat, increased the error in the computational model. This error was due to the erroneous read backs interpreted as sudden settings changes, which the computational model responded to. Another source of error in the computational model is the rounding present in the settings communications from the pump. The settings are rounded to the

nearest integer; this dampens the deviations in values and causes discontinuities. This issues is largely present in the percent systole and heart rate simulations; the stroke volume has enough resolution with the rounding for this to not have a noticeable effect.

3.2 Anatomical Models

The results of the anatomical models are highly qualitative, as the nature of their inclusion in this project is to facilitate the integration of this mock circulatory loop into other research. The depiction of the models at the various stages of construction is provided to provide a pathway to illustrate the construction process of the models.

3.2.1 Aorta

The development of the aortic model from the anatomical results was successful. The workflow presented for generating an in vitro model from human cryoslice data was successful. The rough boundary extraction from ITK-SNAP can be seen in Figure 35; the surface is rough due to the inaccuracy of the automated segmentation methods with cryoslice based data. Figure 36 presents the post-processed mesh of the model using Blender; the surface roughness was greatly reduced. This figure is a rendering of the model after being imported into SolidWorks. The model's cross sectional splines and tangent splines used to create the lofted model are presented in Figure 37. As can be seen, more cross sectional planes were taken at the aortic sinus, due to the more complex boundary shape at this section. The splines tangent to the centerline of the aorta were equally distributed around the perimeter of the lumen. Once the split part design was completed, the machining paths were successfully generated (Figure 38).

The fabrication of the model was successful and the PIV validation was successful. Figure 39 is one of the images taken during the PIV validation. The particles in the flow are clearly depicted. Figure 40 is a contour plot of the series of vector plots created from this

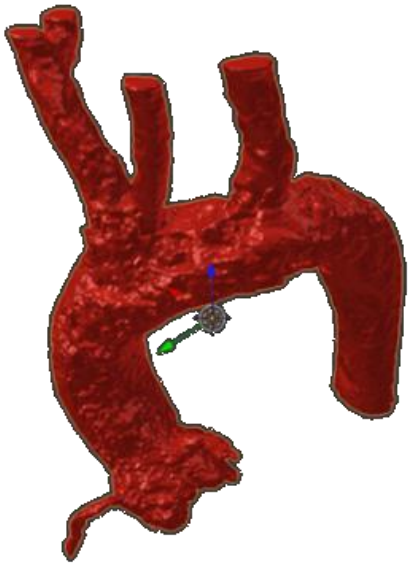

Figure 35: ITK-SNAP tracing results for aorta model.

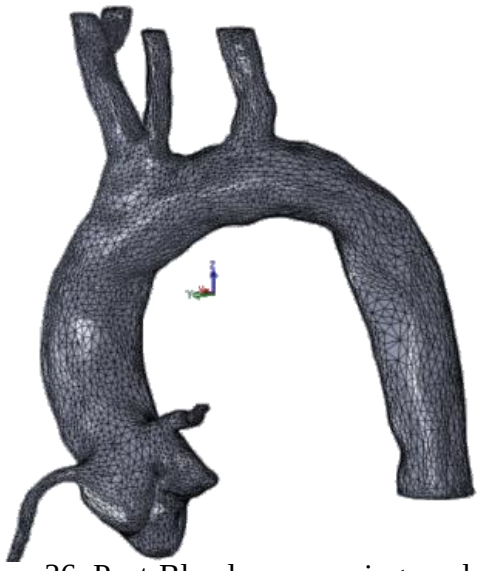

Figure 36: Post-Blender processing model in SolidWorks.

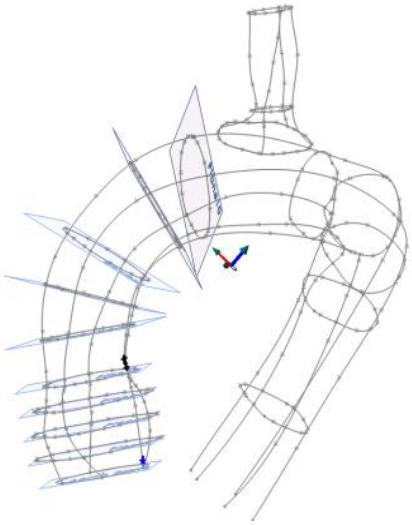

Figure 37: Boundary splines used to create lofted aorta model.

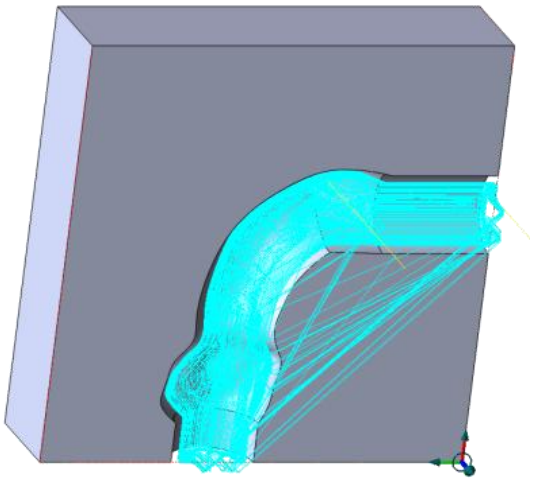

Figure 38: Machining paths used to cut ascending aortic geometry.

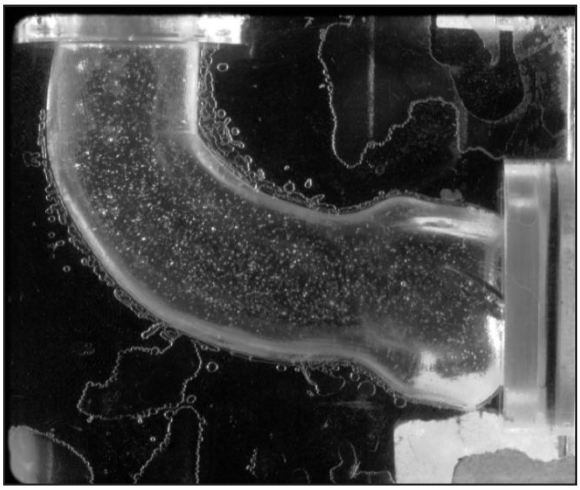

Figure 39: PIV image capture of flow through the aortic model, after exiting a tilting disc valve.

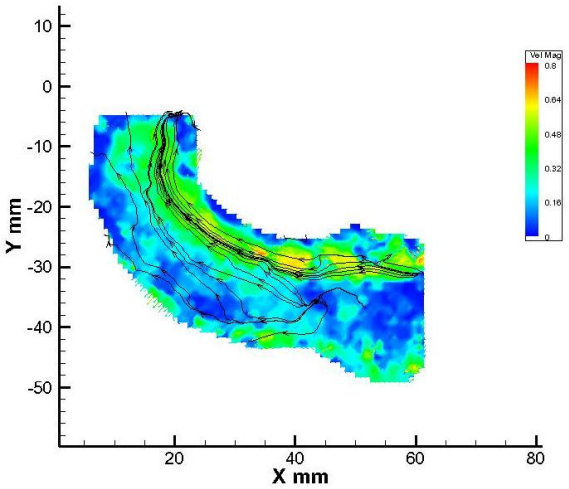

Figure 40: PIV contour plot with streamlines for flow through aortic model. This is the data generated from the image sequence that Figure 39 was taken from.

validation. The streamlines that are present are consistent with the orientation of the tilting disc valve and the exit flow from this prosthesis.

3.2.2 Left Atrium

The generation of the computer model for the left atrium was successful. The complex geometry of the left atrium was successfully extracted using ITK-SNAP (Figure 41 and Figure 42). The model was successfully processed in the same fashion as the aortic model to produce a lofted model shown in Figure 43 and Figure 44. The atrial appendage was captured in the image segmentation, but was truncated in the lofted model. The invaginations of this appendage could not be replicated in the machined model. The truncation was similar to what other groups have done when producing a left atrial model [57]. The left atrium model was not machined due to the lack of investigative need at the time of this project. With the lofted model completed, the steps to fabricate the model are fairly well developed and account for a small percentage of the model development workload.

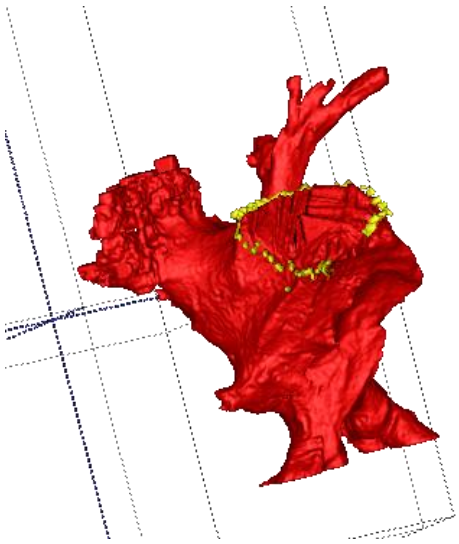

Figure 41: ITK-SNAP tracing results for left atrium from a inferior perspective

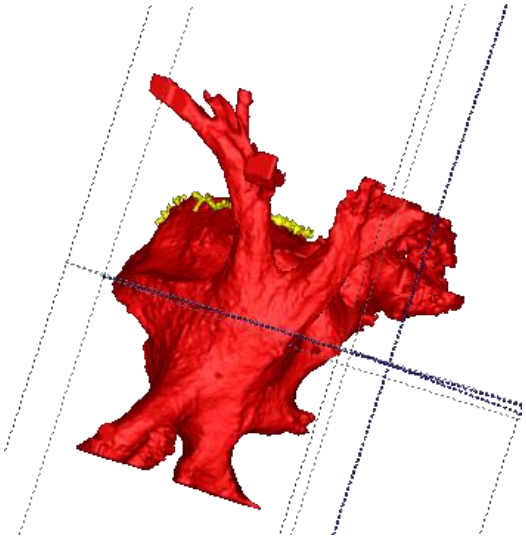

Figure 42: ITK-SNAP tracing results from a dorsal perspective. The pulmonary vein confluence can be seen, with the left atrial appendage in the upper left background.

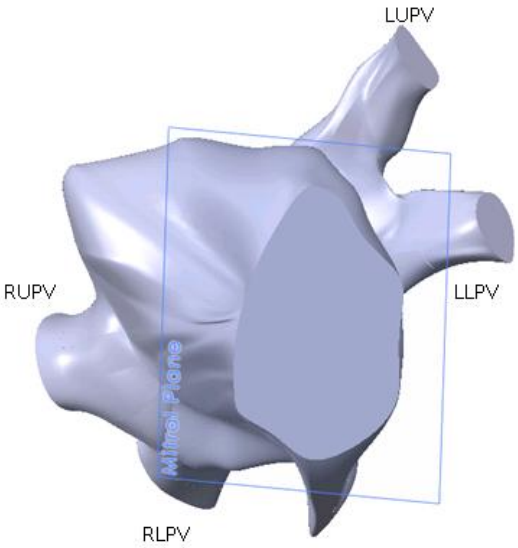

Figure 43: Left atrium model from the mitral plane perspective.

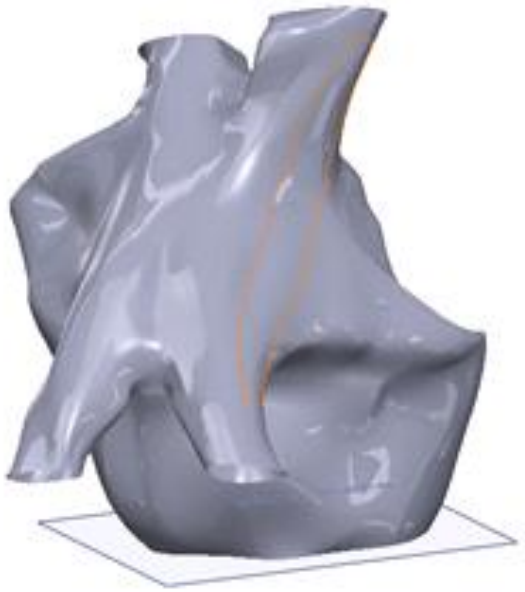

Figure 44: Left atrium model from an oblique dorsal perspective.

3.3 Mock Circulatory Loop

The validation of the mock circulatory loop was performed through the execution of functionality trials that built on the subsystem's performance validations previously discussed. The functionality was assessed by the system's ability to change multiple parameters simultaneously, and sequentially, to determine whether certain conditions could be constructed. These orchestrated events form the basis of the systems implementation and ability to achieve the specific aims of this project.

3.3.1 Computational Model

Using the computational models from each of the subsystem validations, the complete model of the mock circulatory loop was constructed. The architecture of the final model represents a plant and controller design (Figure 45). This enables the controller architecture to be separated from the plant, which is useful for code generation tasks. The controller code can be compiled to a target embedded system and the plant model could be deployed to an xPC target for HIL testing.

The execution time of the computational model is more than that of the experimental time in the MCL. Efforts were made to simplify the network, but due to the pulsatile and dynamic nature of the system, known acceleration tactics were not successful. The model does utilize local solvers for the physical model network of Simscape blocks with a discrete solver running on the remainder of the Simulink blocks. Simplification of the physical system was performed without much success, as the fidelity of the model was lost with replacement of complete physical models with kinematic or dynamic equivalents.

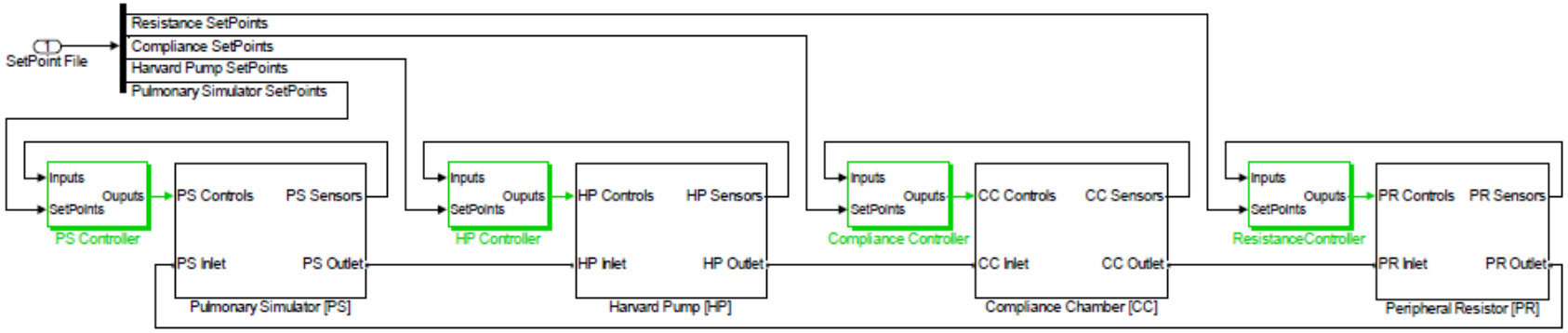

Figure 45: Numerical model of the mock circulatory loop. The control code sections are green, with the plant model elements grouped into black bordered subsystems.

3.3.2 In Vitro Conditions

The simulation of stationary conditions, settings that do not vary in time, is very successful in this system. As seen in Figure 46, the system is able to migrate to new set points for the systemic impedance and maintain the conditions faithfully. This is substantiated by Figure 47, which depicts the overlay of the sections from Figure 46. The similarity in the waveforms in Figure 47 nears the precision of the pressure sensor readings. The performance of the loop for single parameter changes for both cardiac and arterial settings was proven in the subystem validations (Figure 26, Figure 32, Figure 33, Figure 34). When changing settings, there is a period of assimilation in the pressure readings to the new operating point. When migrating from a higher mean arterial pressure to a lower one, there is a period in which the energy stored needs to dissipate. When migrating to a higher mean arterial pressure, the assimilation to the operating point is much faster as the energy dissipation is low and the input energy is high.

Dynamic conditions and events simulations that involve multiple parameter changes in runtime have also been proven in this system. Two challenge events that were simulated were a hemorrhage and a tacchycardic event. Simulating an arterial hemorrhage involves the sudden loss of pressure; a drop in peripheral resistance and an unloading of the soft tissue. This was simulated in the mock circulatory loop as a change in the peripheral resistor value and an increase in the simulated compliance (Figure 48). The transition to tacchycardia was simulated by a sudden increase in cardiac output, with a subsequent decrease in peripheral resistance (Figure 49). The successful execution of these two events communicates that this system can

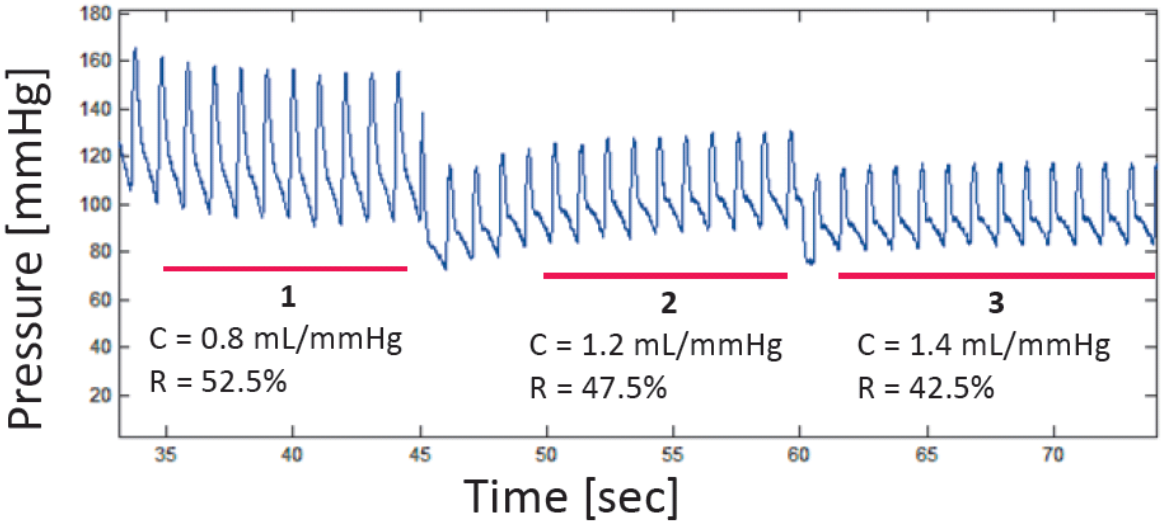

Figure 46: Illustration of arterial impedance change.

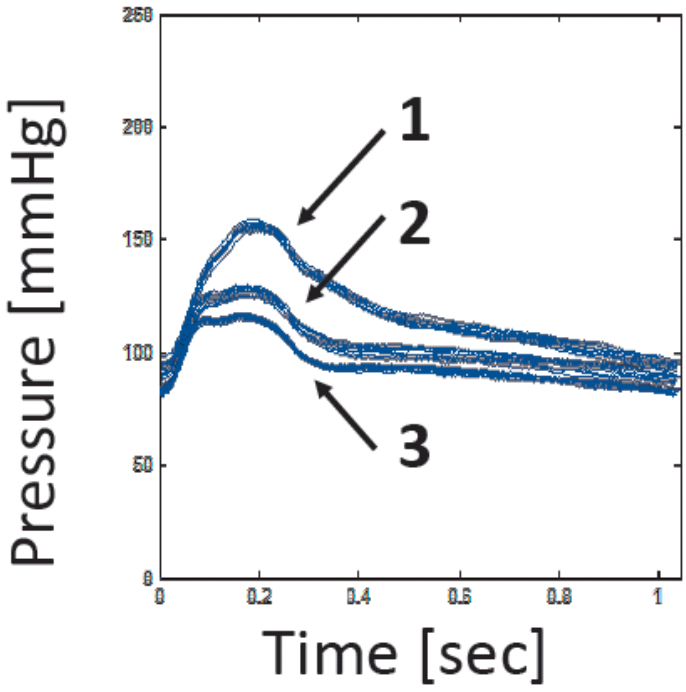

Figure 47: Pressure curve overlay at different arterial impedances, illustrating the reproducibility of the systems conditions. The numbered groups of curves coincide with the enumerated sections of Figure 46.

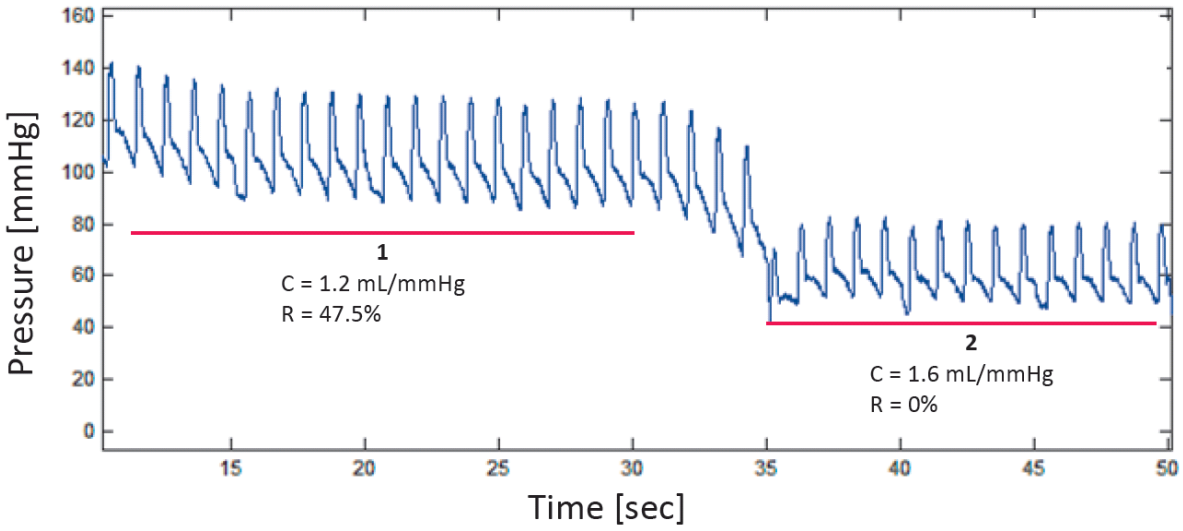

Figure 48: Simulation of a hemorrhagic event in the mock circulatory loop. Sudden drop in peripheral resistance with matched increase in arterial compliance due to the unloading of the soft tissue.

perform multiple set point changes in runtime. This capability allows this system to simulate event sequences and battery testing of conditions that were previously unachievable.

Simulation of patient data is presented in Figure 50 by both the computational model and the in vitro system. This figure also supports the fidelity of the computational model to that of the in vitro system. By using the parameter estimation methods from the Matlab toolboxes, it was found that there was difficulty in effectively modeling the entire waveform. The estimation routines placed emphasis on the catacrotic limb of the waveform, as this accounts for the majority of the cardiac cycle. This left the anacrotic limb underrepresented in the estimation routines. Coupled with the dynamics of the model during systole, it was difficult to establish a successful parameter estimation routine sequence.

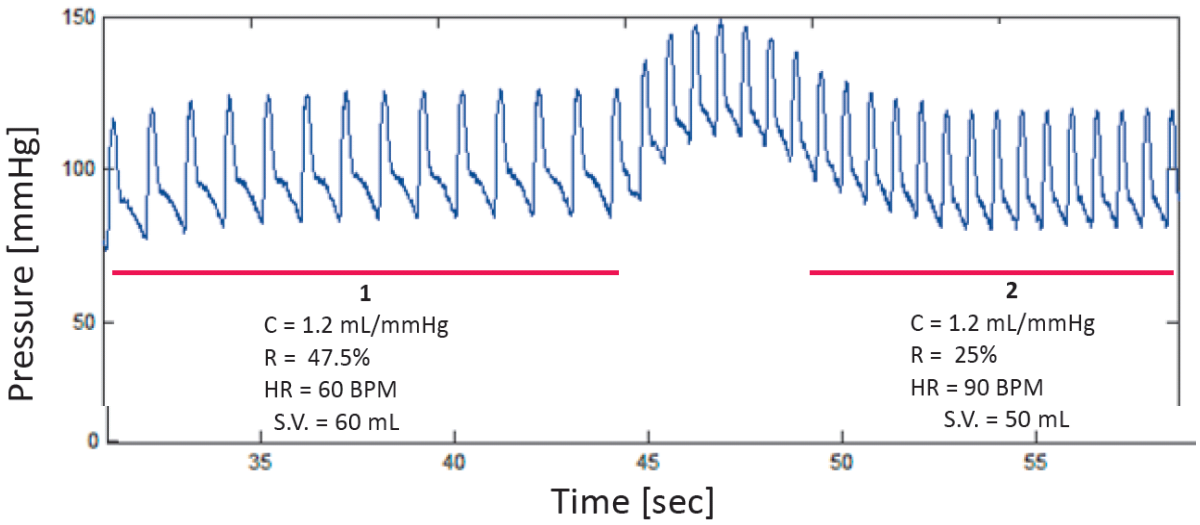

Figure 49: Tacchycardia simulation in the mock circulatory loop. Increase in cardiac output with adjusted peripheral resistance to reduce mean arterial blood pressure.

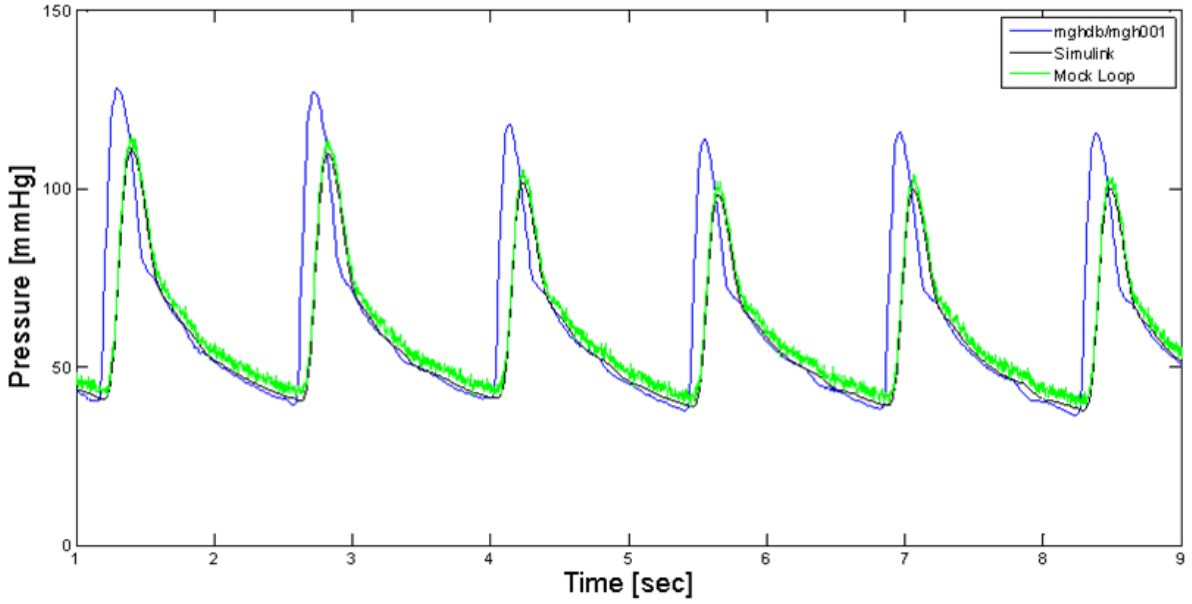

Figure 50: Simulation of PhysioBank patient data using computational model for setting parameter estimation and use mock circulatory loop to replicate the conditions in vitro. The parameter estimation algorithm was biased towards the catacrotic limb, due to the low time in systole for this waveform. Thus, the ability to accurately model the anacrotic limb was reduced.

4 Discussions

4.1 Peripheral Resistor

The importance of simulating accurate physiological conditions of blood pressure in mock circulatory loops is significant to effectively assessing cardiac assist technologies. The goals of integrating a high resolution resistor into the mock circulatory loop and construction of a numerical model of the device were successful. This has provided the capabilities of simulating peripheral systemic resistance to a high degree of accuracy, with the ability to determine operational settings in silico prior to experimental testing.

Real time position determination of orifice size through the read back on the piston position will provide the capability for system delay determination, and control logic capabilities for constructing accurate loop conditions. The use of parameter estimation via a computational model using experimental data as the optimization point is a powerful tool in characterizing custom assemblies.

The automated design allows for resistance changes to be made from a central control interface. The construction of the device provides a geometry that is capable of being controlled accurately, and will not deform over time. These advantages over pinch-tubing methods position this design as a reliable and robust resistor in the mock circulatory loop.

4.2 Compliance Chamber

Real-time compliance control through the use of the direct volume measurement method on the membrane, coupled with a process controller capable of effecting control of the volume distention, allows for a robust method of simulating arterial compliance in a mock circulatory loop. This method lends itself to the fully automated perspective being developed for the mock circulatory loop this assembly is integrated with. It also removes the dependence of inferring

compliance from initial pressure-volume measurements or translating pressure waveforms to estimate compliance changes actuated. The accuracy inherent in this design will expand the investigational capacity of the mock circulatory loop to include simulations of nonlinear compliance and the effects relating to real-time compliance changes. This compliance chamber positions itself as not only a precise experimental tool, but one with a high fidelity computational model.

4.3 Harvard Pump

The ability to remotely actuate condition changes, read back performance values during operation, and use of embedded logic to maintain set points creates a device capable of integration into fully-automated testing systems. Rapid updates to the set points of operation on the pump expand the investigative possibilities, including dynamic analysis. This evaluation of transitions in cardiac function is important in developing higher functionality in the designs of cardiac assist technology. An important facet of the upgrade is the performance read backs from the device during operation. This information is more useful than previous methods of relating results to the set points of the device. Deviation from the set points during operation are not a concern now, as the data obtained is relatable to precisely determined read backs on the performance of the pump. The development of the LabVIEW interface integrates the local upgrades of the pump with the larger data acquisition system for the mock circulatory loop into which this pump is incorporated.

Limitations of the current design pertain to the speed of the motor elements present in the pump. The shunt-wound technology employed for the pump motor is antiquated, and the motor is not as responsive as would be required for expanding the operating region. The migration to a permanent magnet motor of similar power characteristics provides the simplest upgrade in

performance. This motor technology is readily adaptable to the electrical driving board currently employed. Actuation of the stroke volume is not a rapid process, with beat-to-beat changes in set point not easily realized. With an investigation of the maximum torque required for this application, a faster motor could be selected. The refresh rate of the control elements would need to be increased to account for this speed change; this is a minor code revision of the present architecture. The current stroke volume actuation involves the disassembly of the device, which is not advantageous with the application of this upgrade to other pumps. A new technique of applying the stroke volume control should be investigated to allow for a bolt on mechanism for this actuation.

The success of this upgrade to the functionality of this pump has been quickly realized in the expanded capability of data collection in the mock circulatory loop. The rapid transitions to new conditions, and the capability of battery testing, have provided a wealth of functionality in the investigations employing this pump. Data resolution has increased with the elucidation of the precise performance of the pump during these tests, and transitions between settings has allowed for dynamic analysis of the technologies being evaluated. Convenience of the LabVIEW interface positions this upgrade as a user, and automation, friendly design.

4.4 Anatomical Models

The inclusion of anatomical models in the system expanded this mock circulatory loop's investigational application. Taking advantage of the excellent reproducibility that this system provides by using it as a conditions generator for PIV experiments, introduces many investigatory possibilities. Clinical conditions simulations with these accurate anatomical models can provide a wealth of knowledge on the anatomical structure impact on medical device performance. Utilization of the models generated in this work to pursue distensible models will

further the experimental acuity by enabling fluid structure interaction investigations to be performed. Ultimately, the execution of the anatomical work was to expand the studies this system was to perform and provide the workgroup with models that could satisfy many different investigatory needs. Both of these initiatives were met with resounding success.

4.5 Mock Circulatory Loop performance

The mock circulatory loop deployed from this work satisfies the specific aim of a high performance in vitro testing solution. As seen by the steady state and dynamic condition simulations, performance of the system in creating the necessary conditions for evaluating devices or constructing boundary conditions for flow experiments is high. The ability of the system to execute multiple set point changes simultaneously allows for complex events and sequences of conditions to be made rapidly. This capability paves the way for inclusion of control logic governing these settings that replicates the reflexes and physiological controls present in the cardiovascular system.

The Simulink model of the system delivers on one of the specific aim's of this research; provide a computational model that accurately represents the in vitro system. It was shown through the subsystem validations and the simulation of the PhysioBank patient data that the Simscape physical modeling packages allow for precise modeling of these multi-domain systems. The ability to design, simulate and deploy the code from this computational model positions this method as a highly versatile means of developing these complex systems. Ultimately, the acceleration of the computational model was not successful. The accuracy is predominantly due to the inclusion of the full analytical models for the components of the systems. Simplification and discretization of certain computationally intensive components was not successful; the fidelity loss was too great. An accurate model was of more interest than a

lower fidelity faster version. This is one of the known issues with this modeling package, and solutions to this issue may be forthcoming.

5 Conclusion

The objective of producing research tools that would enable investigations that were previously unachievable has been met. The computational tools, in vitro system and anatomical models that enable a range of investigations of conditions are in place. The connection of this work to the PhysioNet data sets allows future investigations to explore applications of this repository that begin to answer fundamental questions regarding the events that are contained in the patients recordings. It lays the groundwork for patient specific modeling during the testing of medical devices, which has become a focus of research for many medical device research groups. The successful creation of models based on the Visible Human Project anatomy connects the future in vitro work by this group to other research efforts based on this data. The connection of this work to larger initiatives was an integral part of the project, and has been deemed successful in its execution.

The products and methods that were utilized in the design and actuation of the mock circulatory loop components were novel applications of these software packages. The adaptation of these tools from proven applications in aerospace and automotive industries takes advantage of the long development by those industries in accurate simulation and robust control design techniques. Illustrating the use of these products in the biomedical field enables many researchers in this field with the capability to execute these high impact tasks on their own.

Future work for this system should take advantage of the range of operation for which this system is capable. Evaluations should include the assessment of left ventricular assist device performance during sudden events, such as those illustrated in the results. The assessment of device controller safety in these events is another avenue of investigation, which could be performed both with the computational model and the mock circulatory loop. The connection of

this system to a PIV system allows for extensive pulsatile flow studies to be completed; evaluation of device outlet flow through a wide range of cardiac and mock circulatory conditions could be performed. Ultimately, it is the extensive range of conditions and reproducibility of the waveforms that empowers the research delivered with this system.

6 Works Cited

[1] Fung, Y. C., 1997, *Biomechanics: Circulation*, Springer-Verlag, New York N.Y.

[2] Iaizzo, P. A., 2009, *Handbook of cardiac anatomy, physiology, and devices*, Springer, New York, NY.

[3] Fung, Y. C., 1993, *Biomechanics: Mechanical Properties of Living Tissues*, Springer-Verlag, New York.

[4] Costanzo, L. S., 2007, *Physiology*, Lippincott Williams & Wilkins, Philadelphia.

[5] Calfee, J. E., and Sudduth, G., 2011, "AEI OUTLOOK SERIES Are Medical Devices Turning the Corner against Heart Failure?," Health Policy, (2).

[6] Dolgin, M., 1994, *Nomenclature and Criteria for Diagnosis of Diseases of the Heart and Great Vessels*, Little Brown & Co.

[7] He, J., Ogden, L. G., Bazzano, L. A., Vupputuri, S., Loria, C., and Whelton, P. K., 2001, "Risk factors for congestive heart failure in US men and women: NHANES I epidemiologic follow-up study," Arch. Intern. Med., **161**(7), pp. 996–1002.

[8] Fonarow, G. C., Abraham, W. T., Albert, N. M., Stough, W. G., Gheorghiade, M., Greenberg, B. H., O'Connor, C. M., Pieper, K., Sun, J. L., Yancy, C. W., and Young, J. B., 2008, "Factors identified as precipitating hospital admissions for heart failure and clinical outcomes: findings from OPTIMIZE-HF," Arch. Intern. Med., **168**(8), pp. 847–854.

[9] Lilly, L. S., and Harvard Medical School, 2003, *Pathophysiology of heart disease: a collaborative project of medical students and faculty*, Lippincott Williams & Wilkins, Philadelphia.

[10] Dhillon, B. S., 2000, *Medical device reliability and associated areas*, CRC Press, Boca Raton.

[11] Patel, S. M., Allaire, P. E., Wood, H. G., Throckmorton, A. L., Tribble, C. G., and Olsen, D. B., 2005, "Methods of failure and reliability assessment for mechanical heart pumps," Artif. Organs, **29**(1), pp. 15–25.

[12] "Draft Guidance for Industry and FDA Staff Heart Valves - Investigational Device Exemption (IDE) and Premarket Approval (PMA) Applications."

[13] International Organization for Standardization, 2005, "Cardiovascular implants — Cardiac valve prostheses," ISO 5840.

[14] Marassi, M., Castellini, P., Pinotti, M., and Scalise, L., 2004, "Cardiac valve prosthesis flow performances measured by 2D and 3D-stereo particle image velocimetry," Exp. Fluids, **36**(1), pp. 176–186.

[15] Sun, W., Li, K., and Sirois, E., 2010, "Simulated elliptical bioprosthetic valve deformation: implications for asymmetric transcatheter valve deployment," J. Biomech., **43**(16), pp. 3085–3090.

[16] Sirois, E., Wang, Q., and Sun, W., 2011, "Fluid Simulation of a Transcatheter Aortic Valve Deployment into a Patient-Specific Aortic Root," Cardiovasc. Eng. Technol., **2**(3), pp. 186–195.

[17] International Organization for Standardization, 1987, "Centrifugal, mixed flow and axial pumps - Code for hydraulic performance tests - Precision class," ISO 5198.

[18] International Organization for Standardization, 2010, "Implants for surgery - Active implantable medical devices, Part 5: Circulatory support Devices," ISO 14708-5.

[19] Altieri, F., Berson, A., Borovetz, H., Butler, K., Byrd, G., Ciarkowski, A. A., Dunn, R., Griffith, B., Hoeppner, D. W., and Jassawalla, J. S., 1998, "Long-Term Mechanical Circulatory Support System Reliability Recommendation American Society for Artificial Internal Organs and Society of Thoracic Surgeons: Long-Term Mechanical Circulatory Support System Reliability Recommendation," Asaio J., **44**(1), p. 108.

[20] Lee, J., 2009, "Long-Term Mechanical Circulatory Support System Reliability Recommendation by the National Clinical Trial Initiative Subcommittee," Asaio J., **55**(6), pp. 534–542.

[21] Bramstedt, K. A., 2002, "Failure mode and effects analysis as an informed consent tool for investigational cardiothoracic devices," Asaio J., **48**(3), pp. 293–295.

[22] International Organization for Standardization, 2007, "Medical devices - Application of risk management to medical devices," ISO 14971.

[23] Wellstead, P. E., 1979, *Introduction to physical system modelling*, Academic Press, London.

[24] 2007, *Cardiovascular and respiratory systems: modeling, analysis, and control*, Society for Industrial and Applied Mathematics, Philadelphia.

[25] Yubing, S., Patricia, L., and Rodney, H., 2011, "Review of Zero-D and 1-D Models of Blood Flow in the Cardiovascular System," Biomed. Eng. Online, **10**(33).

[26] Conlon, M. J., Russell, D. L., and Mussivand, T., 2006, "Development of a mathematical model of the human circulatory system," Ann. Biomed. Eng., **34**(9), pp. 1400–1413.

[27] Liu, Y., 2003, "Design Of A Performance Test Loop For An Artificial Heart Pump," Master's Thesis, University of Virginia, Charlottesville, VA.

[28] Timms, D., Hayne, M., McNeil, K., and Galbraith, A., 2005, "A complete mock circulation loop for the evaluation of left, right, and biventricular assist devices," Artif. Organs, **29**(7), pp. 564–572.

[29] Legendre, D., Fonseca, J., Andrade, A., Biscegli, J. F., Manrique, R., Guerrino, D., Prakasan, A. K., Ortiz, J. P., and Lucchi, J. C., 2008, "Mock circulatory system for the evaluation of left ventricular assist devices, endoluminal prostheses, and vascular diseases," Artif. Organs, **32**(6), pp. 461–467.

[30] Widmaier, E., 2004, *Vander, Sherman, & Luciano's human physiology : the mechanisms of body function.*, McGraw-Hill Higher Education, Boston.

[31] Zappe, R., 1999, *Valve selection handbook*, Gulf Professional Publishing.

[32] Li, J. K.-J., and Zhu, Y., 1994, "Arterial Compliance and Its Pressure Dependence in Hypertension and Vasodilation," Angiology, **45**(2), pp. 113–117.

[33] Gregory, S. D., 2009, "Simulation and development of a mock circulation loop with variable compliance," Master's Thesis, Queensland University of Technology, Brisbane, Australia.

[34] Bank, A. J., and Kaiser, D. R., 1998, "Smooth muscle relaxation: effects on arterial compliance, distensibility, elastic modulus, and pulse wave velocity," Hypertension, **32**(2), pp. 356–359.

[35] Woodruff, S. J., Sharp, M. K., and Pantalos, G. M., 1997, "Compact compliance chamber design for the study of cardiac performance in microgravity," Asaio J., **43**(4), p. 316.

[36] Liu, Y., Allaire, P., Wood, H., and Olsen, D., 2005, "Design and initial testing of a mock human circulatory loop for left ventricular assist device performance testing," Artif. Organs, **29**(4), pp. 341–345.

[37] Rosenberg, G., Phillips, W. M., Landis, D. L., and Pierce, W. S., 1981, "Design and evaluation of the Pennsylvania State University mock circulatory system," Asaio J, **4**(1), pp. 41–49.

[38] Manning, K., 2001, "In Vitro Flow Visualization Study Within An Outlet Cannula Of A Rotary Ventricular Assist Deivce," Dissertation, Virginia Commonwealth University, Richmond, VA USA.

[39] Thatte, S. M., 2006, "In Vitro Flow Visualization Study of the Interface Between Outflow Graft of Ventricular Assist Device and Aorta," Dissertation, Virginia Commonwealth University, Richmond, VA USA.

[40] Gwak, K.-W., Paden, B. E., Noh, M. D., and Antaki, J. F., 2006, "Fluidic operational amplifier for mock circulatory systems," Ieee Trans. Control Syst. Technol., **14**(4), pp. 602 – 612.

[41] Ackerman, M. J., 1998, "The visible human project," Proc. Ieee, **86**(3), pp. 504–511.

[42] Withey, D. J., and Koles, Z. J., 2007, "Medical Image Segmentation: Methods and Software," Joint Meeting of the 6th International Symposium on Noninvasive Functional Source Imaging of the Brain and Heart and the International Conference on Functional Biomedical Imaging, 2007. NFSI-ICFBI 2007, pp. 140–143.

[43] Ma, Z., Tavares, J. M. R. S., Jorge, R. N., and Mascarenhas, T., 2010, "A review of algorithms for medical image segmentation and their applications to the female pelvic cavity," Comput. Methods Biomech. Biomed. Engin., **13**, pp. 235–246.

[44] Pham, D. L., Xu, C., and Prince, J. L., 2000, "Current Methods in Medical Image Segmentation 1," Annu. Rev. Biomed. Eng., **2**(1), pp. 315–337.

[45] Hahn, H. K., 2005, "Morphological Volumetry," Dissertation, University of Bremen, Germany.

[46] "Simtk.org: SimVascular: Cardiovascular Modeling and Simulation Application: Overview" [Online]. Available: https://simtk.org/home/simvascular. [Accessed: 20-Apr-2013].

[47] “MeshLab” [Online]. Available: http://meshlab.sourceforge.net/. [Accessed: 20-Apr-2013].

[48] The Blender Foundation, 2012, “Blender,” Blender.org [Online]. Available: http://www.blender.org/. [Accessed: 14-Dec-2012].

[49] De Zélicourt, D., Pekkan, K., Kitajima, H., Frakes, D., and Yoganathan, A. P., 2005, “Single-Step Stereolithography of Complex Anatomical Models for Optical Flow Measurements,” J. Biomech. Eng., **127**(1), p. 204.

[50] Noorani, R., 2006, *Rapid Prototyping - Principles and Applications*, John Wiley & Sons, Hoboken, NJ.

[51] Gregory, S., Timms, D., Pearcy, M. J., and Tansley, G., 2009, “A naturally shaped silicone ventricle evaluated in a mock circulation loop: A preliminary study,” J. Med. Eng. Technol., **33**(3), pp. 185–191.

[52] Biglino, G., Verschueren, P., Zegels, R., Taylor, A. M., and Schievano, S., 2013, “Rapid prototyping compliant arterial phantoms for in-vitro studies and device testing,” J. Cardiovasc. Magn. Reson., **15**.

[53] Kalejs, M., and Segesser, L. K. v., 2008, “Rapid prototyping of compliant human aortic roots for assessment of valved stents,” Interact. Cardiovasc. Thorac. Surg., **8**, pp. 182–186.

[54] Chua, C. K., Leong, K. F., and Lim, C. C. S., 2010, *Rapid Prototyping: Principles and Applications*, World Scientific, Singapore.

[55] 2012, *Manufacturing Automation: Metal Cutting Mechanics, Machine Tool Vibrations, and CNC Design*, Cambridge University Press.

[56] Arcaute, K., Palafox, G. N., Medina, F., and Wicker, R. B., “Complex silicone aorta models manufactured using a dip-spin coating technique and water-soluble molds,” Proceedings of the 2003 Summer Bioengineering Conference, pp. 1093–1094.

[57] Tanné, D., Bertrand, E., Kadem, L., Pibarot, P., and Rieu, R., 2009, “Assessment of left heart and pulmonary circulation flow dynamics by a new pulsed mock circulatory system,” Exp. Fluids, **48**(5), pp. 837–850.

[58] MAESTRINI, D., 1959, “[S. Baglioni and the law of the heart],” Il Policlin. Sezione Prat., **66**(7), pp. 224–230.

[59] Jauhar, S., 2004, “The artificial heart,” N Engl J Med, **350**(6).

[60] Liotta, D., Wieting, D. W., Hall, C. W., Chidoni, J. J., and DeBakey, M. E., 1967, “In vitro and in vivo flow studies in blood pumps,” Asaio J., **13**(1), pp. 280–287.

[61] Wildevuur, C. R. H., Mrava, G. L., Crosby, M. J., Wright, J. I., Hladky, H. L., Andreson, G. J., Pierson, R. M., Kon, T., and Nosé, Y., 1968, “An artificial heart sensitive to atrial volume,” Asaio J., **14**(1), p. 276.

[62] Snyder, M. F., Rideout, V. C., and Hillestad, R. J., 1968, “Computer modeling of the human systemic arterial tree,” J. Biomech., **1**(4), pp. 341–353.

[63] Liu, Y., Allaire, P., Wu, Y., Wood, H., and Olsen, D., 2006, “Construction of an Artificial Heart Pump Performance Test System,” Cardiovasc. Eng., **6**(4), pp. 151–158.

[64] Timms, D. L., 2005, “Design, development and evaluation of centrifugal ventricular assist devices.”

[65] Timms, D. L., Gregory, S. D., Greatrex, N. A., Pearcy, M. J., Fraser, J. F., and Steinseifer, U., 2011, “A Compact Mock Circulation Loop for the In Vitro Testing of Cardiovascular Devices,” Artif. Organs, **35**(4), pp. 384–391.

[66] Timms, D., Hayne, M., Tan, A., and Pearcy, M., 2005, “Evaluation of left ventricular assist device performance and hydraulic force in a complete mock circulation loop,” Artif. Organs, **29**(7), pp. 573–580.

[67] Gregory, S. D., Greatrex, N., Timms, D., Gaddum, N., Pearcy, M. J., and Fraser, J. F., 2010, “Simulation and enhancement of a cardiovascular device test rig,” J. Simul., **4**(1), pp. 34–41.

[68] Pantalos, G. M., Koenig, S. C., Gillars, K. J., Giridharan, G. A., and Ewert, D. L., 2004, “Characterization of an Adult Mock Circulation for Testing Cardiac Support Devices,” Asaio J., **50**(1), pp. 37–46.

[69] Pantalos, G. M., Koenig, S. C., Gillars, K. J., and Ewert, D. L., 2002, “Mock circulatory system for testing cardiovascular devices,” Proceedings of the Second Joint EMBS/BMES Conference, IEEE, Houston, TX, pp. 1597– 1598 vol.2.

[70] Rosenberg, G., 1972, “A mock circulatory system for in vitro studies of artificial hearts,” Pennsylvania State University.

[71] Sharp, M. K., Richards, C. M., Gillars, K. J., Giridharan, G., and Pantalos, G. M., 2008, “The Influence of Mock Circulation Input Impedance on Valve Acceleration During In Vitro Cardiac Device Testing,” Asaio J., **54**(4), pp. 341–346.

[72] Koenig, S. C., Pantalos, G. M., Gillars, K. J., Ewert, D. L., Litwak, K. N., and Etoch, S. W., 2004, “Hemodynamic and Pressure-Volume Responses to Continuous and Pulsatile Ventricular Assist in an Adult Mock Circulation,” Asaio J., **50**(1), pp. 15–24.

[73] Giridharan, G. A., and Skliar, M., 2006, “Physiological control of blood pumps using intrinsic pump parameters: a computer simulation study,” Artif. Organs, **30**(4), pp. 301–307.

[74] Pantalos, G. M., Ionan, C., Koenig, S. C., Gillars, K. J., Horrell, T., Sahetya, S., Colyer, J., and Gray Jr, L. A., 2010, “Expanded Pediatric Cardiovascular Simulator for Research and Training,” Asaio J., **56**(1), p. 67.

[75] Neal, M. L., and Kerckhoffs, R., 2010, “Current progress in patient-specific modeling,” Brief. Bioinform., **11**(1), pp. 111–126.

[76] Syncardia Systems, Inc., “Patient Simulator and Training Center (Mock Circulation Tank); User’s Manual” [Online]. Available: http://www.perfusion.ws/Syncardia/TAH-t%20Training%20Center%20User%20Manual.pdf. [Accessed: 16-Dec-2012].

[77] Kar, B., Delgado III, R. M., Frazier, O., Gregoric, I. D., Harting, M. T., Wadia, Y., Myers, T. J., Moser, R. D., and Freund, J., 2005, “The effect of LVAD aortic outflow-graft placement on hemodynamics and flow: Implantation technique and computer flow modeling,” Tex. Heart Inst. J., **32**(3), p. 294.

[78] Long, Q., Merrifield, R., Yang, G. Z., Kilner, P. J., Firmin, D. N., and Xu, X. Y., 2003, "The influence of inflow boundary conditions on intra left ventricle flow predictions.," J. Biomech. Eng., **125**(6), p. 922.

[79] Moody, G. B., Mark, R. G., and Goldberger, A. L., 2011, "PhysioNet: Physiologic signals, time series and related open source software for basic, clinical, and applied research," Proceedings of the 33rd Annual International Conference of the IEEE Engineering in Medicine and Biology Society (EMBS), Boston, Massachusetts, pp. 8327–8330.

[80] Hsu, P. L., Cheng, S. J., Saumarez, R. C., Dawes, W. N., and McMahon, R. A., 2008, "An extended computational model of the circulatory system for designing ventricular assist devices," Asaio J., **54**(6), p. 594.

[81] Lévine, J., and Müllhaupt, P., eds., 2010, *Advances in the theory of control, signals and systems with physical modeling*, Springer, Berlin.

[82] Johansson, P., and Andersson, B., 2008, "Comparison of simulation programs for supercapacitor modelling," Master's Thesis, Chalmers University of Technology, Gothenberg, Sweden.

[83] Kornecki, A., and Zalewski, J., 2009, "Certification of software for real-time safety-critical systems: state of the art," Innov. Syst. Softw. Eng., **5**(2), pp. 149–161.

[84] The MathWorks, 2010, *Simscape 3.0 User's Guide*, The MathWorks, Natick, MA.

[85] Yu, Y. C., and Gopalakrishnan, S., 2009, "Elastance control of a mock circulatory system for ventricular assist device test," American Control Conference, 2009. ACC'09., pp. 1009–1014.

[86] Taylor, C. E., and Miller, G. E., 2012, "Implementation of an Automated Peripheral Resistance Device in a Mock Circulatory Loop With Characterization of Performance Values Using Simulink Simscape and Parameter Estimation," J. Med. Devices, **6**(4), p. 045001.

[87] Enocksson, S., 2011, "Modeling in MathWorks Simscape by building a model of an automatic gearbox," Master's Thesis, Uppsala University, Uppsala, Sweden.

[88] Marlin, T. E., 2000, *Process control: designing processes and control systems for dynamic perfomance*, McGraw-Hill, Boston.

[89] Watton, J., 2009, *Fundamentals of fluid power control*, Cambridge University Press, New York.

[90] Lipták, B., 2006, *Instrument engineers' handbook*, CRC Taylor & Francis, Boca Raton Fla. [u.a.].

[91] Merritt, H. E., 1991, *Hydraulic Control Systems*, Wiley.

[92] Miller, S., 2009, "Modeling Physical Systems as Physical Networks with the Simscape Language", Podium presentation at the 6th Vienna International Conference on Mathematical Modelling, Vienna, Austria.

[93] Segur, J. B., and Oberstar, H. E., 1951, "Viscosity of glycerol and its aqueous solutions," Ind. Eng. Chem., **43**(9), pp. 2117–2120.

[94] 2011, “Density of Glycerine-Water Solutions,” Dow Chem. Corp. Website [Online]. Available: http://www.dow.com/glycerine/resources/table4_3140.htm.

[95] Papaioannou, T. G., Mathioulakis, D. S., Nanas, J. N., Tsangaris, S. G., Stamatelopoulos, S. F., and Moulopoulos, S. D., 2002, “Arterial compliance is a main variable determining the effectiveness of intra-aortic balloon counterpulsation: quantitative data from an in vitro study,” Med. Eng. Phys., **24**(4), pp. 279–284.

[96] Komaragiri, U., Begley, M. R., and Simmonds, J. G., 2005, “The Mechanical Response of Freestanding Circular Elastic Films Under Point and Pressure Loads,” J. Appl. Mech., **72**(2), pp. 203–212.

[97] Ugural, A., 1999, *Stresses in plates and shells*, WCB/McGraw Hill, Boston.

[98] Reddy, J., 1999, *Theory and analysis of elastic plates*, Taylor & Francis, Philadelphia PA.

[99] Olin, C., 1971, “Pulsatile flow studies of prosthetic aortic valves,” Scand. Cardiovasc. J., **5**(1), pp. 1–12.

[100] Yeboa, K. C., Camp, T. A., and Figliola, R. S., 2009, “Modeling of Free Pulmonary Regurgitation and Analysis of Mock Circulatory System”, presentation at the 2009 Biomaterial Day, Clemson University.

[101] Wolf, L., and Clinch, J. M., 1972, “Mock circulatory system for intra-aortic balloon testing,” Ieee Trans. Biomed. Eng., **19**(1), pp. 38–46.

[102] Harvard Apparatus Inc., “Series 1400 Pulsatile Blood Pumps User’s Manual.”

[103] Harvard Apparatus Inc., “Model 665 Intermediate Ventilator User’s Manual.”

[104] Eckhardt, H., 1998, *Kinematic design of machines and mechanisms*, McGraw-Hill, New York.

[105] 2011, “Viscosity of Aqueous Glycerine Solutions,” Dow Chem. Corp. Website [Online]. Available: http://www.dow.com/glycerine/resources/table18.htm.

[106] Dorsi, J. M., 1990, “Testing a multiple disk pump for use as an artificial ventricle.,” Master’s Thesis, Texas A&M University, College Station, TX.

[107] Mojica-Santiago, J. A., Villongco, C. A., Krummen, D. E., Frank, L. R., and McCulloch, A. D., 2011, “Reconstructing Patient-Specific Models of the Dyssynchronous Failing Heart using CT and DTMR Images”, Poster presentation at the Biomedical Engineering Society Annual Meeting, Hartford, CT.

[108] Gorder, R., 2010, “Mass Transport and Shear Stress within the Carotid Artery Bifurcation: A Study of Flow Effects on Atherosclerosis,” Master’s Thesis, University of Washington, Seattle, WA.

[109] Shankar, P. N., and Kumar, M., 1994, “Experimental determination of the kinematic viscosity of glycerol-water mixtures,” Proc. Math. Phys. Sci., **444**(1922), pp. 573–581.

[110] The MathWorks, 2010, *Simulink 7.0 User’s Guide*, The MathWorks, Natick, MA.

[111] Toliyat, H. A., and Kliman, G. B., 2004, *Handbook of electric motors*, CRC, Boca Raton.

[112] Microchip Technology Inc., 2009, “PIC18F2455/2550/4455/4550 Data Sheet.”

[113] Microchip Technology Inc., 2005, “MPLAB(R) C18 C Compiler User’s Guide.”

Appendix A

This section is provided as a reference for the code architectures and hardware integration developed during the course of this project. The information contained in this section only pertains to controllers that were internally developed, and not commercially available.

A.1: Compliance Chamber Controller

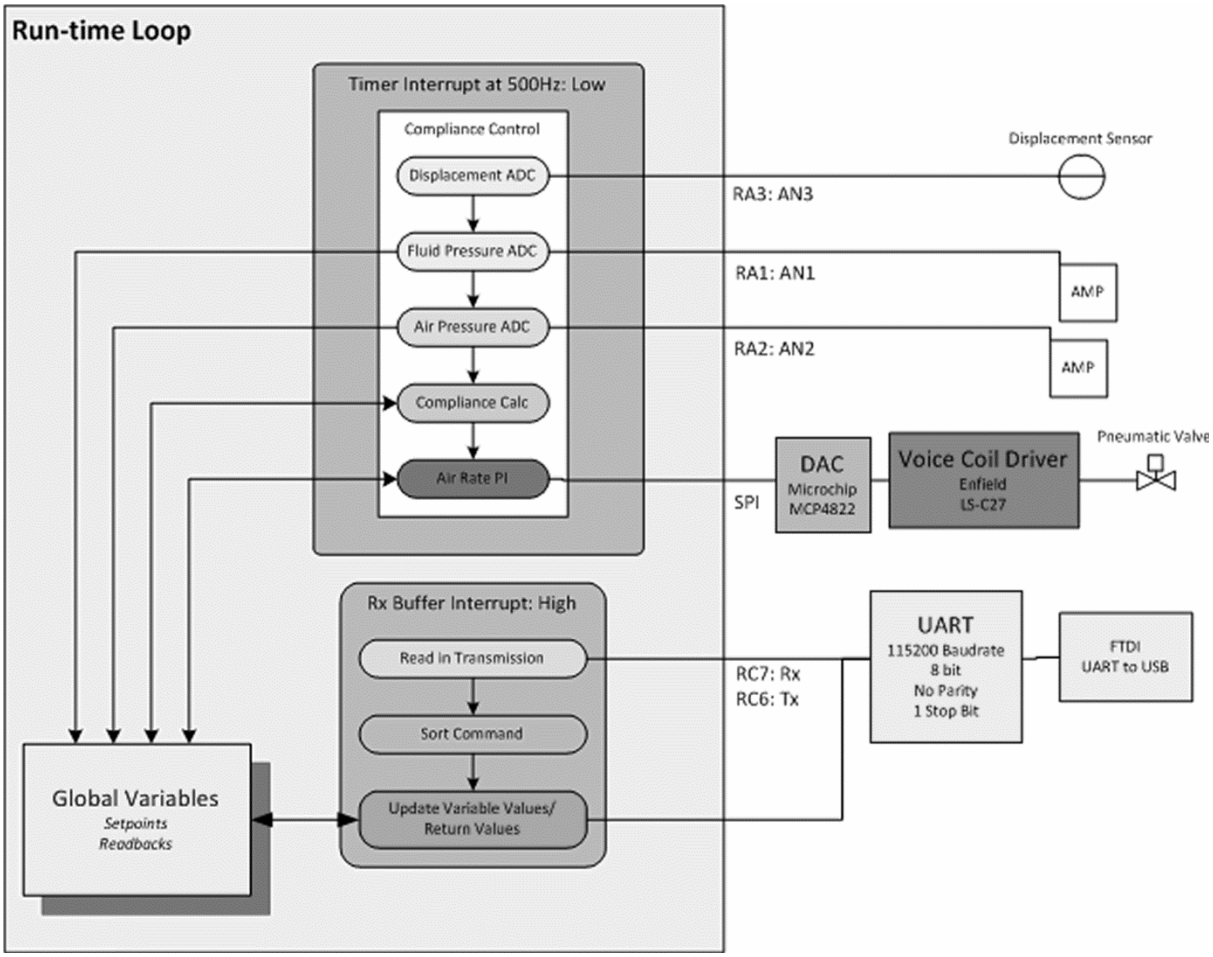

Figure 51: Compliance chamber control architecture, illustrating code section execution and connections to the hardware.

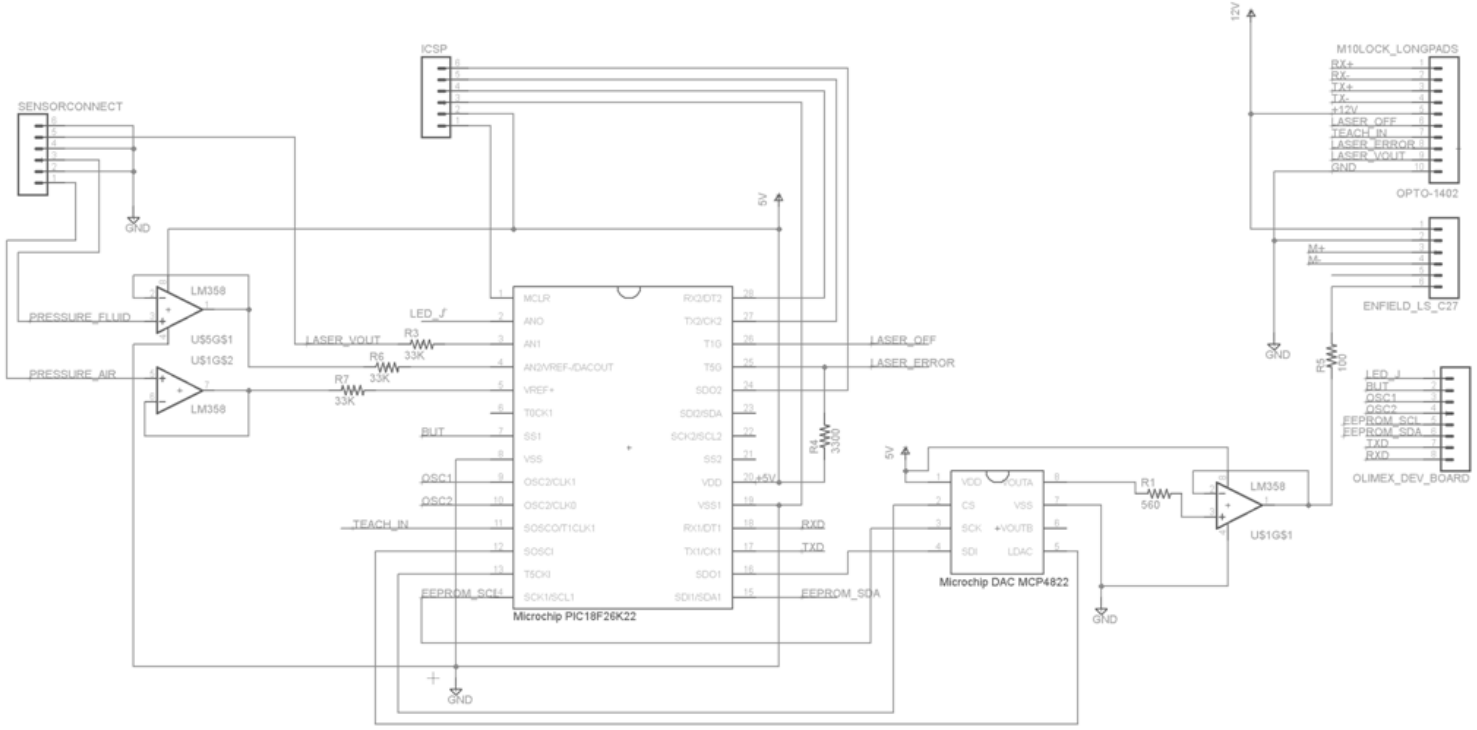

Figure 52: Circuit diagram of compliance chamber controller.

A.2: Harvard Pump Controller

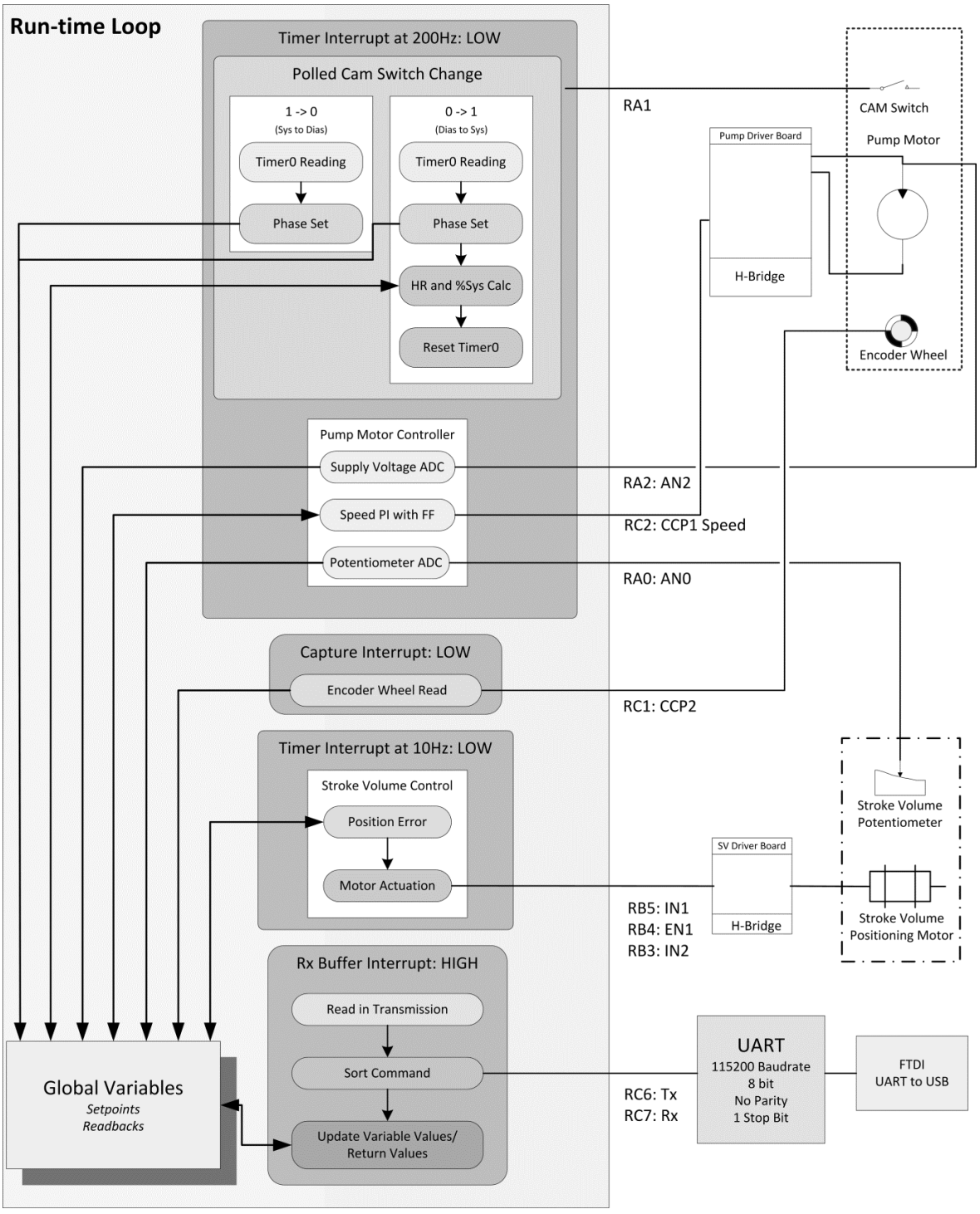

Figure 53: Harvard pump control architecture, illustrating code section execution and connections to the hardware.

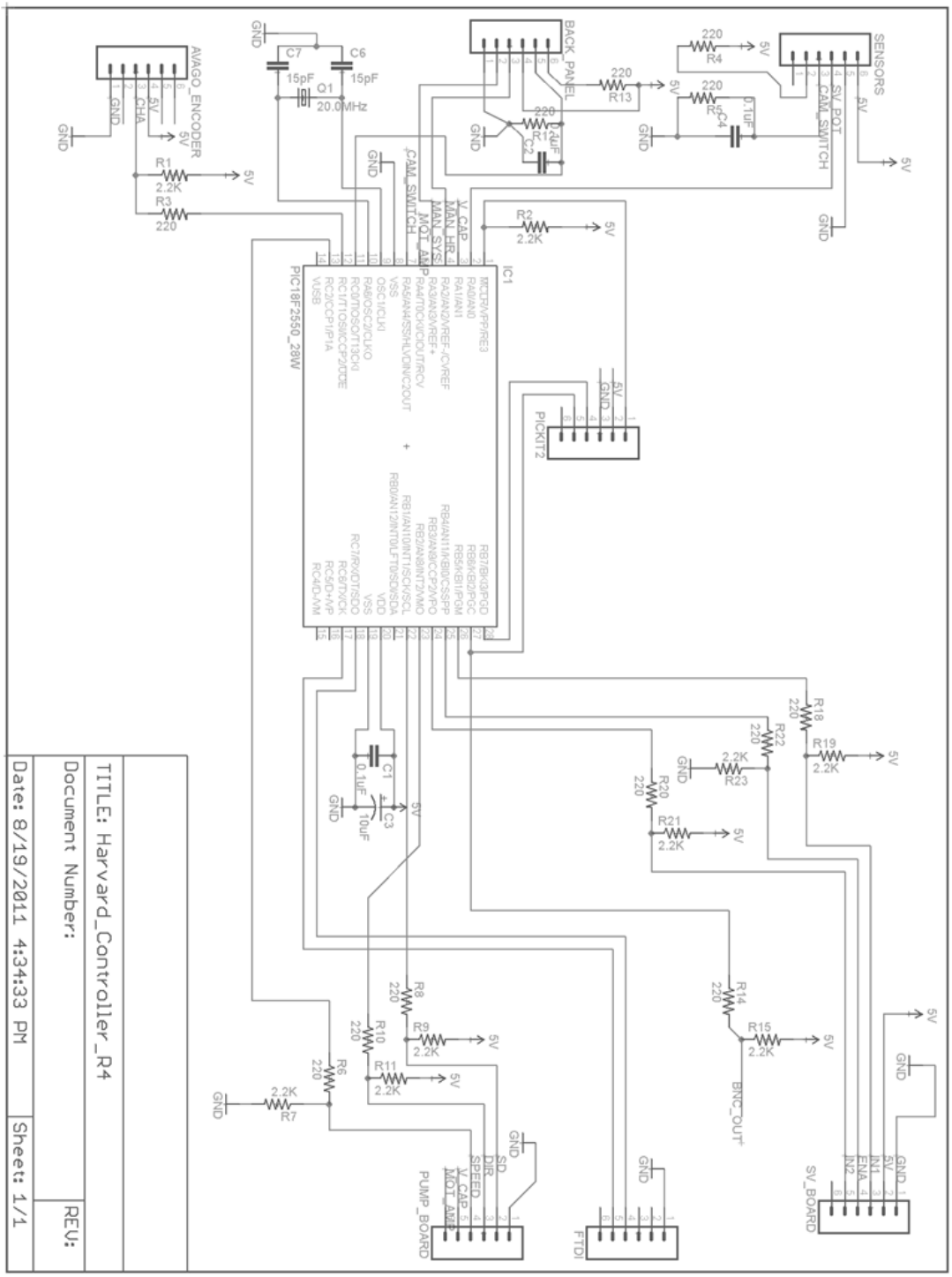

Figure 54: Circuit diagram of Harvard Pump controller.

Appendix B

The following appendix details the LabVIEW block diagrams that are responsible for the function of the mock circulatory loop Dashboard VI.

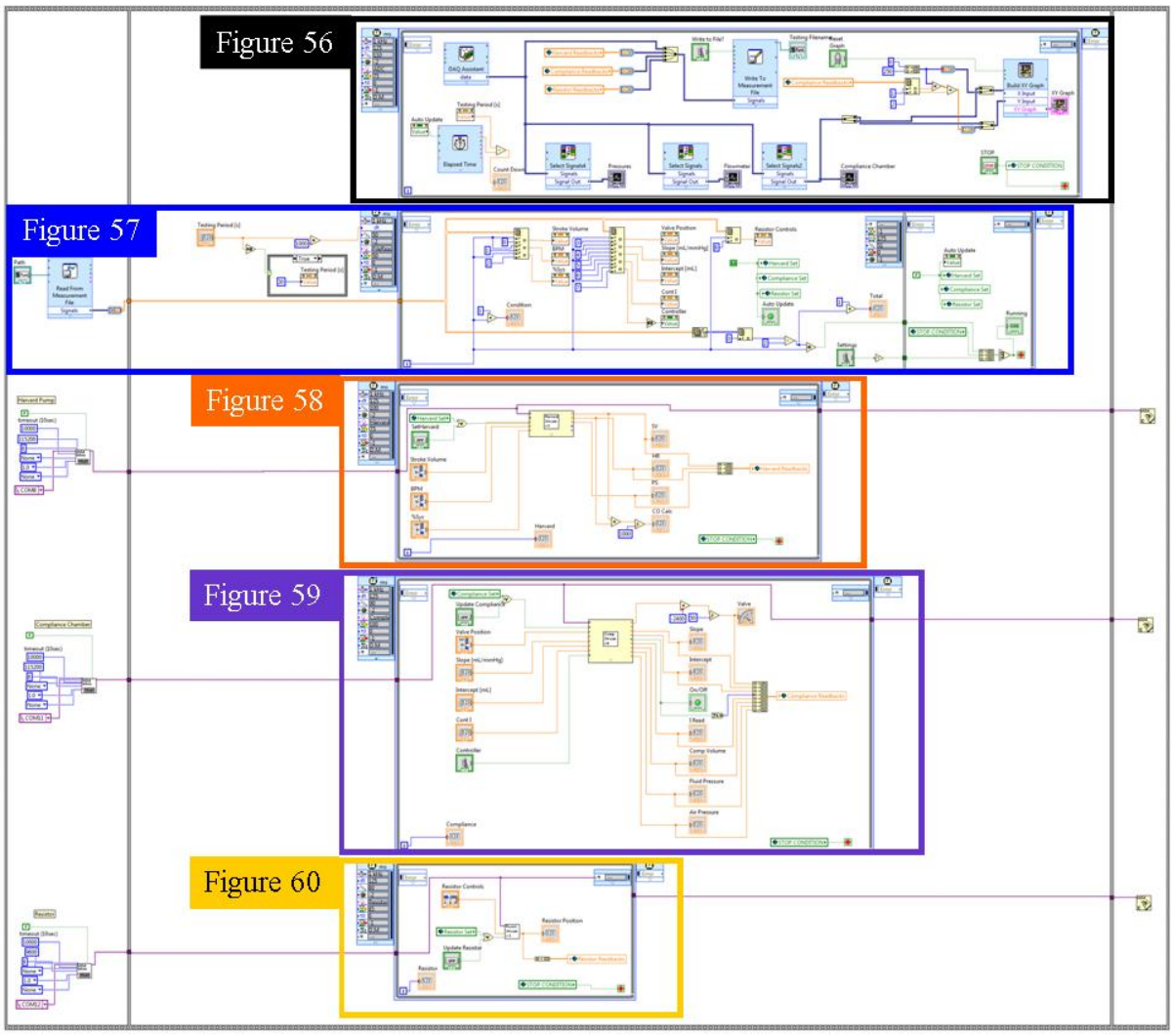

Figure 55: Block diagram of the Dashboard VI used to control the mock circulatory loop. Due to the size of the block diagram, it cannot be effectively displayed in one figure. This illustration acts as a roadmap for the subsequent figures that display enlarged sections of this figure. The delineation in the figures is by section of code encapsulated by its respective control loop. The initialization of the serial communications in the far left column, and the termination scripts in the far right, have not been included in the subsequent figures.

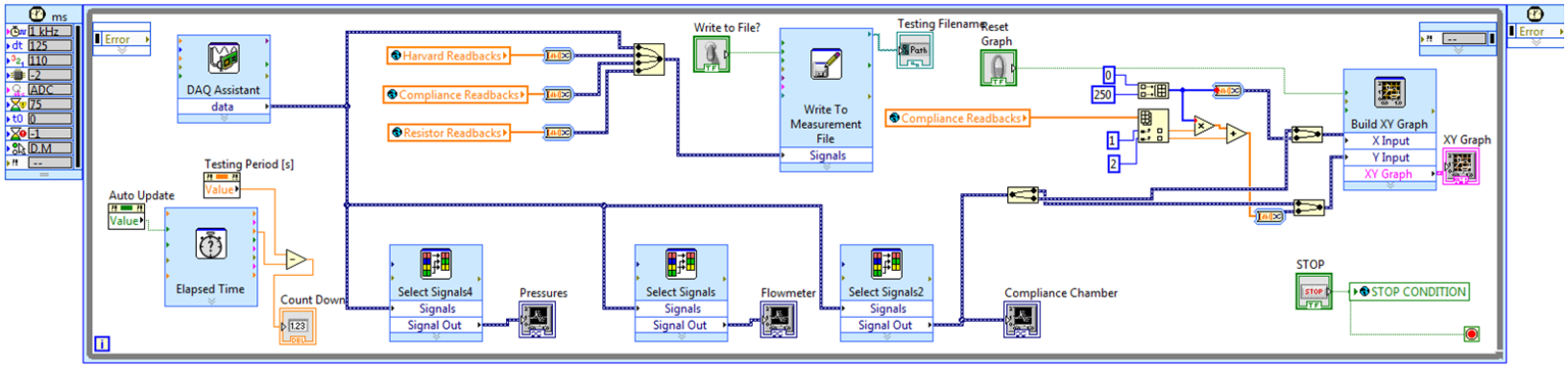

Figure 56: Dashboard block diagram section logging subsystem read backs(orange blocks) and sensor readings (DAQ assistant block far left) to the output file (Write to Measurement File block).

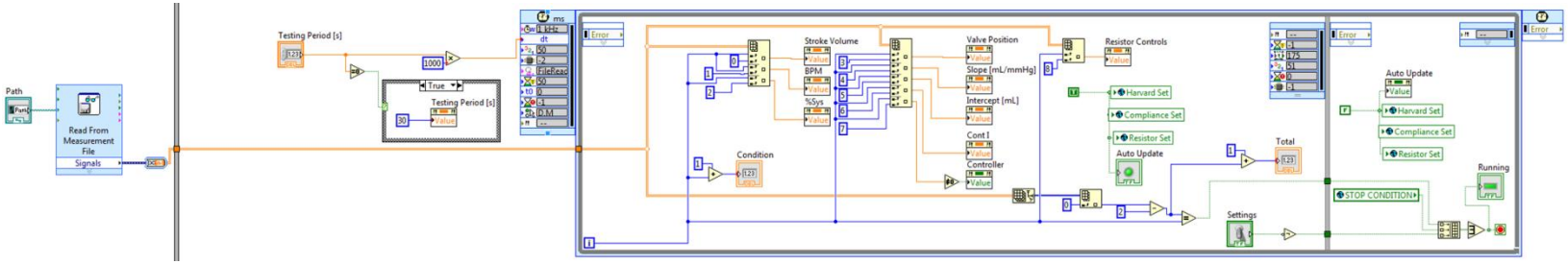

Figure 57: Dashboard block diagram section that reads the experiment file generated by the Conditions Designer program, and executes the set point changes at times throughout the experiment. The file is identified by the path entered by the user (far left) and imported as a numerical array; rows denote sets of set points with the first column indicating the time. The settings are parsed to the various subsystems global variables, which will be updated to the controls when the respective loops controlling the subsystem settings are executed.

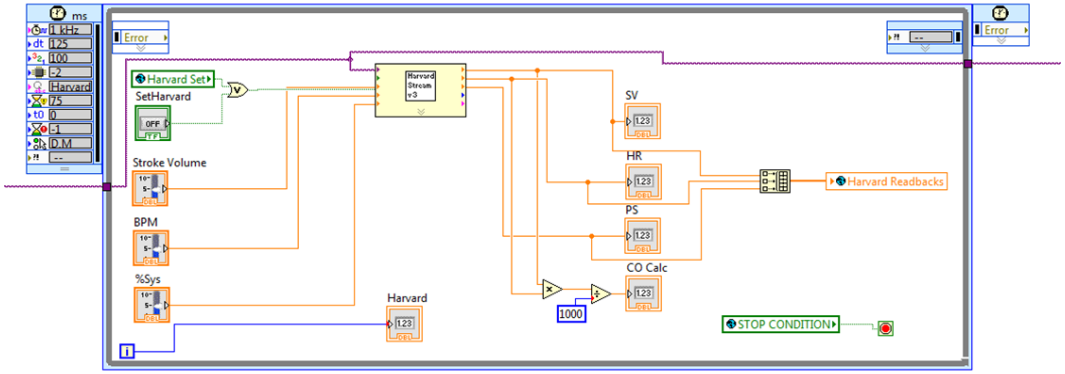

Figure 58: Control section that updates the Harvard Pump controller. The global set points are on the left, which connect to the serial communication block (center). Updates are output from the serial communication block to update the read back indicators. These read backs are connected to a global variable array (far right) that is used by the logging section of the code to record the settings to file.

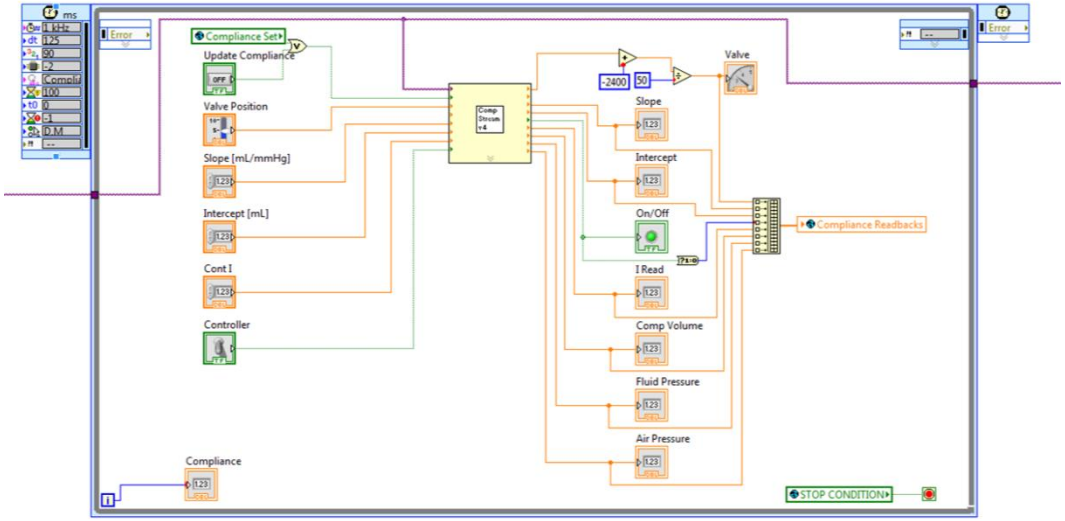

Figure 59: Control section for the Compliance Chamber, which shares the architecture with the Harvard Pump section in Figure 58.

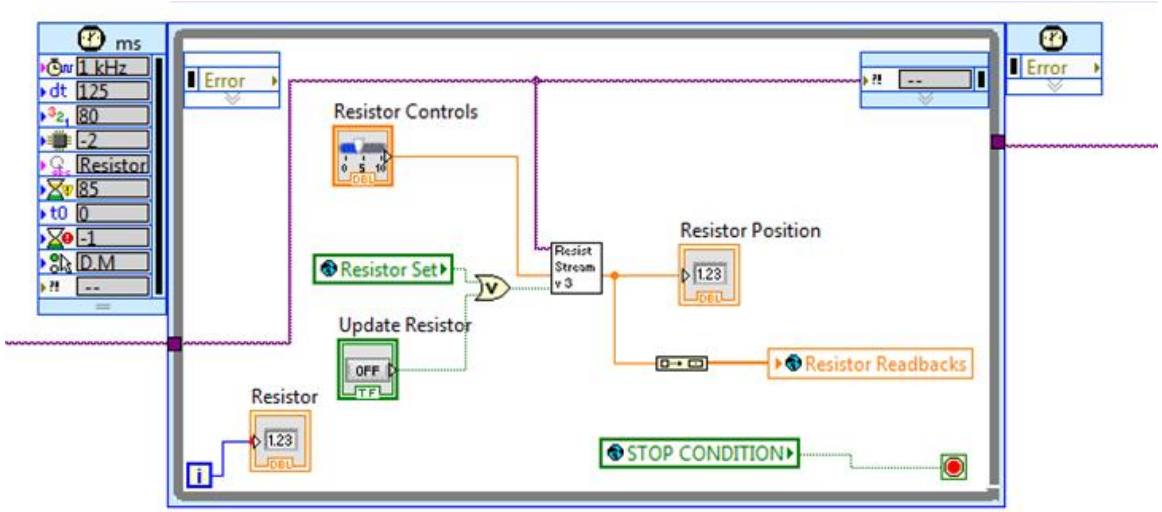

Figure 60: Peripheral resistor control code section. Position of the piston is the only set point for this subsystem, which otherwise shares the same code architecture as the Harvard Pump (Figure 58).

Vita

Charles Edward Taylor was born on July 21, 1983 in Hollywood, California USA. He graduated from Loyola High School of Los Angeles, California in 2001. During his college years, he held various biomedical engineering positions. In his first two years of college, he worked for Charles River Laboratories Transgenic Services Division as a technician in their isolation vivariums. During the summer between his third and fourth years, he interned at Stanford Medical Centers Biomedical Engineering and Biotechnology Department where he received training on a wide range of medical devices in use at the facility. At the end of his fourth year, he worked for Kalypsys, Inc. as a part-time employee assisting the Analytical Chemistry Department. He received his Bachelor of Science in Bioengineering from the University of California, San Diego in 2005. In the following years, he worked at Kalypsys, Inc. as an analytical chemist developing high throughput physical property assays. He enrolled at Virginia Commonwealth University in the fall of 2008 to pursue his Doctorate in Biomedical Engineering.